doi.org/10.26434/chemrxiv.14204210.v1

Selective Manganese-Catalyzed Dimerization and Cross-Coupling of Terminal Alkynes

Stefan Weber, Luis F. Veiros, Karl Kirchner

Submitted date: 11/03/2021 • Posted date: 16/03/2021

Citation information: Weber, Stefan; Veiros, Luis F.; Kirchner, Karl (2021): Selective Manganese-Catalyzed Dimerization and Cross-Coupling of Terminal Alkynes. ChemRxiv. Preprint. https://doi.org/10.26434/chemrxiv.14204210.v1

For the first time, an efficient manganese-catalyzed dimerization of terminal alkynes to afford 1,3-enynes is described. This reaction is atom economic, implementing an inexpensive, earth abundant non-precious metal catalyst. The pre-catalyst is the bench-stable alkyl bisphosphine Mn(I) complex fac-[Mn(dippe)(CO)3(CH2CH2CH3)]. The catalytic process is initiated by migratory insertion of a CO ligand into the Mn-alkyl bond to yield an acyl intermediate which undergoes rapid C-H bond cleavage of the alkyne forming an active Mn(I) acetylide catalyst [Mn(dippe)(CO)2(C≡CPh)(η2-HC≡CPh)] together with liberated butanal. A range of aromatic and aliphatic terminal alkynes were efficiently and selectively converted into head-to-head Z-1,3-enynes and head-to-tail gem-1,3-enynes, respectively, in good to excellent yields. Moreover, cross-coupling of aromatic and aliphatic alkynes yields selectively head-to-tail gem-1,3-enynes. In all cases, the reactions were performed at 70 °C with a catalyst loading of 1-2 mol %. A mechanism based on DFT calculations is presented.

File list (3)

Selective Manganese-Catalyzed Dimerization and Cross-Coupling of Terminal Alkynes

Stefan Weber,[1] Luis F. Veiros,[2] and Karl Kirchner*, [1]

[1]Institute of Applied Synthetic Chemistry, Vienna University of Technology, Getreidemarkt 9, A-1060 Vienna, AUSTRIA

[2] Centro de Química Estrutural and Departamento de Engenharia Química, Instituto Superior Técnico, Universidade de Lisboa, Av Rovisco Pais, 1049-001 Lisboa, PORTUGAL

ABSTRACT: For the first time, an efficient manganese-catalyzed dimerization of terminal alkynes to afford 1,3-enynes is described. This reaction is atom economic, implementing an inexpensive, earth abundant non-precious metal catalyst. The pre-catalyst is the bench-stable alkyl bisphosphine Mn(I) complex *fac*-[Mn(dippe)(CO)$_3$(CH$_2$CH$_2$CH$_3$)].

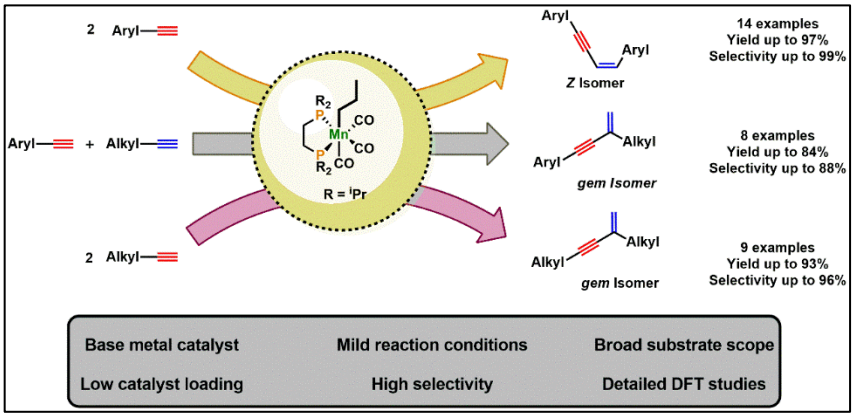

The catalytic process is initiated by migratory insertion of a CO ligand into the Mn-alkyl bond to yield an acyl intermediate which undergoes rapid C-H bond cleavage of the alkyne forming an active Mn(I) acetylide catalyst [Mn(dippe)(CO)$_2$(C≡CPh)(η^2-HC≡CPh)] together with liberated butanal. A range of aromatic and aliphatic terminal alkynes were efficiently and selectively converted into head-to-head Z-1,3-enynes and head-to-tail gem-1,3-enynes, respectively, in good to excellent yields. Moreover, cross-coupling of aromatic and aliphatic alkynes yields selectively head-to-tail gem-1,3-enynes. In all cases, the reactions were performed at 70 °C with a catalyst loading of 1-2 mol %. A mechanism based on DFT calculations is presented.

INTRODUCTION

CO ligands in Mn(I) alkyl carbonyl complexes are known to undergo migratory insertions to form highly reactive coordinatively unsaturated acyl complexes which can be trapped in the presence of strong field ligands such as CO or tertiary phosphines - *a well-known textbook reaction*.[1] The classic reaction is the formation of Mn(CO)$_5$(η^1-COCH$_3$) from Mn(CO)$_5$(CH$_3$) in the presence of CO.[2-4] On the other hand, these acyl 16e$^-$ intermediates can be utilized to activate dihydrogen, possibly also molecules featuring weakly polar E-H (E = e.g., C, Si, B) bonds. For instance, dihydrogen is able to react with transition-metal acyl complexes to afford aldehydes and metal hydride complexes. This process is accompanied by H-H and metal-σ-C bond cleavage and is typically the final step in both stoichiometric and catalytic hydroformylations of alkenes (Scheme 1).[5,6]

Scheme 1. Formation of a Mn(I) Hydride and Acetylide Species *via* Alkyl Migration followed by Aldehyde Release upon E-H Bond Cleavage

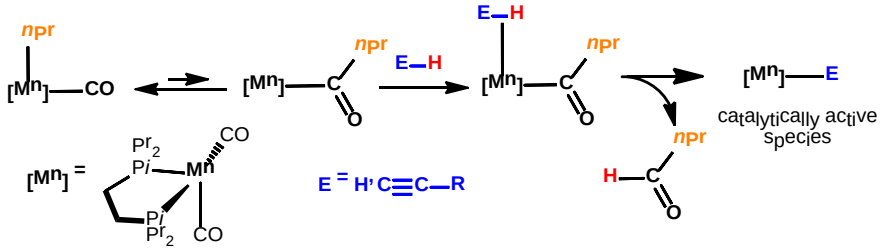

We have recently described the hydrogenation of alkenes and nitriles utilizing Mn(I) complexes *fac*-[Mn(dpre)$(CO)_3$(R)] (dpre = 1,2-bis(di-*n*-propylphosphino) ethane, R = CH_3, CH_2CH_3, $CH_2CH_2CH_3$) and *fac*-[Mn(dippe)$(CO)_3$($CH_2CH_2CH_3$) (dippe = 1,2-bis(di-*iso*-propylphosphino)ethane) where we took advantage of the migratory insertion and hydrogenolysis processes to create the active 16e$^-$ Mn(I) hydride catalysts (Scheme 1).[7]

Here, we describe the activity of *fac*-[Mn(dippe)$(CO)_3$($CH_2CH_2CH_3$)] (**1**) as pre-catalyst for the dimerization of terminal aromatic and aliphatic alkynes to afford selectively head-to-head Z-1,3-enynes and head-to-tail gem-1,3-enynes, respectively. The initiation step involves C-H bond activation of the terminal alkyne forming an active Mn(I) acetylide catalyst together with free butanal (Scheme 1). This is the first example of a manganese catalyzed dimerization and cross coupling of terminal alkynes,[8,9] which proceeds without any additives under mild conditions.

RESULTS AND DISCUSSION

The catalytic performance of **1** was first investigated for the dimerization of phenylacetylene as model substrate. Selected optimization experiments are depicted in Table 1. With **1** as pre-catalyst and a catalyst loading of 2 mol% quantitative formation of 1,3-enyne was observed at 70 °C (Table 1, entry 1). No reaction took place with complexes **2** and **3** (Table 1 entries 2 and 3) emphasizing the crucial role of the alkyl substituents at the phosphine donors. It should be noted that high selectivity towards the formation of the *Z*-isomer (>95 %) is attributed to the use of **1** as catalyst, where only small amounts of *E*-isomer (<5 %) and no formation of geminal isomer were detected. Upon optimization reactions (for details see SI), the catalyst loading could be decreased to 1 mol% (Table 1, entry 6). Only traces of product could be detected at room temperature (Table 1, entry 7).

Having established the optimized reaction conditions, a broad variety of different aromatic substrates was investigated. Excellent yields could be achieved for substrates containing a halide or an electron withdrawing-group in the para- or ortho-position (Table 2, **5**-**7**, **12** and **13**). Slightly lower yields were achieved for aryl-substrates, containing electron-donating groups such as alkyl- or methoxy-groups (Table 2, **8**-**11**). Amine functionalities are tolerated (Table 2, **14, 15** and **17**), however, the reactivity of the system is decreased. Good yield could be achieved with 2-ethynylthiophene as substrate (Table 2, **16**). No conversion was observed for 2-ethynylpyridine and 2-ethynylaniline, presumably due to coordination of the nitrogen donor blocking the vacant coordination site of the active Mn(I) acetylide catalyst.

Table 1. Optimization reaction for the dimerization of phenylacetylene catalyzed by 1.

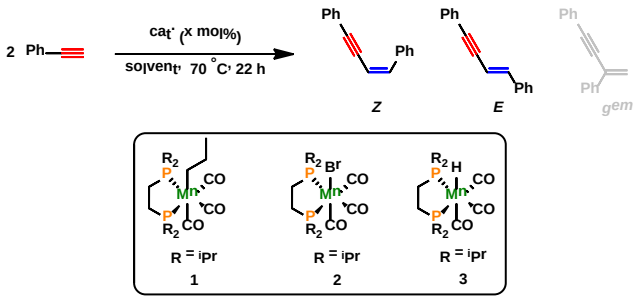

entry	catalyst (mol%)	solvent	conversion [%]	*Z:E ratio*
1	1 (2)	THF	>99	96:4
2	2 (2)	THF	-	n.d.
3	3 (2)	THF	-	n.d.
4	1 (2)	toluene	17	95: 5
5	1 (2)	$CHCl_3$	12	97:3
6[a]	**1 (1)**	**THF**	**>99**	**97:3**
7[a,b]	1 (1)	THF	traces	n.d.

Reaction conditions: phenylacetylene (1.1 mmol), 0.5 mL anhydrous solvent, 70 °C, 22 h, conversion and isomer ratio determined by GC-MS. [a] 18 h. [b] 25 °C.

The investigation of aliphatic alkynes unveiled an unexpected observation. Apart from lower reactivity of aliphatic systems, which led to higher catalyst loadings and prolonged reaction times, the product changed drastically. Instead of head-to-head dimerization, massive formation of head-to-tail product and only small amounts of *Z*-1,3-enyne and no *E*-1,3-enyne were detected. Excellent yields could be achieved for linear aliphatic substrates such as 1-hexyne or 1-octyne (Table 3, **18** and **19**). Lower reactivity was observed for 3-phenyl-1-propyne (Table 3, **22**). Interestingly, a ratio of 39:61 *gem*:*Z* was observed for trimethylsilylacetylene (Table 3, **23**). Cyclic aliphatic systems (Table 3, **24** – **26**) gave excellent yields with high selectivity towards the geminal isomer.

Encouraged by these findings, we aimed for the cross-coupling of aromatic with aliphatic alkynes yielding geminal 1,3-enynes. Cross-coupling of alkynes is a challenging field due the high number of possible cross- and homo-coupling products. The results are represented in Table 4. A detailed table of all detected isomers is provided the SI. We were able to couple a variety of aromatic substrates with cyclopropylacetylene (Table 4, **27**-**30**). The highest yields were achieved if electron donating groups, such as *t*Bu or OMe are present in the *para*-position. These substrates show lower tendency to dimerize under the given reaction conditions. Phenylacetylene and 1-chloro-4-phenylacetylene showed a higher amount of dimerization for the investigated systems, which lowers the amount of cross-coupling product. Good to excellent yields were achieved for the coupling of 4-ethynylanisole with 6-chloro-1-hexyne as well as

1-ethynylcyclohexene. Furthermore, **1** is suitable for cross-coupling of two aliphatic substrates (cyclopropylacetylene and 1-ethynylcyclohexene, Table 4, **34**).

Table 2. Scope and limitation of the dimerization of aromatic alkynes catalyzed by 1.

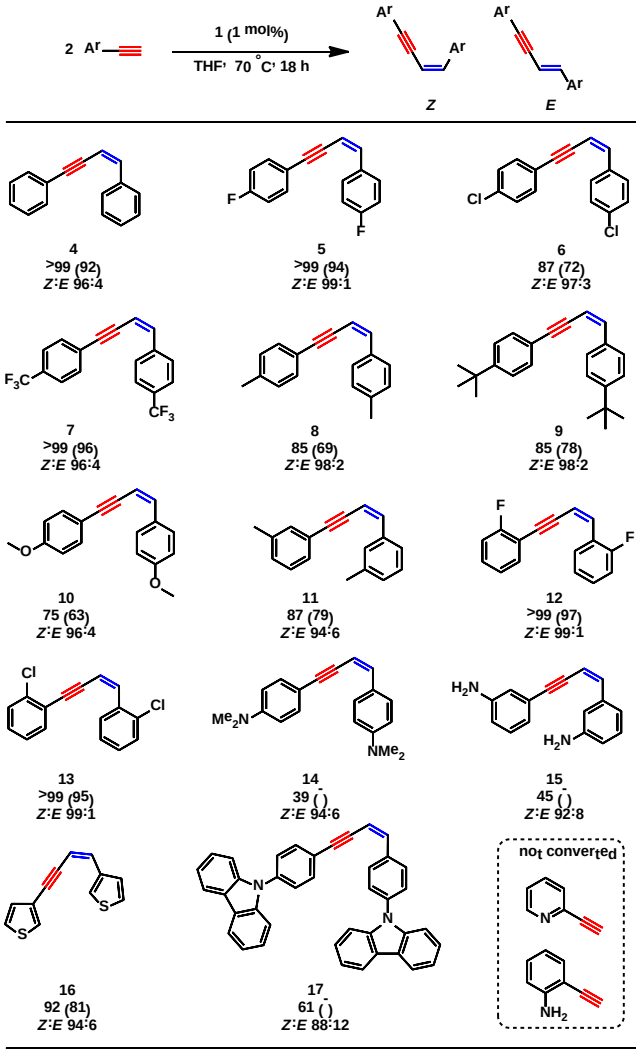

Reaction conditions: alkyne (1.1 mmol), **1** (1 mol%), 0.5 mL anhydrous THF, 70 °C, 18 h, conversion and isomer ratio determined by GC-MS, isolated yield given in parenthesis.

The homogeneity of the system was confirmed upon addition of one drop of mercury, whereas no decrease of reactivity and selectivity was observed for the dimerization of phenylacetylene. In presence of 1 equivalent of PMe_3, only traces of product formation could be detected, which indicates an inner-sphere mechanism. Kinetic isotope effects of 1.49 and 2.44 were detected for the dimerization of phenylacetylene *vs.* phenylacetylene-d_1 and 1-octyne *vs.* 1-octyne-d_1, respectively, as depicted in Scheme 2.

Table 3. Scope and limitation of the dimerization of aliphatic alkynes catalyzed by 1.

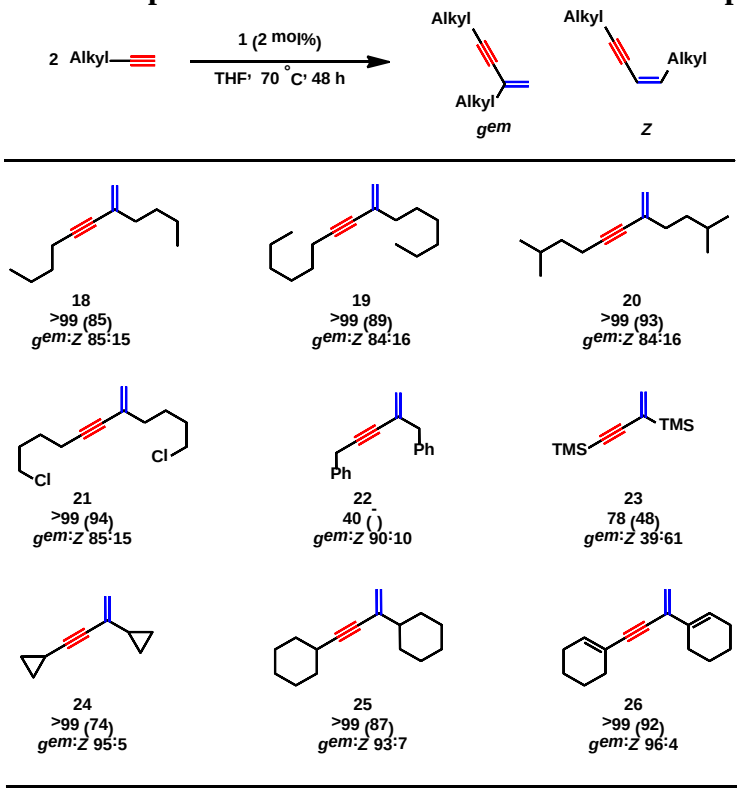

Reaction conditions: alkyne (1.1 mmol), **1** (2 mol%), 0.5 mL anhydrous THF, 70 °C, 48 h, conversion and isomer ratio determined by GC-MS, isolated yield given in parenthesis.

Table 4. Scope and limitation of the cross-coupling alkynes catalyzed by 1.

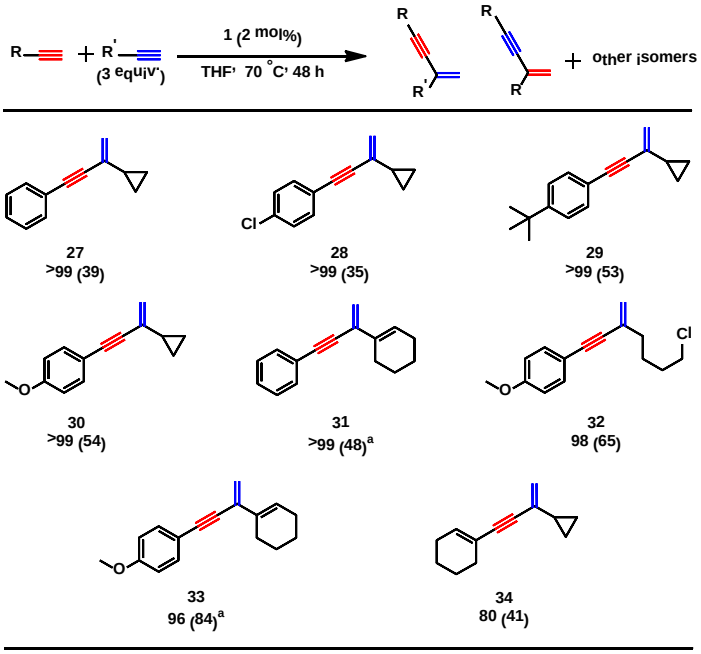

Reaction conditions: alkyne 1 (1.1 mmol, 1 equiv.), alkyne 2 (3.3 mmol, 3 equiv.), **1** (2 mol%), 0.5 mL anhydrous THF, 70 °C, 48 h, conversion of alkyne 1 determined by GC-MS, isolated yield given in parenthesis. [a] Yield determined by GC-MS using hexadecane as standard.

This suggests that the activation of the C-H bond is the rate determining step during the reaction. These findings are in line with theoretical calculation since the C-H activation upon product release shows the highest energy barrier in the catalytic reaction (*vide infra*). Interestingly, the ratio of *gem*:*Z* for 1-octyne-d_1 is drastically increased to 97:3 (85:17 for 1-octyne).

Scheme 2. Determination of the KIE for the dimerization of phenylacetylene (a) and 1-octyne (b) catalyzed by 1.

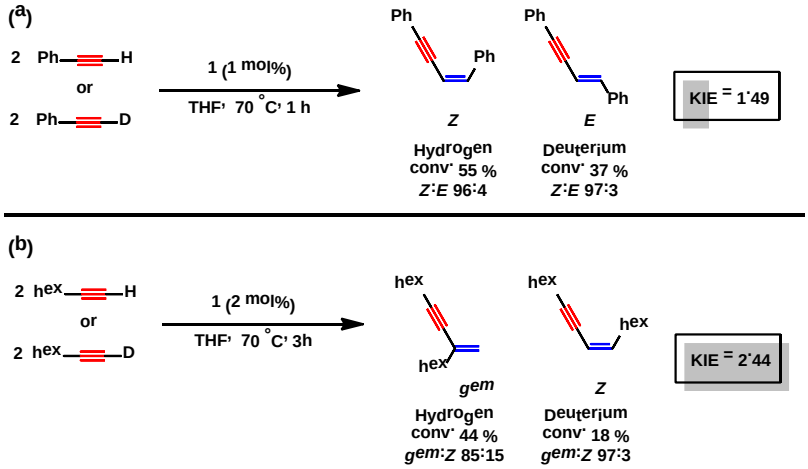

In order to get more insight into the dimerization of terminal alkynes, we performed DFT-calculations[10] based on *fac*-[Mn(dippe)(CO)$_3$(CH$_2$CH$_2$CH$_3$)] (**1**) as the pre-catalyst and employing phenylacetylene as the substrate. The free energy profile calculated for the formation of the active species, previous to the initiation of the catalytic cycle, is represented in Figure 1.

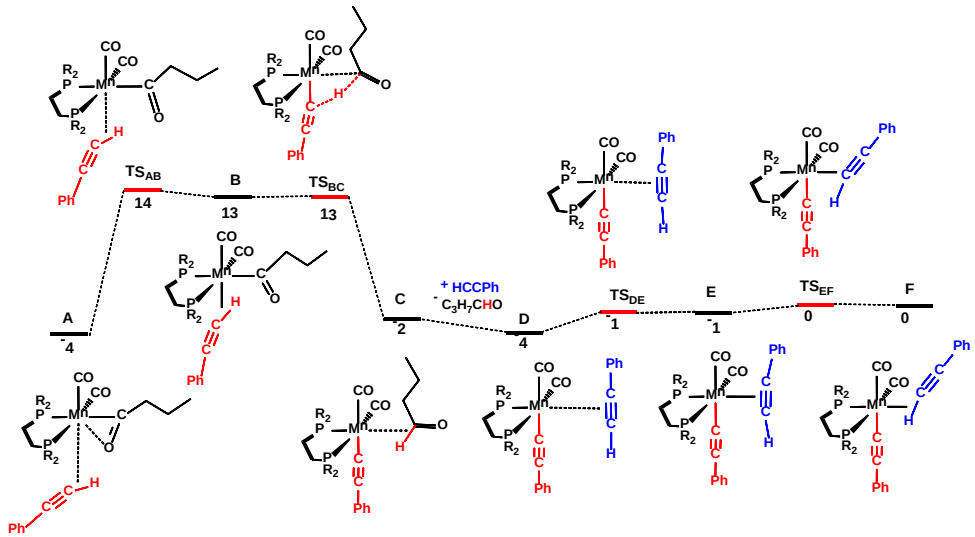

Figure 1. Free Energy Profile Calculated for the Formation of the Active Acetylide Catalyst. Free Energies (kcal/mol) are Referred to [Mn(dippe)(CO)$_2$(C≡CPh)(η^2-*C*,*H*-HC≡CPh)] (**F** in the calculations).

Catalyst initiation, starting from **1**, has been reported previously.[7] Experimental mechanistic studies revealed that *n*-butanal is liberated during the catalytic reaction as detected by ^{1}H - NMR spectroscopy.

The first step following formation of an acyl intermediate is coordination of one phenylacetylene molecule, from **A** to **B**, and, then, there is H-transfer from the newly bonded acetylene ligand to the carbonyl C-atom, with formation of aldehyde, from **B** to **C**. This part of the path includes the highest barrier in the profile, $\Delta G^{\ddagger}$ = 18 kcal/mol, from **A** to **TS$_{AB}$**.

From **C**, butanal is liberated and exchanges with a second substrate molecule that slips from η^2-coordination in **E** to a κ^2-mode in **F**. This is the initial active species in the catalytic cycle, and its formation follows a series of steps fairly easy ($\Delta G^{\ddagger}$ = 4 kcal/mol) and almost thermoneutral (ΔG = 2 kcal/mol), from **C** to **F**.

Scheme 3. Simplified Catalytic Cycle for the (Z)-Selective Dimerization of Terminal Alkynes.

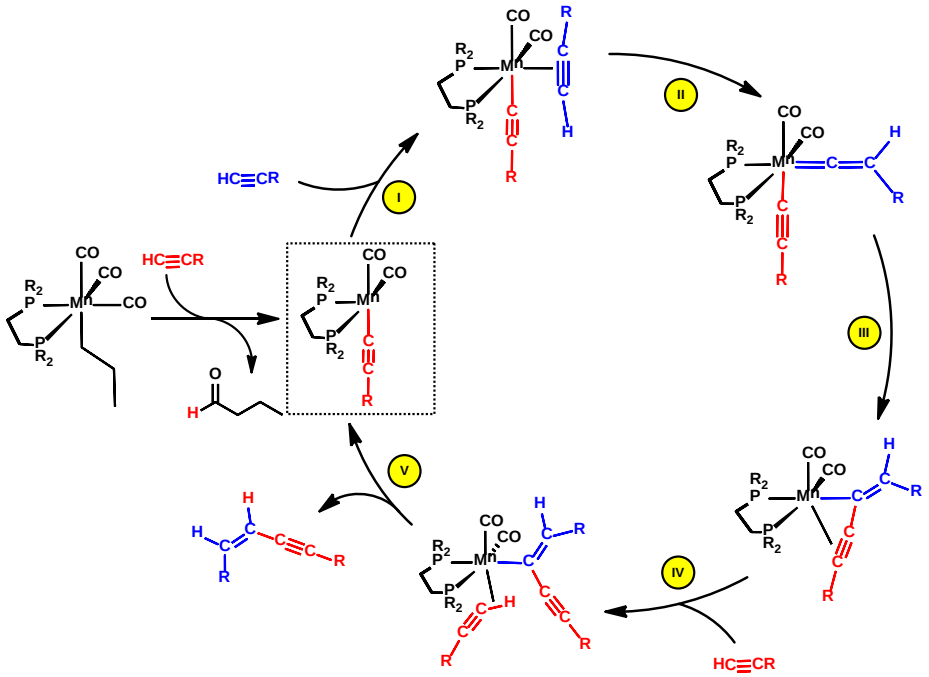

Scheme 3 depicts a summary of the catalytic cycle. Similarly to what is known for ruthenium- as well as iron-based systems,[11,12,9g] our calculations unveiled a classical acetylene-vinylidene mechanism. In particular, an incoming acetylene substrate undergoes a 1,2-H-shift (**II**) yielding a vinylidene intermediate which suffers nucleophilic attack from the neighboring acetylide ligand (**III**) resulting in the formation of an alkynyl vinyl complex. Proton transfer from a second acetylene molecule leads to the liberation the final 1,3-enyne and recovery of the initial acetylide species (**IV**, **V**).

The free energy profile obtained for the first part of the path (**II** and **III** in the cycle of Scheme 3) is represented in Figure 2. Here, formation of the two isomers of the alkynyl vinyl intermediate, with *Z* and *E* conformations around the C=C double bond, is considered. Thus, the left part of the profile regards formation of the intermediate with the *E*-vinylalkynyl ligand, from **F** (the last species in the profile of Figure 1) to **H$_E$**. This is a single-step path, with simultaneous H-shift on the acetylene ligand and C–C coupling between this and the neighbor acetylide. The corresponding barrier is $\Delta G^{\ddagger}$ = 15 kcal/mol and the process is favorable, from the thermodynamic point of view, with ΔG = –30 kcal/mol.

The right-hand part of the profile in Figure 2 regards formation of the vinylalkynyl intermediate with this ligand in a *Z*-conformation, from **F** to **H$_Z$**. In this case, the overall process takes two consecutive

steps. First, there is H-shift within the acetylene ligand, forming a vinylidene acetylide intermediate, from **F** to **G**$_Z$, in an exergonic step (ΔG = –9 kcal/mol) with a barrier of $\Delta G^{\ddagger}$ = 13 kcal/mol (**TS**$^{Z}_{FG}$). Then, in a second step, there is C–C coupling between the two ligands, the vinylidene and the acetylide, from **G**$_Z$ to **H**$_Z$, in a facile step with a barrier of only $\Delta G^{\ddagger}$ = 4 kcal/mol (from **G**$_Z$ to **TS**$^{Z}_{GH}$) and a balance of ΔG = –26 kcal/mol.

From the profile in Figure 2, it is clear that the *Z*-alkynylvinyl intermediate (**H**$_Z$) is the most stable of the two isomers by 5 kcal/mol and also the one that is formed more easily, with a barrier 2 kcal/mol lower than the one associated with formation of the *E* isomer (**H**$_E$): **TS**$^{Z}_{FG}$ vs. **TS**$^{E}_{FH}$. The final part of the mechanism corresponds to the formation of the 1,3-enyne product from the alkynylvinyl intermediates (**IV** and **V** in the cycle of Scheme 3). The corresponding free energy profile is represented in Figure 3 for the two isomers, *Z* and *E*. The left hand side of the profile concerns formation of the *E*-enyne (in **K**$_E$) from the corresponding *E*- alkynylvinyl intermediate (**H**$_E$), while on the right side there is the equivalent profile for the formation of the product with a *Z* conformation, from **H**$_Z$ to **K**$_Z$. Two equivalent mechanisms were obtained, both composed by two steps: first coordination of a new phenylacetylene molecule and, then, H-transfer from coordinated acetylene to the alkynylvinyl ligand with formation of the product. The barrier associated with the formation of the *Z*-enyne ($\Delta G^{\ddagger}$ = 25 kcal/mol, from **H**$_Z$ to **TS**$^{Z}_{IJ}$ or **TS**$^{Z}_{JK}$) is 7 kcal/mol lower than the one corresponding to the formation of its *E*-counterpart indicating that the *Z*-isomer is the most favorable product, as observed. Interestingly, the last step (associated with **TS**$^{Z}_{JK}$) corresponds to H-transfer and being the rate-determining step corroborates the kinetic isotopic effect experimentally detected and discussed above (see Scheme 2).

The mechanism of *Z*-*E* isomerization between the two forms of the alkynylvinyl intermediates (**H**$_E$ and **H**$_Z$) was also studied and the profile obtained is presented in the SI. The corresponding rearrangement around the C=C double bond of the ligand has an overall barrier of $\Delta G^{\ddagger}$ = 24 kcal/mol that, being 1 kcal/mol lower than the one calculated for the catalytic cycle, indicates that the isomerization process is faster, or at least competitive, compared with enyne formation.

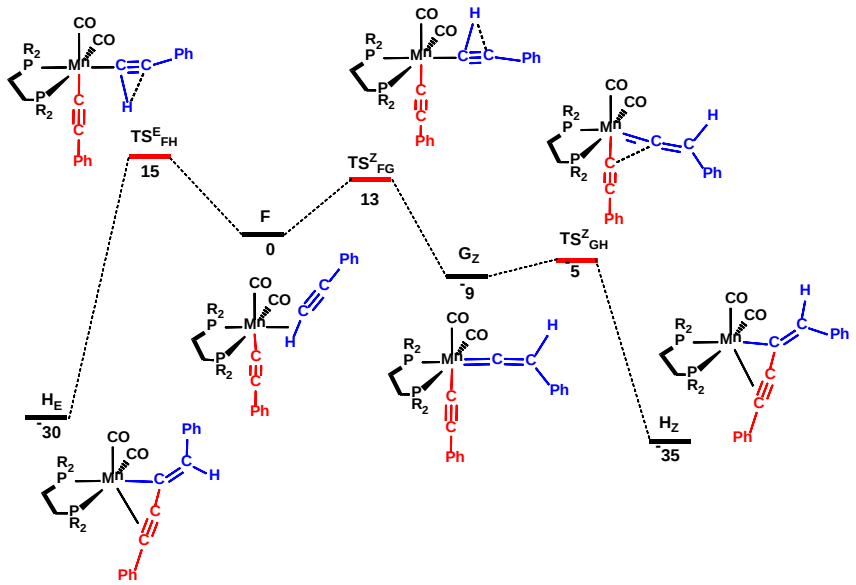

Figure 2. Free Energy Profile Calculated for the Dimerization of Terminal Alkynes. Free Energies (kcal/mol) are Referred to [Mn(dippe)(CO)$_2$(C≡CPh)(η^2-HC≡CPh)] (**F** in the calculations)

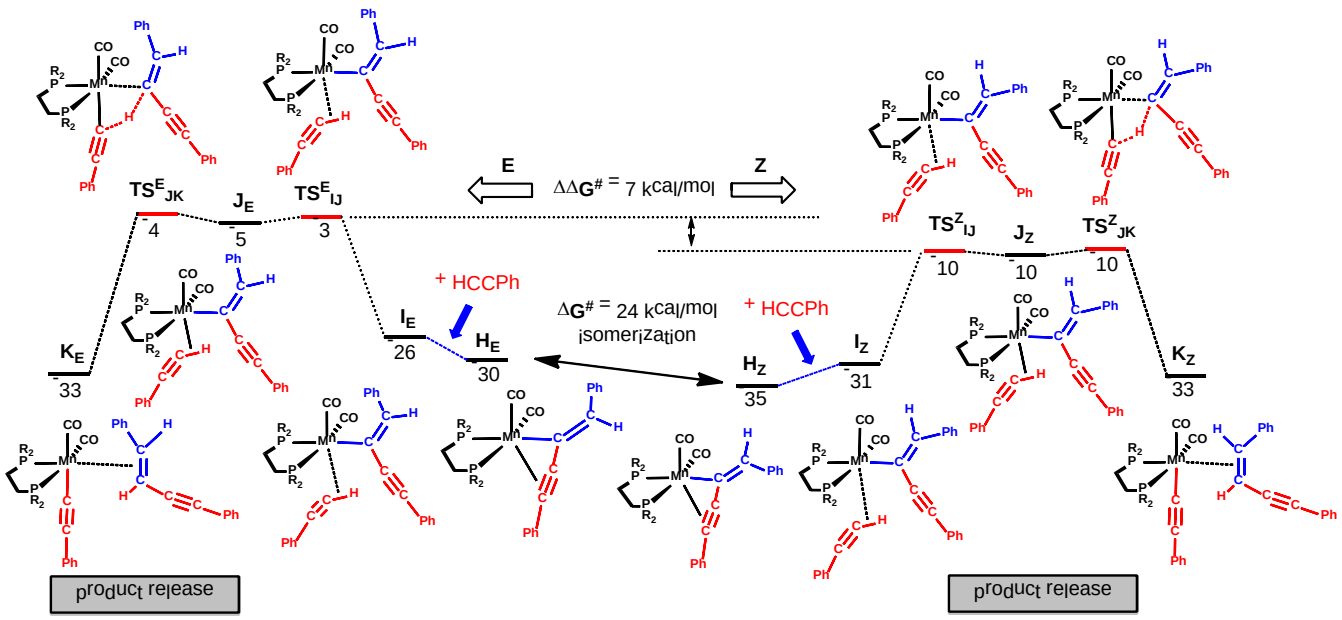

Figure 3. Free Energy Profile Calculated for the Dimerization of Terminal Alkynes. Free Energies (kcal/mol) are Referred to [Mn(dippe)(CO)$_2$(C≡CPh)(η^2-HC≡CPh)] (**F** in the calculations)

CONCLUSION

In sum, an efficient and highly selective additive-free manganese-catalyzed dimerization and cross-coupling of terminal alkynes to afford enynes is described. To the best of our knowledge, this is the first example of a well-defined Mn(I)-based catalyst for such a process. The pre-catalyst is the alkyl bisphosphine Mn(I) complex *fac*-[Mn(dippe) (CO)$_3$(CH$_2$CH$_2$CH$_3$)] (**1**) which is air-stable for several weeks in the solid state. The initiation step involves migratory insertion of a CO ligand into the Mn-alkyl bond followed by C-H bond activation of the terminal alkyne to form the 16e$^-$ Mn(I) acetylide complex [Mn(dippe)(CO)$_2$(HC≡CR)]. This species is an efficient catalyst for the regio- and stereoselective head-to-head dimerization of terminal aromatic and aliphatic alkynes giving 1,3-enynes and head-to-tail gem-1,3-enynes, respectively, in high yields with up to 99% selectivity. Additionally, complex **1** is also capable to promote cross-dimerizations of aromatic with aliphatic alkynes yielding geminal l 1,3-enynes. DFT calculations disclosed in the case of aromatic alkynes an acetylene-vinylidene mechanism and indicate that the *Z*-1,3-enyne is a kinetic product, resulting from a lower energy barrier, compared with the one associated with the formation of its *E*-counterpart as depicted in Scheme 2. Based on the kinetic isotope effects of 1.49 and 2.44 detected for the dimerization of phenylacetylene *vs.* phenylacetylene-d_1 and 1-octyne *vs.* 1-octyne-d_1, respectively, the activation of the C-H bond appears to be the rate determining step. These findings are in line with theoretical calculation since the C-H activation upon product release shows the highest energy barrier in the catalytic reaction.

Supporting Information

^{1}H- and ^{13}C{^{1}H}-NMR spectra of all compounds and complete computational details (PDF)
Cartesian coordinates for DFT-optimized structures (XYZ)

ACKNOWLEDGMENT

Financial support by the Austrian Science Fund (FWF) is gratefully acknowledged (Project No. P 33016-N). Centro de Química Estrutural acknowledges the financial support of Fundação para a Ciência e Tecnologia (UIDB/00100/2020).

REFERENCES

(1) Calderazzo, F. Synthetic and Mechanistic Aspects of Inorganic Insertion Reactions. Insertion of Carbon Monoxide. *Angew. Chem. Int. Ed.* **1977**, 16, 299-311.

(2) (a) Coffield, T. H.; Closson, R. D.; Kozikowski, J. Acyl Manganese Pentacarbonyl Compounds. *J. Org. Chem.* **1957**, *22*, 598. (b) Noack, K.; Calderazzo, F. Carbon monoxide insertion reactions. V. The carbonylation of methylmanganese pentacarbonyl with carbon-13 monoxide. *J. Organomet. Chem.* **1967**, *10*, 101−104.

(3) Casey, C. P.; Bunnell, C. A.; Calabrese, J. C. Synthesis, Crystal Structure, and Stability of Pyruvoylpenta-carbonylmanganese(I). *J. Am. Chem. Soc.* **1976**, *98* ,1166-1171 and references therein.

(4) Food, T. C.; Jensen, J. E.; Staller, J. A. Stereochemistry at Manganese of the Carbon Monoxide Insertion in Pentacarbonylmethylmanganese(I). The Geometry of the Intermediate *J. Am. Chem. Soc.* **1981**, *103*, 4410-4414.

(5) Birbeck, J. M.; Haynes, A.; Adams, H.; Damoense, L.; Otto, S. Ligand Effects on Reactivity of Cobalt Acyl Complexes. *ACS Catal.* **2012**, *2*, 2512−2523.

(6) (a) Ojima, I.; Tsai, C.-Y.; Tzamarioudaki, M.; Bonafoux, D. The Hydroformylation Reaction; Wiley: New York, **2004**. (b) van Leeuwen, P. W. N. M. In *Homogeneous Catalysis: Understanding the Art*; 1st ed.; Springer: Dordrecht, **2005**. (c) Claver, C.; van Leeuwen, P. W. N. M. In *Rhodium Catalyzed Hydroformylation*; Claver, C., van Leeuwen, P. W. N. M., Eds.; Kluwer Academic Publishers: Dordrecht, The Netherlands, **2000**.

(7) (a) Weber, S.; Veiros, L. F.; Kirchner, K. Old Concepts, New Application: Additive-free Hydrogenation of Nitriles Catalyzed by a Bench-Stable Alkyl Mn(I) Complex. *Adv. Synth. Catal.* **2019**, *361*, 5412-5420. (b) Weber, S.; Stöger, B.; Veiros, L. F.; Kirchner, K. Rethinking Old Concepts - Hydrogenation of Alkenes Catalyzed by Bench-Stable Alkyl Mn(I) Complexes. *ACS Catal.* **2019**, *9*, 9715-9720.

(8) Liang, Q.; Hayashi, K.; Song, D. Catalytic Alkyne Dimerization without Noble Metals. *ACS Catal.* **2020**, *10*, 4895-4905.

(9) For recent examples of base-metal catalyzed alkyne dimerizations, see: (a) Midya, G. C.; Paladhi, S.; Dhara, K.; Dash, J. Iron Catalyzed Highly Regioselective Dimerization of Terminal Aryl Alkynes. *Chem. Commun.* **2011**, *47*, 6698−6700. (b) Midya, G. C.; Parasar, B.; Dhara, K.; Dash, J. Ligand Mediated Iron Catalyzed Dimerization of Terminal Aryl Alkynes: Scope and Limitations. *Org. Biomol. Chem.* **2014**, *12*, 1812−1822. (c) Bhunia, M.; Sahoo, S. R.; Vijaykumar, G.; Adhikari, D.; Mandal, S. K. Cyclic (Alkyl)amino Carbene Based Iron Catalyst for Regioselective Dimerization of Terminal Arylalkynes. *Organometallics* **2016**, *35*, 3775−3780. (d) Xue, F.; Song, X.; Lin, T. T.; Munkerup, K.; Albawardi, S. F.; Huang, K.-W.; Hor, T. S. A.; Zhao, J. Dimerization of Terminal Aryl Alkynes Catalyzed by Iron(II) Amine-Pyrazolyl Tripodal Complexes with *E/Z* Selectivity Controlled by tert-Butoxide. *ACS Omega* **2018**, *3*, 5071−5077. (e) Rivada-Wheelaghan, O.; Chakraborty, S.; Shimon, L. J. W.; Ben-David, Y.; Milstein, D. Z-Selective (Cross-) Dimerization of Terminal Alkynes Catalyzed by an Iron Complex. *Angew. Chem., Int. Ed.* **2016**, *55*, 6942−6945. (f) Gorgas, N.; Alves, L. G.; Stöger, B.; Martins, A. M.;

Veiros, L. F.; Kirchner, K. Stable, Yet Highly Reactive Nonclassical Iron(II) Polyhydride Pincer Complexes: Z-Selective Dimerization and Hydroboration of Terminal Alkynes. *J. Am. Chem. Soc.* **2017**, *139*, 8130−8133. (g) Gorgas, N.; Stöger, B.; Veiros, L. F.; Kirchner, K. Iron(II) Bis(acetylide) Complexes as Key Intermediates in the Catalytic Hydrofunctionalization of Terminal Alkynes. *ACS Catal.* **2018**, *8*, 7973−7982. (h) Liang, Q.; Osten, K. M.; Song, D. Iron-Catalyzed gem-Specific Dimerization of Terminal Alkynes. *Angew. Chem., Int. Ed.* 2017, *56*, 6317−6320. (i) Liang, Q.; Sheng, K.; Salmon, A.; Zhou, V. Y.; Song, D. Active Iron(II) Catalysts toward gem-Specific Dimerization of Terminal Alkynes. *ACS Catal.* **2019**, *9*, 810−818. (j) Field, L. D.; Ward, A. J.; Turner, P. The Dimerization and Cyclotrimerization of Acetylenes Mediated by Phosphine Complexes of Cobalt(I), Rhodium(I), and Iridium(I). Aust. J. Chem. 1999, 52, 1085−1092. (k) Hilt, G.; Hess, W.; Vogler, T.; Hengst, C. Ligand and Solvent Effects on Cobalt(I)-Catalysed Reactions: Alkyne Dimerisation Versus [2+2+2]-Cyclotrimerisation Versus Diels−Alder Reaction Versus [4+2+2]-Cycloaddition. *J. Organomet. Chem.* **2005**, *690*, 5170−5181. (l) Beattie, J. W.; Wang, C.; Zhang, H.; Krogman, J. P.; Foxman, B. M.; Thomas, C. M. Dimerization of Terminal Alkynes Promoted by a Heterobimetallic Zr/Co Complex. *Dalton Trans.* **2020**, *49*, 2407−2411. (m) Xu, D.; Sun, Q.; Quan, Z.; Wang, C.; Sun, W. Cobalt-Catalyzed Dimerization and Homocoupling of Terminal Alkynes. Asian *J. Org. Chem.* **2018**, *7*, 155−159. (n) Zhuang, X.; Chen, J.-Y.; Yang, Z.; Jia, M.; Wu, C.; Liao, R.-Z.; Tung, C.-H.; Wang, W. Sequential Transformation of Terminal Alkynes to 1,3-Dienes by a Cooperative Cobalt Pyridonate Catalyst. *Organometallics* **2019**, *38*, 3752−3759. (o) Grenier-Petel, J.-C.; Collins, S. K. Photochemical Cobalt-Catalyzed Hydroalkynylation To Form 1,3-Enynes. *ACS Catal.* **2019**, *9*, 3213−3218. (p) Ueda, Y.; Tsurugi, H.; Mashima, K. Cobalt-Catalyzed (*E*)-Selective Cross-Dimerization of Terminal Alkynes via a Mechanism Involving Co(0/II) Redox Cycles. *Angew. Chem., Int. Ed.* **2020**, *59*, 1552−1556. (q) Chen, J.-F.; Li, C. Cobalt-Catalyzed gem-Cross-Dimerization of Terminal Alkynes. *ACS Catal.* **2020**, *10*, 3881−3889.

(10) (a) Parr, R. G.; Yang, W. Density Functional Theory of Atoms and Molecules; Oxford University Press: New York, 1989. (b) Calculations performed at the M06/(6-311++G**)//PBE0/(SDD,6-31G**) level using the GAUSSIAN 09 package. Single-point energy calculations included solvent effects (benzene) using the PCM/SMD model. A full account of the computational details and a complete list of references are provided as SI.

(11) (a) Jia, G.; Meek, D. W.; Gallucci, J. C. Synthesis and Reactivity of Ruthenium Hydride Complexes Containing Chelating Triphosphines. 4. Reactions of Ruthenium Hydride Complexes Containing Triphosphines with Olefins. *Organometallics* **1990**, *9*, 2549–2555. (b) Bianchini, C.; Peruzzini, M.; Zanobini, F.; Frediani, P.; Albinati, A. A Ruthenium(II) Enynyl Complex Mediates the Catalytic Dimerization of 1-Alkynes to Z-1,4-Disubstituted Enynes. *J. Am. Chem. Soc.* **1991**, *113*, 5453–5454. (c) Jia, G.; Meek, D. W. Synthesis and Reactivity of Ruthenium Hydride Complexes of Chelating Triphosphines. 5. Reactions of Acetylenes with RuHCl(Cyttp) and RuH_4(Cyttp) {Cyttp = $C_6H_5P[CH_2CH_2CH_2P(c\text{-}C_6H_{11})_2]_2$}. *Organometallics* **1991**, *10*, 1444–1450. (d) Eaves, S. G.; Yufit, D. S.; Skelton, B. W.; Lynam, J. M.; Low, P. J. Reactions of alkynes with *cis*-$RuCl_2(dppm)_2$: exploring the interplay of vinylidene, alkynyl and η^3-butenynyl complexes. *Dalton Trans.* **2015**, *44*, 21016-21024.

(12) Katayama, H.; Ozawa, F. Vinylidene Ruthenium Complexes in Catalysis. *Coord. Chem. Rev.* **2004**, *248*, 1703–1715.

Selective Manganese-Catalyzed Dimerization and Cross-Coupling of Terminal Alkynes

Stefan Weber,[†] Luis F. Veiros,[§] and Karl Kirchner*[, †]

[†]Institute of Applied Synthetic Chemistry, Vienna University of Technology, Getreidemarkt 9, A-1060 Vienna, AUSTRIA

[§] Centro de Química Estrutural and Departamento de Engenharia Química, Instituto Superior Técnico, Universidade de Lisboa, Av Rovisco Pais, 1049-001 Lisboa, PORTUGAL

1. General information

All reactions were performed under an inert atmosphere of argon by using Schlenk techniques or in a MBraun inert-gas glovebox. The solvents were purified according to standard procedures. The deuterated solvents were purchased from Aldrich and dried over 3 Å molecular sieves.

Complexes *fac*-[Mn(dippe)$(CO)_3$(Pr)][1] (dippe = 1,2-bis(di-*iso*-propylphosphino)ethane) (**1**), *fac*-[Mn(dippe)$(CO)_3$(Br)][2] (**2**) and *fac*-[Mn(dippe)$(CO)_3$(H)][3] (**3**) were synthesized according to literature. Phenylacetylene-d_1 (>98 % D) and 1-octyne-d_1 (>98 % D) was synthesized from phenylacetylene, 1-octyne, *n*-BuLi and D_2O.

^{1}H- and ^{13}C{^{1}H}- NMR spectra were recorded on a Bruker AVANCE-400 spectrometer. ^{1}H and ^{13}C{^{1}H}-NMR spectra were referenced internally to residual protio-solvent and solvent resonances, respectively, and are reported relative to tetramethylsilane (δ = 0 ppm).

GC–MS analysis was conducted on a ISQ LT Single quadrupole MS (Thermo Fisher) directly interfaced to a TRACE 1300 Gas Chromatographic systems (Thermo Fisher), using a Rxi-5Sil MS (30 m, 0.25mm ID) cross-bonded dimethyl polysiloxane capillary column.

High-resolution accurate mass spectra were recorded on an Agilent 6545 QTOF equipped with an Agilent MMI ion source (Agilent Technologies, Santa Clara, CA, USA) which can be operated in mixed ESI and APCI mode. Measured accurate mass data for confirming calculated elemental compositions were within ±3 ppm accuracy.

2. Synthetic procedures

Optimization reactions for the dimerization of phenylacetylene

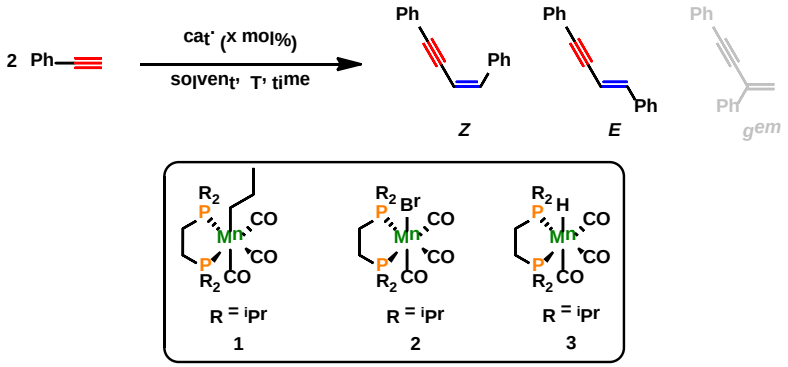

Inside an Ar-flushed glovebox an 8 mL-screw cap vial was charged with complex **1,2** or **3** (0.5 - 2 mol%) and phenylacetylene (1.1 mmol, 1 eq.). A stirring bar was added and 0.5 mL THF were added. The vial was sealed, transferred out of the glovebox, and heated (if required) to the indicated temperature for the indicated time. The color of the mixture changes from colorless to dark brown upon reaction progress. The reaction mixture was allowed to reach room temperature and exposed to air. A sample was taken for GC-MS analysis.

Full Table of optimization reaction

Table S1. Full table of optimization reaction for the dimerization of phenylacetylene catalyzed by complex **1**.

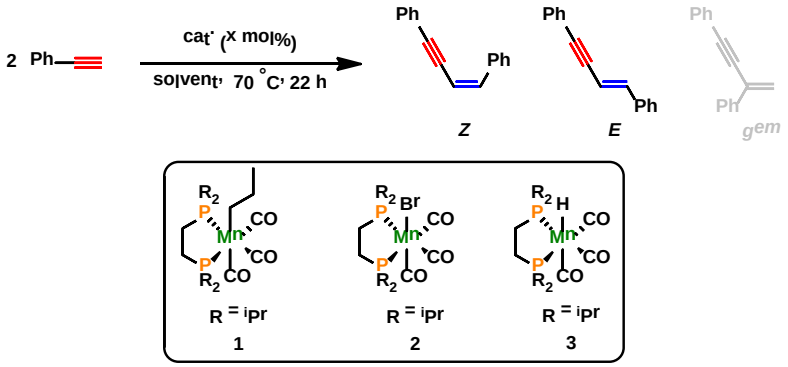

entry	catalyst (mol%)	solvent	conversion [%]	*Z:E ratio*
1	**1** (2)	THF	>99	96:4
2	**2** (2)	THF	-	n.d.
3	**3** (2)	THF	-	n.d.

4	**1** (2)	DME	97	95:5
5	**1** (2)	iPrOH	97	97:3
6	**1** (2)	toluene	17	95: 5
7	**1** (2)	$CHCl_3$	12	97:3
8[a]	**1 (1)**	**THF**	**>99**	**97:3**
9[a]	**1** (1)	neat	95	96:4
10[a]	**1** (0.5)	THF	82	96:4
11[a,b]	**1** (0.5)	THF	traces	n.d.
12[a,b]	(0.5)	neat	38	98:2

Reaction conditions: 1.12 mmol phenylacetylene, 0.5 mL anhydrous solvent, 70 °C, 22 h, conversion and isomer ratio determined by GC-MS. [a] 18 h. [b] 25 °C.

General procedure for the dimerization of aromatic alkynes

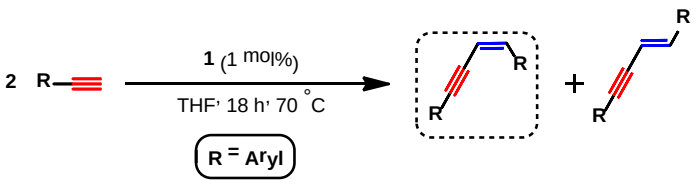

Inside an Ar-flushed glovebox an 8 mL-screw cap vial was charged with **1** (4.5 mg, 1 mol%) and substrate (1.1 mmol, 1 eq.). A stirring bar was added and 0.5 mL THF were added. The vial was sealed, transferred out of the glovebox, and heated to 70 °C for 18 h. The color of the mixture changes from colorless to dark brown upon heating. The reaction mixture was allowed to reach room temperature and exposed to air. A sample was taken for GC-MS analysis. The solvent was removed under reduced pressure. The crude products were isolated by flash chromatograph (2-3 g silica 60 in a Pasteur pipette) using light petroleum/Et_2O as eluent.

General procedure for the dimerization of aliphatic alkynes

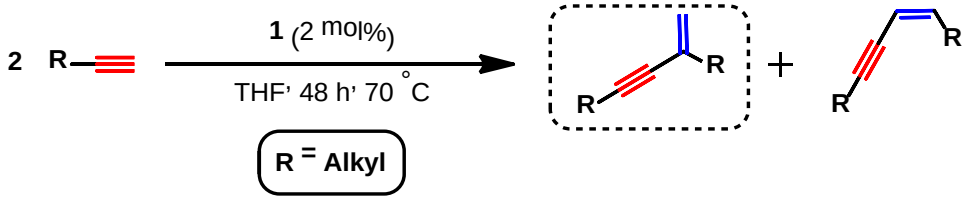

Inside an Ar-flushed glovebox an 8 mL-screw cap vial was charged with **1** (9 mg, 2 mol%) and substrate (1.1 mmol, 1 eq.). A stirring bar was added and 0.5 mL THF were added. The vial was sealed, transferred out of the glovebox, and heated to 70 °C for 48 h. The color of the mixture changes from colorless to orange upon heating. The reaction mixture was allowed to reach room temperature and exposed to air. A sample was taken for GC-MS analysis. The solvent was removed under reduced pressure. The crude products were isolated by flash chromatograph (2-3 g silica 60 in a Pasteur pipette) using light petroleum/Et_2O as eluent.

General procedure for cross coupling of alkynes

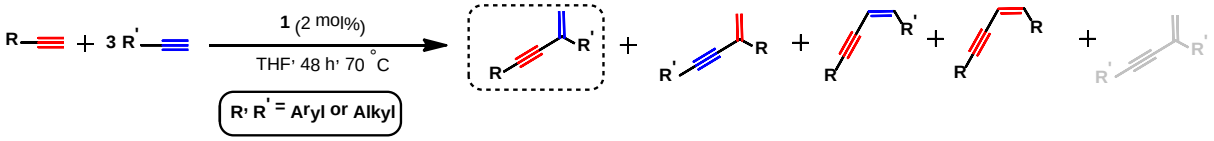

Inside an Ar-flushed glovebox an 8 mL-screw cap vial was charged with **1** (9 mg, 2 mol%), alkyne (1.1 mmol, 1 eq.) and the coupling partner alkyne (3.3 mmol, 3 eq.). A stirring bar was added and 0.5 mL THF were added. The vial was sealed, transferred out of the glovebox, and heated to 70 °C for 48 h. The color of the mixture changes from colorless to red upon heating. The reaction mixture was allowed to reach room temperature and exposed to air. A sample was taken for GC-MS analysis. The solvent was removed under reduced pressure. The crude products were isolated by flash chromatograph.

Additional table of cross coupling of alkynes

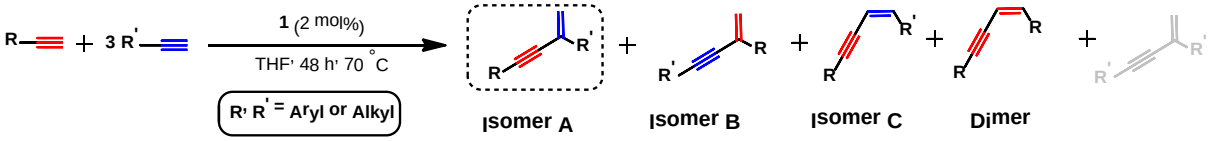

Table S2. Isomer ratio for the cross coupling of alkynes

Alkyne 1 (1 eq.)	Alkyne 2 (3 eq.)	Conversion Alkyne 1 [%]	A [%]	B [%]	C [%]	Dimer [%]
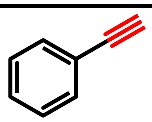	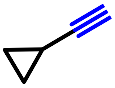	>99	52	21	9	18
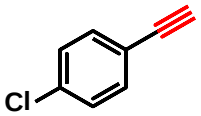	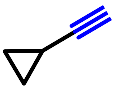	>99	38	18	3	32
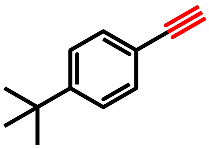	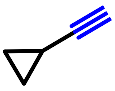	>99	58	18	9	58
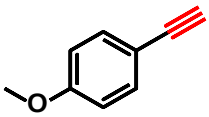	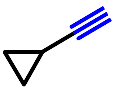	>99	60	22	10	7
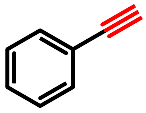	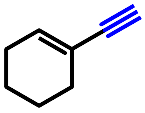	>99	48	32	n.d.	21
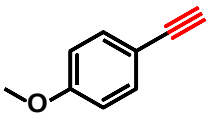	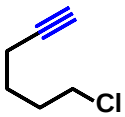	98	72	15	n.d.	10
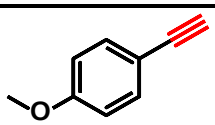	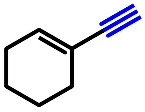	96	84	n.d.	n.d.	12
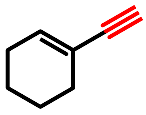	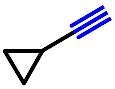	80	47	15	6	5

Detection of 1-butanal

Inside an Ar-flushed glovebox an NMR tube was charged with **1** (4.5 mg, 1 mol%) and phenylacetylene (1.1 mmol, 1 eq.). 0.5 mL THF-*d8* were added. The NMR tube was sealed, transferred out of the glovebox and heated to 70 °C for 2 h. ^{1}H-NMR was recorded.

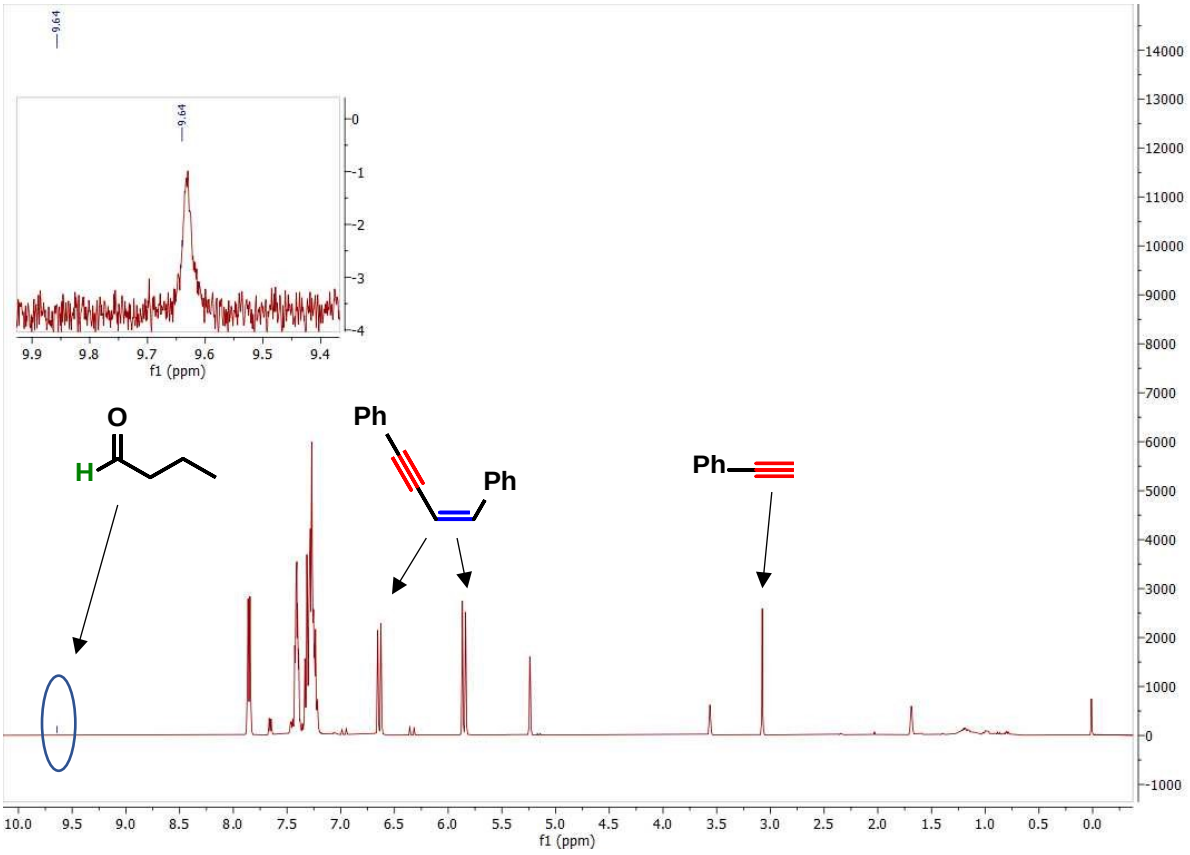

3. Computational Details

The computational results presented have been achieved in part using the Vienna Scientific Cluster (VSC). All calculations were performed using the GAUSSIAN 09 software package.[11] Geometry optimizations were obtained using the PBE0 functional without symmetry constraints and a basis set (b1) consisting of the Stuttgart/Dresden ECP (SDD) basis set[12] to describe the electrons of Mn, and a standard 6-31G(d,p) basis set[13] for all other atoms. The PBE0 functional uses a hybrid generalized gradient approximation (GGA), including 25 % mixture of Hartree-Fock[14] exchange with DFT[15] exchange-correlation, given by Perdew, Burke and Ernzerhof functional (PBE).[16] Transition state optimizations were performed with the Synchronous Transit-Guided Quasi-Newton Method (STQN) developed by Schlegel *et al*,[17] following extensive searches of the Potential Energy Surface. Frequency calculations were performed to confirm the nature of the stationary points, yielding one imaginary frequency for the transition states and none for the minima. Each transition state was further confirmed by following its vibrational mode downhill on both sides and obtaining the minima presented on the energy profiles. The electronic energies (E_{b1}) were converted to free energy at 298.15 K and 1 atm (G_{b1}) by using zero point energy and thermal energy corrections based on structural and vibration frequency data calculated at the same level.

Single point energy calculations were performed on the geometries obtained at the PBE0/b1 level using the M06 functional, and an improved basis set (b2) corresponding to same basis set for the Mn-atom and a 6-311++G(d,p) basis set[18] for the rest of the elements (b2). The M06 functional is a hybrid meta-GGA functional developed by Truhlar and Zhao,[19] and it was shown to perform very well for the kinetics of transition metal molecules, providing a good description of weak and long range interactions.[20] Solvent effects (THF) were considered in the M06/b2//PBE0/b1 calculations using the Polarizable Continuum Model (PCM) initially devised by Tomasi and coworkers[21] with radii and non-electrostatic terms of the SMD solvation model, developed by Truhlar *et al*.[22] The free energy values presented (G_{b2}^{soln}) were derived from the electronic energy values obtained at the M06/b2//PBE0/b1 level, including solvent effects (E_{b2}^{soln}), according to the following expression:

$$G_{b2}^{soln} = E_{b2}^{soln} + G_{b1} - E_{b1}$$

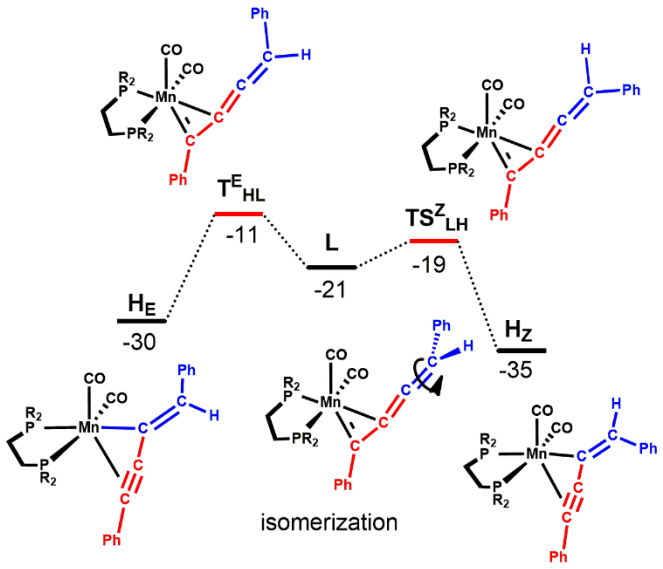

Figure S1. Free Energy Profile Calculated for the Isomerization of $\mathbf{H_E}$ and $\mathbf{H_Z}$ of Terminal Alkynes. Free Energies (kcal/mol) are Referred to [Mn(dippe)(CO)$_2$(C≡CPh)(η^2-HC≡CPh)] (**F** in the calculations)

4. Characterization of organic products

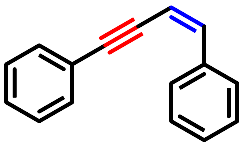

(Z)-but-1-en-3-yne-1,4-diyldibenzene[4] (**4**), yellow oil, 106 mg (92%). ^{1}H NMR (δ, 400 MHz, CD_2Cl_2, 20 ºC): 7.87 – 7.81 (m, 2H), 7.46 – 7.36 (m, 2H), 7.35 – 7.19 (m, 6H), 6.63 (d, J = 11.9 Hz, 1H), 5.84 (d, J = 11.9 Hz, 1H) ppm. ^{13}C{^{1}H} NMR (δ, 101 MHz, CD_2Cl_2, 20 ºC): 138.7, 136.6, 131.4, 128.7, 128.6, 128.5, 128.3, 123.4, 107.2, 95.8, 88.1 ppm.

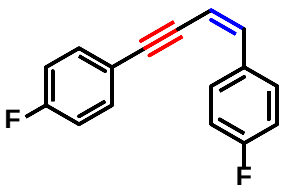

(Z)-4,4'-(but-1-en-3-yne-1,4-diyl)bis(fluorobenzene)[4] (**5**), yellow oil, 114 mg (92%). ^{1}H NMR (δ, 400 MHz, CD_2Cl_2, 20 ºC): 8.04 – 7.81 (m, 2H), 7.59 – 7.42 (m, 2H), 7.15 – 7.03 (m, 4H), 6.69 (d, J = 12.0 Hz, 1H), 5.90 (d, J = 11.9 Hz, 1H) ppm. ^{13}C{^{1}H} NMR (δ, 101 MHz, CD_2Cl_2, 20 ºC): 162.7 (d, J_{C-F} = 250 Hz), 162.5 (d, J_{C-F} = 249 Hz), 137.4, 133.4, 133.3, 132.9, 132.9, 130.6, 130.5, 115.9, 115.6, 115.3, 115.3, 106.8, 106.7, 94.6, 87.6 ppm.

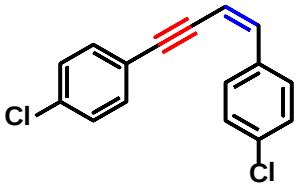

(Z)-4,4'-(but-1-en-3-yne-1,4-diyl)bis(chlorobenzene)[5] (**6**), purified by column chromatography (15g SiO_2, PE/Et_2O 1:1) slightly yellow solid, 99 mg (92%). ^{1}H NMR (δ, 400 MHz, CD_2Cl_2, 20 °C): 7.90 – 7.82 (m, 2H), 7.49 – 7.31 (m, 6H), 6.70 (d, *J* = 11.9 Hz, 1H), 5.95 (d, *J* = 12.0 Hz, 1H) ppm. ^{13}C{^{1}H} NMR (δ, 101 MHz, CD_2Cl_2, 20 °C): 139.2, 136.6, 136.1, 135.6, 134.3, 131.6, 130.4, 130.1, 123.3, 109.2, 96.7, 90.3 ppm.

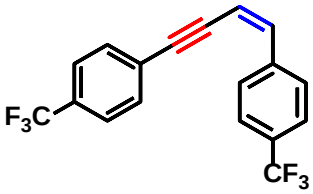

(Z)-4,4'-(but-1-en-3-yne-1,4-diyl)bis(trifluoromethylbenzene)[5] (**7**), brownish oil, 166 mg (96%). ^{1}H NMR (δ, 400 MHz, CD_2Cl_2, 20 °C): 8.03 (dt, J = 8.8, 0.8 Hz, 2H), 7.70 – 7.60 (m, 6H), 6.84 (d, J = 11.9 Hz, 1H), 6.09 (d, J = 11.9 Hz, 1H) ppm. ^{13}C{^{1}H} NMR (δ, 101 MHz, CD_2Cl_2, 20 °C): 141.3, 139.7, 133.4, 131.9, 131.7, 131.5, 131.4, 130.5, 128.4, 127.1 - 126.8 (m, -CF_3), 124.4, 124.2, 111.0, 96.6, 91.2 ppm.

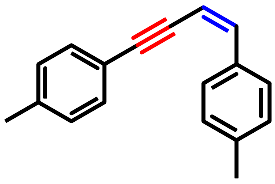

(Z)-4,4'-(but-1-en-3-yne-1,4-diyl)bis(methylbenzene)[4] (**8**), yellow oil, which slowly crystallized upon standing, 81 mg (69%). ^{1}H NMR (δ, 400 MHz, CD_2Cl_2, 20 °C): 7.88 – 7.81 (m, 2H), 7.44 – 7.36 (m, 2H), 7.28 – 7.15 (m, 5H), 6.67 (d, J = 11.9 Hz, 1H), 5.87 (d, J = 11.9 Hz, 1H), 2.38 (s, 6H) ppm. ^{13}C{^{1}H} NMR (δ, 101 MHz, CD_2Cl_2, 20 °C): 140.6, 140.6, 140.1, 135.8, 133.1, 131.0, 130.8, 130.5, 122.2, 108.1, 97.6, 89.6, 23.1, 22.9 ppm.

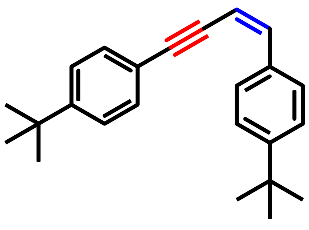

(Z)-4,4'-(but-1-en-3-yne-1,4-diyl)bis(tert-butylbenzene)[4] (**9**), purified by column chromatography (15g SiO_2, PE/Et_2O 3:1) yellow solid, 125 mg (78%). ^{1}H NMR (δ, 400 MHz, CD_2Cl_2, 20 °C): 7.95 – 7.88 (m, 2H), 7.52 – 7.39 (m, 7H), 6.70 (d, J = 11.9 Hz, 1H), 5.90 (d, J = 11.9 Hz, 1H), 1.37 (s, 9 H), 1.36 (s, 9H) ppm. ^{13}C{^{1}H} NMR (δ, 101 MHz, CD_2Cl_2,

20 °C): 153.6, 139.9, 135.6, 132.8, 130.2, 127.4, 127.2, 127.0, 122.2, 108.2, 97.6, 89.6, 36.4, 36.4, 32.7, 32.6 ppm.

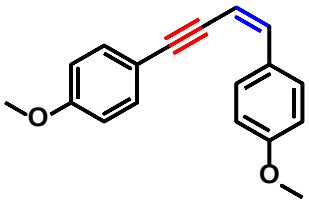

(Z)-4,4'-(but-1-en-3-yne-1,4-diyl)bis(methoxybenzene)[4] (**10**), purified by column chromatography (15g SiO_2, PE/Et_2O 1:1) yellow solid, 84 mg (63%). ^{1}H NMR (δ, 400 MHz, CD_2Cl_2, 20 °C): 7.95 – 7.88 (m, 2H), 7.50 – 7.42 (m, 2H), 6.97 – 6.87 (m, 4H), 6.63 (d, J = 11.9 Hz, 1H), 5.81 (d, J = 11.8 Hz, 1H), 3.84 (s, 3H), 3.83 (s, 3H) ppm. ^{13}C{^{1}H} NMR (δ, 101 MHz, CD_2Cl_2, 20 °C): 161.5, 161.5, 139.0, 134.5, 131.8, 131.4, 130.0, 127.5, 117.3, 115.8, 115.3, 106.6, 97.1, 59.03, 57.0, 56.9 ppm.

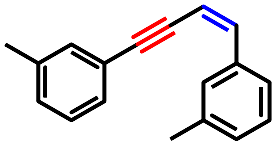

(Z)-3,3'-(but-1-en-3-yne-1,4-diyl)bis(methylbenzene)[5] (**13**), yellow oil, 93 mg (79%). ^{1}H NMR (δ, 400 MHz, CD_2Cl_2, 20 °C): 7.83 (td, J = 1.8, 0.9 Hz, 1H), 7.72 (dt, J = 7.7, 1.5 Hz, 1H), 7.36 – 7.23 (m, 4H), 7.20 - 7.12 (m, 2H), 6.69 (d, J = 12.0 Hz, 1H), 5.91 (d, J = 11.9 Hz, 1H), 2.40 (s, 3H), 2.36 (s, 3H) ppm. ^{13}C{^{1}H} NMR (δ, 101 MHz, CD_2Cl_2, 20 °C): 140.5, 140.1, 139.7, 138.3, 133.7, 131.1, 131.1, 130.2, 130.1, 130.0, 127.7, 125.0, 108.8, 97.7, 89.8, 23.0, 22.7 ppm.

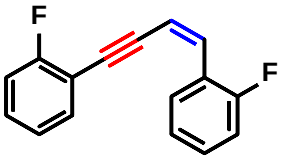

(Z)-2,2'-(but-1-en-3-yne-1,4-diyl)bis(fluorobenzene)[5] (**14**), slightly yellow oil, 118 mg (97%). ^{1}H NMR (δ, 400 MHz, CD_2Cl_2, 20 °C): 8.62 (td, J = 7.8, 1.8 Hz, 1H), 7.48 (td, J = 7.4, 1.9 Hz, 1H), 7.42 – 7.28 (m, 2H), 7.27 – 7.06 (m, 4H), 7.02 (d, J = 12.1 Hz, 1H), 6.07 (d, J = 12.1 Hz, 1H) ppm. ^{13}C{^{1}H} NMR (δ, 101 MHz, CD_2Cl_2, 20 °C): 165.7, 163.2, 163.2, 160.7, 135.0, 132.2, 132.2, 132.1, 132.0, 130.4, 130.2, 125.9, 125.9, 125.8, 125.6, 125.5, 117.3, 117.1, 117.0, 116.7, 113.4, 113.3, 110.2, 94.2, 91.5 ppm.

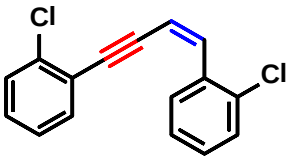

(Z)-2,2'-(but-1-en-3-yne-1,4-diyl)bis(chlorobenzene)[5] (**15**), brownish solid, 131 mg (95%). ^{1}H NMR (δ, 400 MHz, CD_2Cl_2, 20 °C): 8.62 – 8.54 (m, 1H), 7.53 – 7.47

(m, 1H), 7.45 – 7.40 (m, 2H), 7.37 – 7.22 (m, 4H), 7.16 (d, J = 12.0 Hz, 1H), 6.13 (d, J = 12.1 Hz, 1H) ppm. $^{13}C\{^{1}H\}$ NMR (δ, 101 MHz, CD_2Cl_2, 20 °C): 137.5, 137.2, 135.8, 135.4, 135.4, 131.6, 131.3, 131.2, 128.5, 128.4, 124.8, 111.0, 94.7, 93.9 ppm.

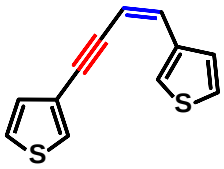

(Z)-3,3'-(but-1-en-3-yne-1,4-diyl)dithiophene (**16**)[4], brownish oil, 89 mg (81%). ^{1}H NMR (δ, 400 MHz, $CDCl_3$, 20 °C): 7.81 (d, J = 3.1, 1H), 7.69 (d, J = 5.1, 1H), 7.50 (d, J = 3.0), 7.31 (s, 2H), 7.19 (d, J = 5.0, 1H), 6.73 (d, J = 11.7 Hz, 1H), 5.79 (d, J = 11.6 Hz, 1H) ppm. $^{13}C\{^{1}H\}$ NMR (δ, 101 MHz, $CDCl_3$, 20 °C): 138.8, 132.7, 129.6, 128.5, 127.8, 125.6, 125.5, 125.2, 122.5, 106.0, 91.1, 88.1 ppm.

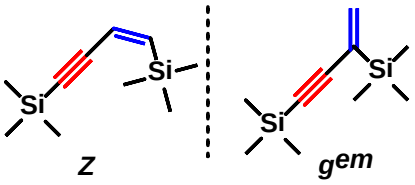

(Z)-but-1-en-3-yne-1,4-diylbis(trimethylsilane) (*Z*-siomer) and but-3-en-1-yne-1,3-diylbis(trimethylsilane) (*gem*-isomer)[4] (**18**), colorless oil, 48 mg (48%) combined yield of *Z*-isomer and *gem*-isomer. ^{1}H NMR (δ, 400 MHz, $CDCl_3$, 20 °C): 6.26 (d, J = 15.1 Hz, 1H)(*Z*-isomer), 6.16 (d, J = 15.1 Hz, 1H)(*Z*-isomer), 6.12 (d, J = 3.4 Hz, 1H) (*gem*-isomer), 5.70 (d, J = 3.4 Hz, 1H) (*gem*-isomer), 0.19 (s, 9H) (*Z*-isomer), 0.19 (s, 9H) (*Z*-isomer), 0.19 (s, 6H) (*gem*-isomer), 0.16 (s, 6H) (*gem*-isomer) ppm. $^{13}C\{^{1}H\}$ NMR (δ, 101 MHz, $CDCl_3$, 20 °C): 146.5, 135.2, 135.0, 124. 9, 106.9, 105.4, 98.9, 98.9, 0.4, 0.0, -0.4, -1.95 ppm.

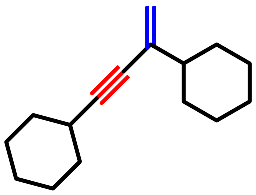

But-3-en-1-yne-1,3-diyldicyclohexane[6] (**19**), yellow oil, 103 mg (87%).^{1}H NMR (δ, 400 MHz, $CDCl_3$, 20 °C): 5.17 (d, J = 2.2 Hz, 1H), 5.13 – 5.09 (m, 1H), 1.92 – 1.59 (m, 16H), 1.56 – 1.39 (m, 6H), 1.39 – 1.02 (m, 16H) ppm. $^{13}C\{^{1}H\}$ NMR (δ, 101 MHz, $CDCl_3$, 20 °C): 138.0, 117.2, 94.8, 80.2, 45.3, 32.8, 32.34, 32.0, 31.8, 29.6, 26.3, 26.1, 26.0, 24.8, 20.2, 20.0 ppm.

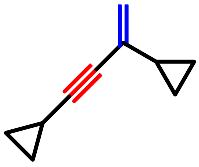

But-3-en-1-yne-1,3-diyldicyclopropane[7] (**20**), colorless liquid, 53 mg (74%). ^{1}H NMR (δ, 400 MHz, $CDCl_3$, 20 °C): 5.24 (d, J = 2.0 Hz, 1H), 5.18 (d, J = 2.0 Hz, 1H), 1.56 – 1.45 (m, 1H), 1.35 – 1.20 (m, 2H), 1.15-0.98 (m, 1H), 0.84 – 0.75 (m, 1H), 0.72 – 0.61 (m, 4H) ppm. ^{13}C{^{1}H} NMR (δ, 101 MHz, $CDCl_3$, 20 °C): 134.2, 117.5, 93.7, 72.8, 16.6, 8.7, 5.7, 0.0.

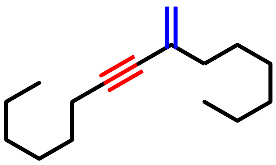

9-methylenepentadec-7-yne[6] (**21**), colorless liquid, 99 mg (89 %). ^{1}H NMR (δ, 400 MHz, $CDCl_3$, 20 °C): 5.13 (d, *J* = 2.5 Hz, 1H), 5.05 (q, *J* = 1.5 Hz, 1H), 2.23 (t, *J* = 7.0 Hz, 2H), 2.04 (t, *J* = 7.6 Hz, 2H), 1.51 – 1.39 (m, 4H), 1.39 – 1.29 (m, 3H), 1.29 – 1.15 (m, 12H), 0.91 - 0.77 (m, 6H). ^{13}C{^{1}H} NMR (δ, 101 MHz, $CDCl_3$, 20 °C): 142.6, 119.3, 91.0, 81.0, 37.6, 31.7, 31.4, 28.8, 28.6, 28.6, 28.1, 22.6, 22.6, 19.3, 14.1, 14.0.

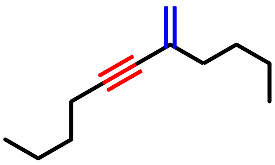

7-methyleneundec-5-yne[7] (**22**), slightly yellow liquid, 70 mg (85%). ^{1}H NMR (δ, 400 MHz, $CDCl_3$, 20 °C): 5.20 (dt, J = 2.2, 0.7 Hz, 1H), 5.12 (dt, J = 2.5, 1.3 Hz, 1H), 2.31 (t, J = 7.0 Hz, 2H), 2.16 – 2.07 (m, 2H), 1.56 – 1.39 (m, 7H), 1.32 (dt, J = 8.4, 7.0 Hz, 2H), 0.91 (td, J = 7.3, 5.2 Hz, 6H).^{13}C{^{1}H} NMR (δ, 101 MHz, $CDCl_3$, 20 °C): 142.6, 119.3, 90.0, 81.3, 37.3, 30.9, 30.3, 22.0, 22.0, 19.0, 13.9, 13.6.

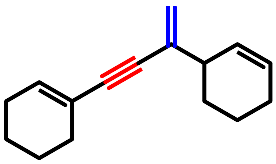

1-(3-(cyclohex-2-en-1-yl)but-3-en-1-yn-1-yl)cyclohex-1-ene[7] (**23**), yellowish oil, which slowly crystallizes upon standing, 98 mg (92%). ^{1}H NMR (δ, 400 MHz, $CDCl_3$, 20 °C): 6.10 (d, J = 11.9 Hz, 1H,), 6.07 – 6.04 (m, 1H), 5.95 (t, J = 3.4 Hz, 1H), 5.41 (d, J = 11.8 Hz, 1H), 2.61 (td, J = 6.2, 5.1, 3.2 Hz, 2H), 2.20 – 2.08 (m, 6H), 1.71 – 1.54 (m, 6H).^{13}C{^{1}H} NMR (δ, 101 MHz, $CDCl_3$, 20 °C): 141.5, 137.3, 134.1, 132.6, 121.3, 104.0, 96.2, 86.7, 28.9, 27.1, 26.1, 25.8, 22.7, 22.3, 22.0, 21.6.

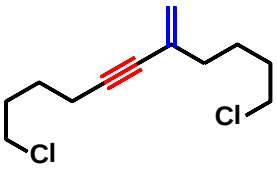

1,11-dichloro-7-methyleneundec-5-yne[8] (**24**), colorless oil, 111 mg (94%). %). ^{1}H NMR (δ, 400 MHz, $CDCl_3$, 20 °C): 5.25 – 5.21 (m, 1H), 5.16 (q, J = 1.5 Hz, 1H), 3.60 – 3.56 (m, 2H), 3.56 – 3.52 (m, 2H), 2.36 (t, J = 6.9 Hz, 2H), 2.16 (t, J = 7.3 Hz, 2H), 1.96 – 1.86 (m, 2H), 1.83 – 1.76 (m, 2H), 1.74 – 1.64 (m, 4H). ^{13}C{^{1}H} NMR (δ, 101 MHz, $CDCl_3$, 20 °C): 141.7, 120.4, 89.4, 81.3, 44.9, 44.6, 36.6, 31.7, 31.6, 25.9, 25.3, 18.6.

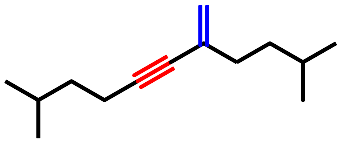

2,10-dimethyl-7-methyleneundec-5-yne (**25**), colorless oil, 91 mg (93 %). ^{1}H NMR (δ, 400 MHz, $CDCl_3$, 20 °C): 5.19 (dt, J = 2.1, 0.7 Hz, 1H), 5.14 – 5.11 (m, 1H), 2.31 (t, J = 7.4 Hz, 2H), 2.15 – 2.09 (m, 2H), 1.70 (dq, J = 13.4, 6.7 Hz, 1H), 1.57 (dp, J = 13.3, 6.6 Hz, 1H), 1.47 – 1.36 (m, 4H), 0.90 (dd, J = 6.6, 5.0 Hz, 12H). ^{13}C{^{1}H} NMR (δ, 101 MHz, $CDCl_3$, 20 °C): 142.8, 119.1, 90.1, 81.0, 37.7, 37.6, 35.5, 27.4, 27.2, 22.5, 22.2, 17.3. HRMS (APCI) *m/z* calculated for $C_{14}H_{24}$ $[M-H]^+$: 193.1878, found 193.1847.

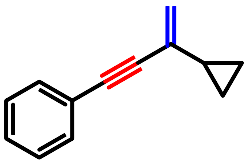

(3-cyclopropylbut-3-en-1-yn-1-yl)benzene[9] (**26**), purified by column chromatography (10 g SiO_2, PE), colorless oil, 65 mg (39%). ^{1}H NMR (δ, 400 MHz, $CDCl_3$, 20 °C): 7.46 – 7.39 (m, 2H), 7.34 – 7.28 (m, 3H), 5.42 (d, J = 1.7 Hz, 1H), 5.39 (d, J = 1.7 Hz, 1H), 1.64 (tt, J = 8.1, 5.0 Hz, 1H), 0.83 – 0.76 (m, 2H), 0.74 (ddt, J = 10.8, 5.2, 2.8 Hz, 2H).). ^{13}C{^{1}H} NMR (δ, 101 MHz, $CDCl_3$, 20 °C): 133.9, 131.3, 128.3, 128.2, 123.1, 118.9, 89.5, 86.6, 16.5, 5.9.

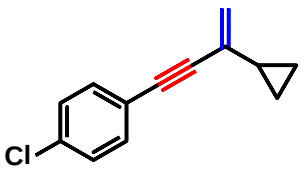

1-chloro-4-(3-cyclopropylbut-3-en-1-yn-1-yl)benzene (**27**), purified by column chromatography (10 g SiO_2, PE), colorless solid, 71 mg (35%). ^{1}H NMR (δ, 400 MHz, $CDCl_3$, 20 °C): 7.29 – 7.24 (m, 2H), 7.23 – 7.17 (m, 2H), 5.36 (d, J = 1.7 Hz, 1H), 5.31 (d, J = 1.7 Hz, 1H), 1.59 – 1.50 (m, 1H), 0.67 (tt, J = 8.1, 2.4 Hz, 4H). ^{13}C{^{1}H} NMR (δ, 101 MHz, $CDCl_3$, 20 °C): 134.3, 133.6, 132.8, 128.6, 121.6, 119.4, 88.7, 88.0, 16.7, 5.95. HRMS (APCI) *m/z* calculated for $C_{13}H_{11}Cl$ $[M-H]^+$: 203.0549, found 203.0618.

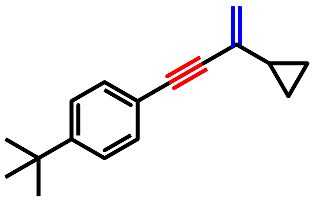

1-(tert-butyl)-4-(3-cyclopropylbut-3-en-1-yn-1-yl)benzene (**28**), purified by column chromatography (10 g SiO_2, PE), colorless oil, 119 mg (53%). ^{1}H NMR (δ, 400 MHz, $CDCl_3$, 20 °C): 7.37 – 7.34 (m, 2H), 7.32 (d, J = 8.8 Hz, 2H), 5.40 (d, J = 1.8 Hz, 1H), 5.36 (d, J = 1.8 Hz, 1H), 1.63 (tt, J = 8.4, 4.9 Hz, 1H), 1.31 (s, 9H), 0.82 – 0.76 (m, 2H), 0.76 – 0.68 (m, 2H). ^{13}C{^{1}H} NMR (δ, 101 MHz, $CDCl_3$, 20 °C): 151.5, 134.0, 131.4, 125.3, 120.1, 118.5, 89.6, 85.8, 30.8, 34.8, 16.5, 5.9. HRMS (APCI) *m/z* calculated for $C_{17}H_{20}$ [M-H]$^+$: 225.1565, found 225.1631.

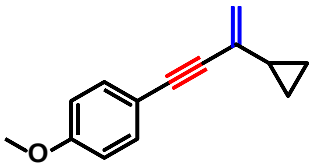

1-(3-cyclopropylbut-3-en-1-yn-1-yl)-4-methoxybenzene[10] (**29**), purified by column chromatography (10 g SiO_2, PE/EE 20:1), orange oil, 107 mg (54%). ^{1}H NMR (δ, 400 MHz, $CDCl_3$, 20 °C): 7.38 – 7.33 (m, 2H), 6.87 – 6.81 (m, 2H), 5.38 (d, J = 2.4 Hz, 1H), 5.35 (d, J = 1.8 Hz, 1H), 3.81 (s, 3H), 1.67 – 1.56 (m, 1H), 0.81 – 0.77 (m, 2H), 0.75 – 0.68 (m, 2H). ^{13}C{^{1}H} NMR (δ, 101 MHz, $CDCl_3$, 20 °C): 159.6, 134.1, 133.1, 118.2, 115.2, 113.9, 89.5, 85.2, 55.3, 16.5, 5.9.

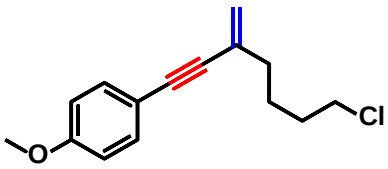

1-(7-chloro-3-methylenehept-1-yn-1-yl)-4-methoxybenzene (**30**), purified by column chromatography (10 g SiO_2, PE), orange oil, 161 mg (65%). ^{1}H NMR (δ, 400 MHz, $CDCl_3$, 20 °C): 7.38 (dd, J = 9.1, 2.5 Hz, 2H), 6.88 – 6.82 (m, 2H), 5.39 (d, J = 2.0 Hz, 1H), 5.27 (q, J = 1.4 Hz, 1H), 3.81 (s, 3H), 3.58 (t, J = 6.5 Hz, 2H), 2.31 – 2.24 (m, 2H), 1.88 – 1.81 (m, 2H), 1.79 – 1.72 (m, 2H). ^{13}C{^{1}H} NMR (δ, 101 MHz, $CDCl_3$, 20 °C): 159.6, 142.2, 133.1, 131.2, 120.9, 115.3, 110.1, 89.5, 88.2, 55.3, 44.9, 36.5, 31.8, 25.4. HRMS (APCI) *m/z* calculated for $C_{15}H_{17}ClO$ [M-H]$^+$: 249.0968, found 249.1043.

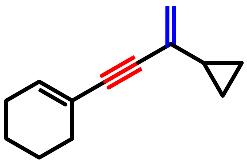

1-(3-cyclopropylbut-3-en-1-yn-1-yl)cyclohex-1-ene (**31**), purified by column chromatography (10 g SiO_2, PE), slightly yellow oil, 71 mg (41%). ^{1}H NMR (δ, 400

MHz, $CDCl_3$, 20 °C): 6.08 (tt, J = 3.6, 1.6 Hz, 1H), 5.30 (d, J = 1.8 Hz, 1H), 5.23 (d, J = 1.9 Hz, 1H), 2.15 – 2.04 (m, 4H), 1.66 – 1.50 (m, 5H), 0.73 – 0.61 (m, 4H). $^{13}C\{^1H\}$ NMR (δ, 101 MHz, $CDCl_3$, 20 °C): 135.1, 134.1, 117.8, 91.5, 83.8, 29.2, 25.7, 22.3, 21.5, 16.5, 5.8. HRMS (APCI) *m/z* calculated for $C_{13}H_{16}$ $[M-H]^+$: 173.1252, found 173.1325.

5. NMR Spectra

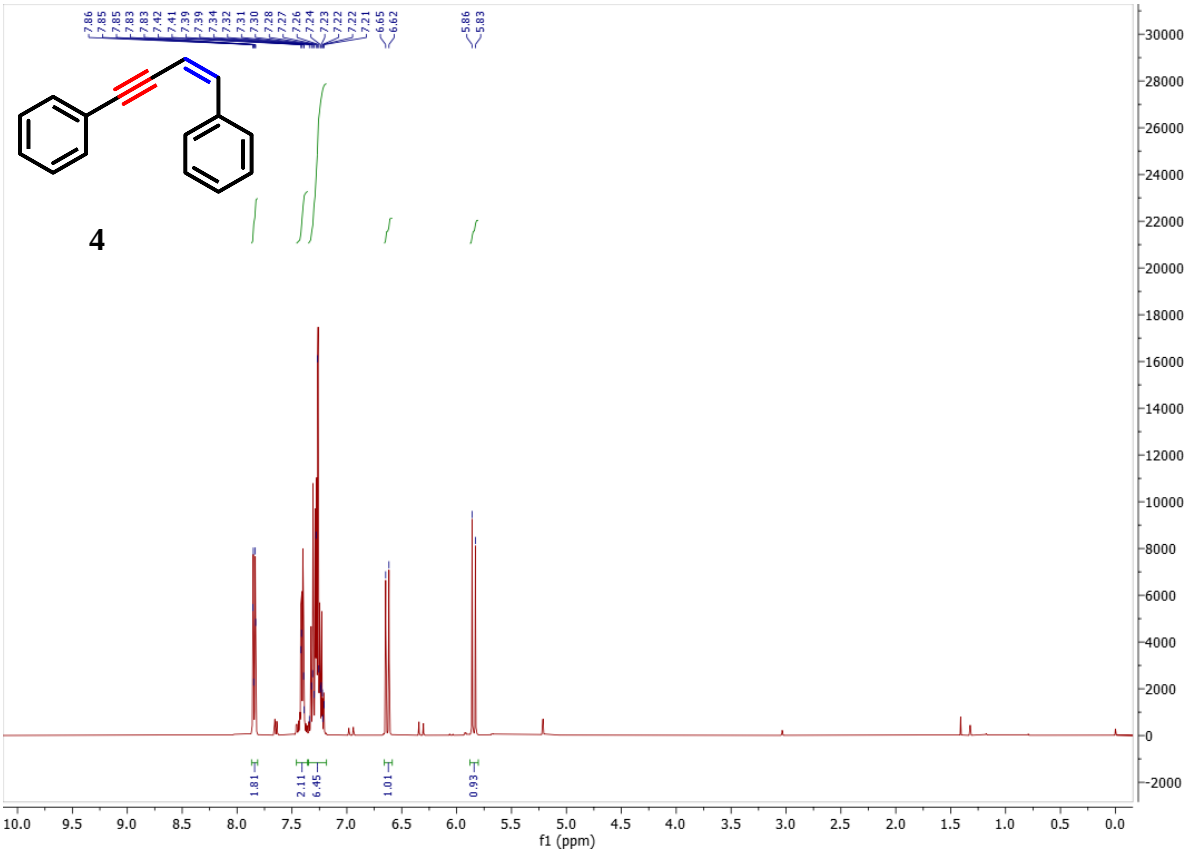

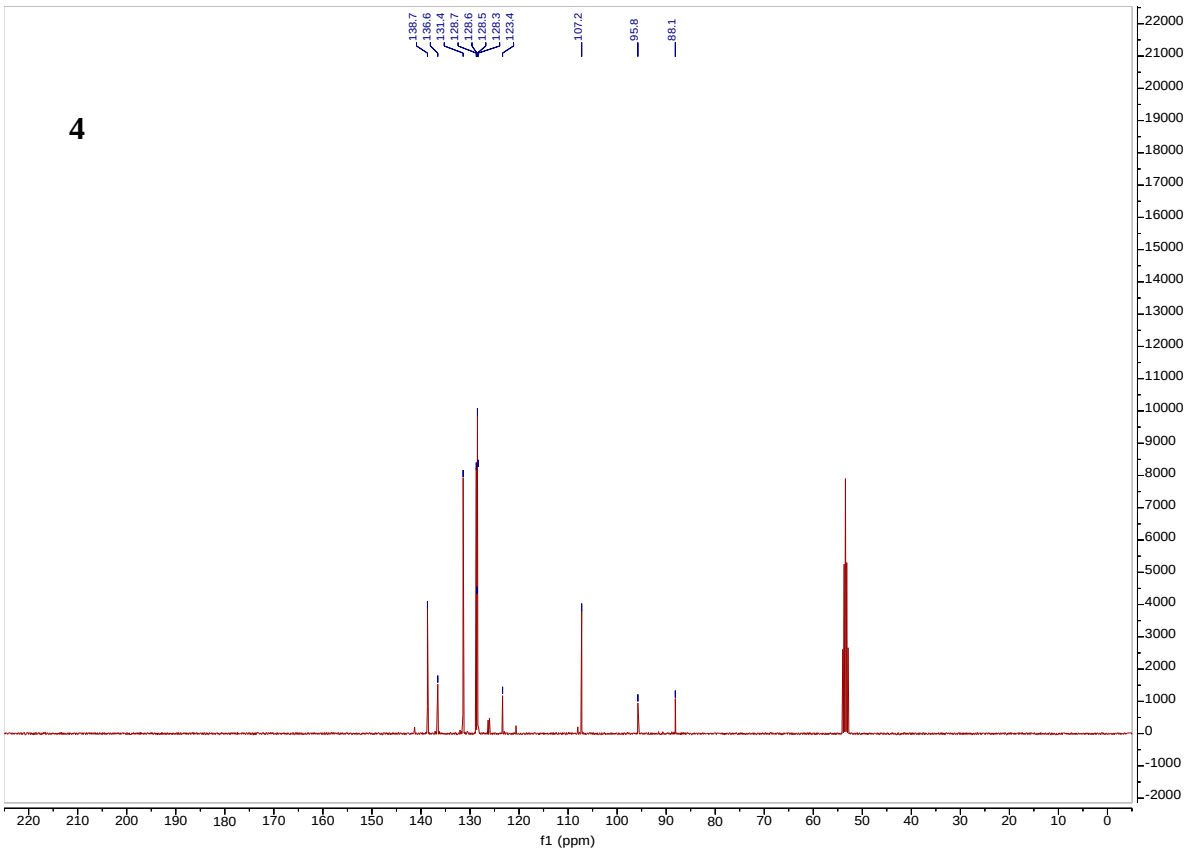

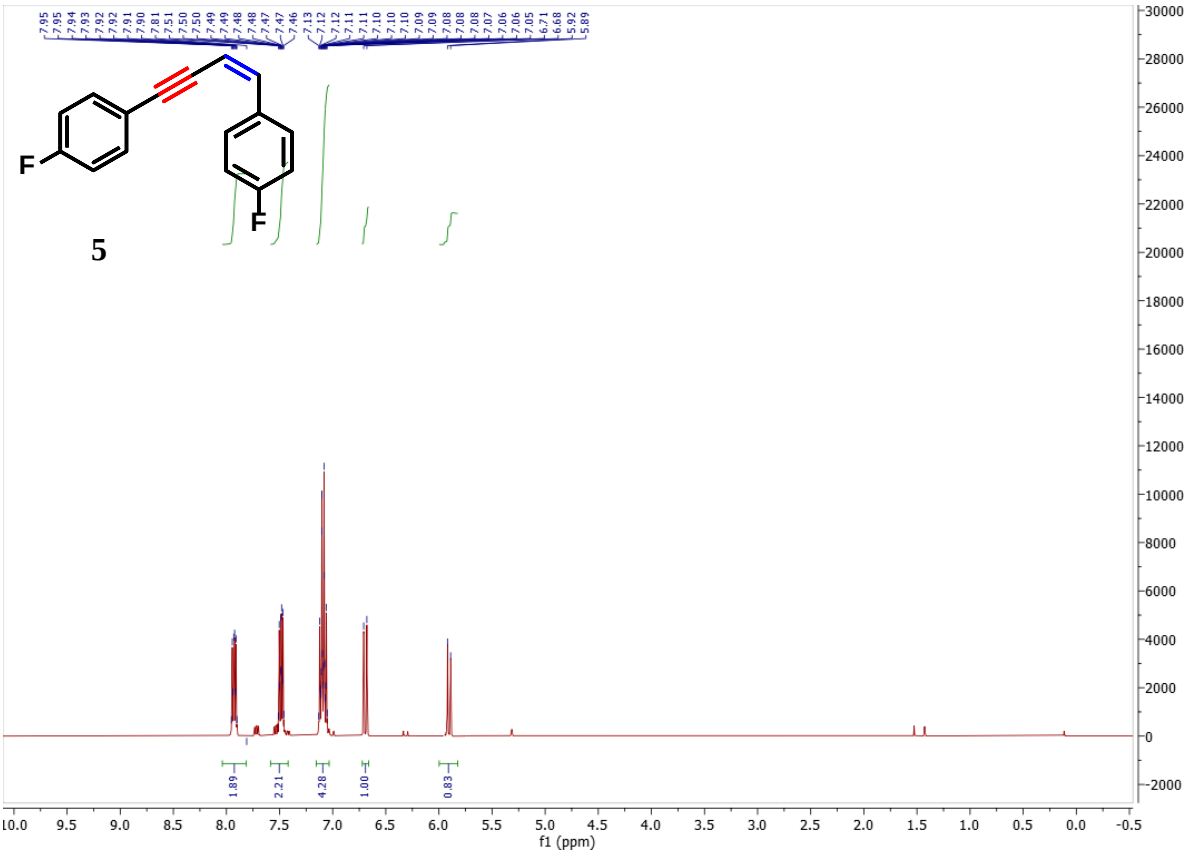
F
F
5
1.89
2.21
4.28
1.00
0.83
f1 (ppm)

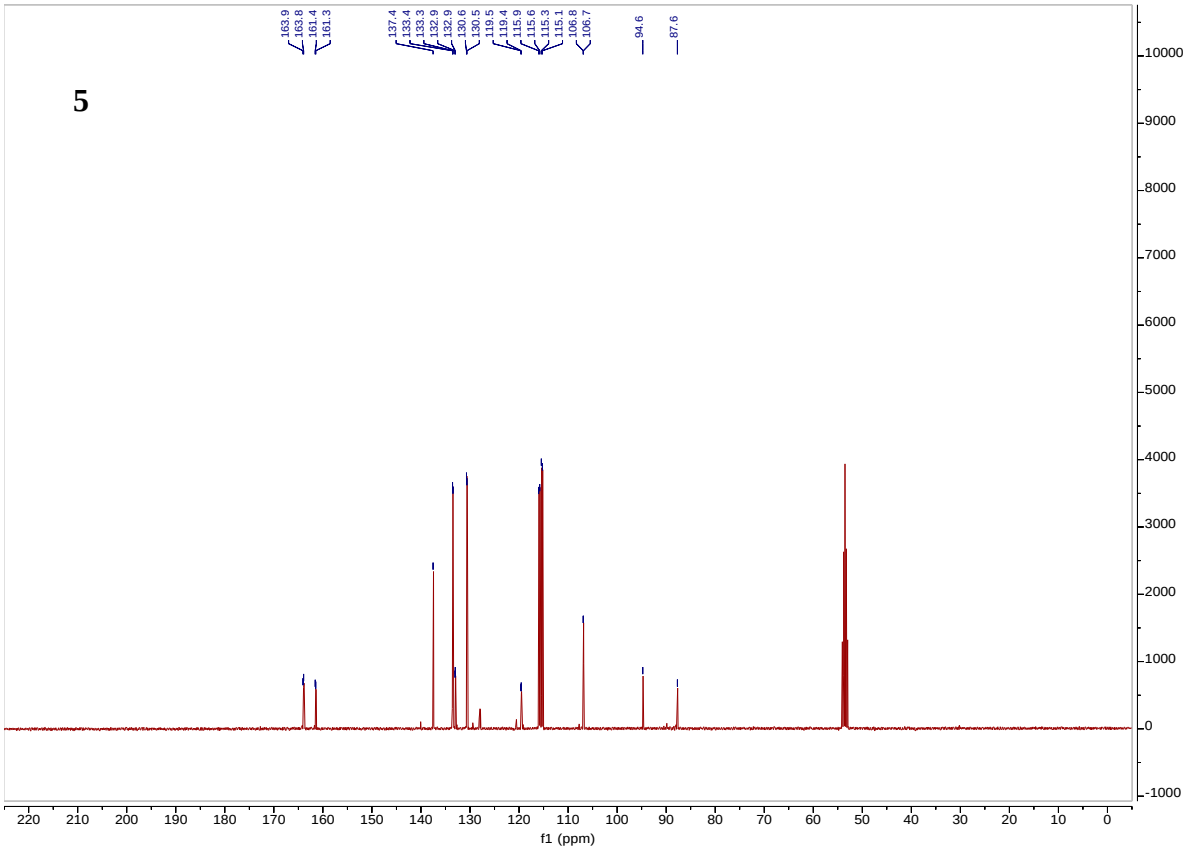
5
f1 (ppm)

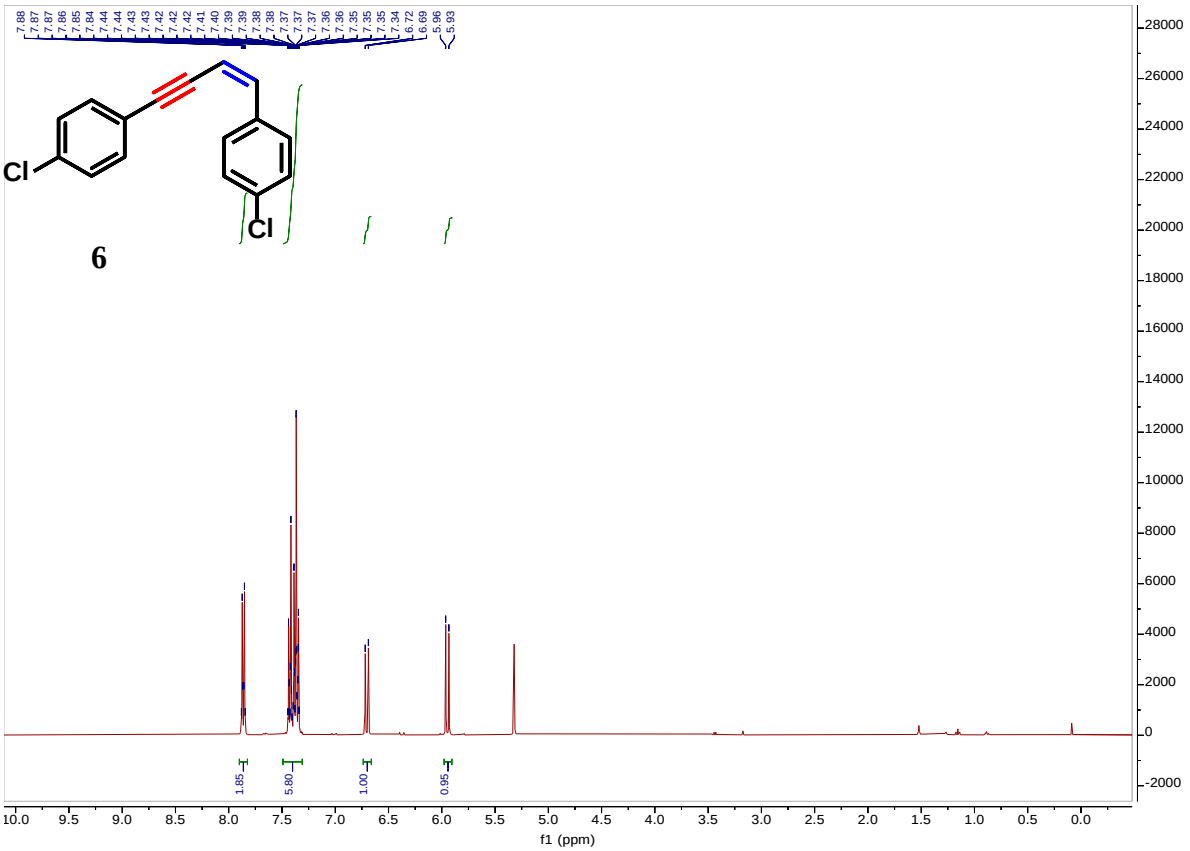
7.88
7.87
7.87
7.86
7.85
7.84
7.44
7.44
7.43
7.43
7.42
7.42
7.42
7.41
7.40
7.39
7.39
7.38
7.38
7.37
7.37
7.37
7.36
7.36
7.35
7.35
7.35
7.34
6.72
6.69
5.96
5.93
Cl
Cl
6
28000
26000
24000
22000
20000
18000
16000
14000
12000
10000
8000
6000
4000
2000
0
-2000
1.85
5.80
1.00
0.95
10.0
9.5
9.0
8.5
8.0
7.5
7.0
6.5
6.0
5.5
5.0
4.5
4.0
3.5
3.0
2.5
2.0
1.5
1.0
0.5
0.0
f1 (ppm)

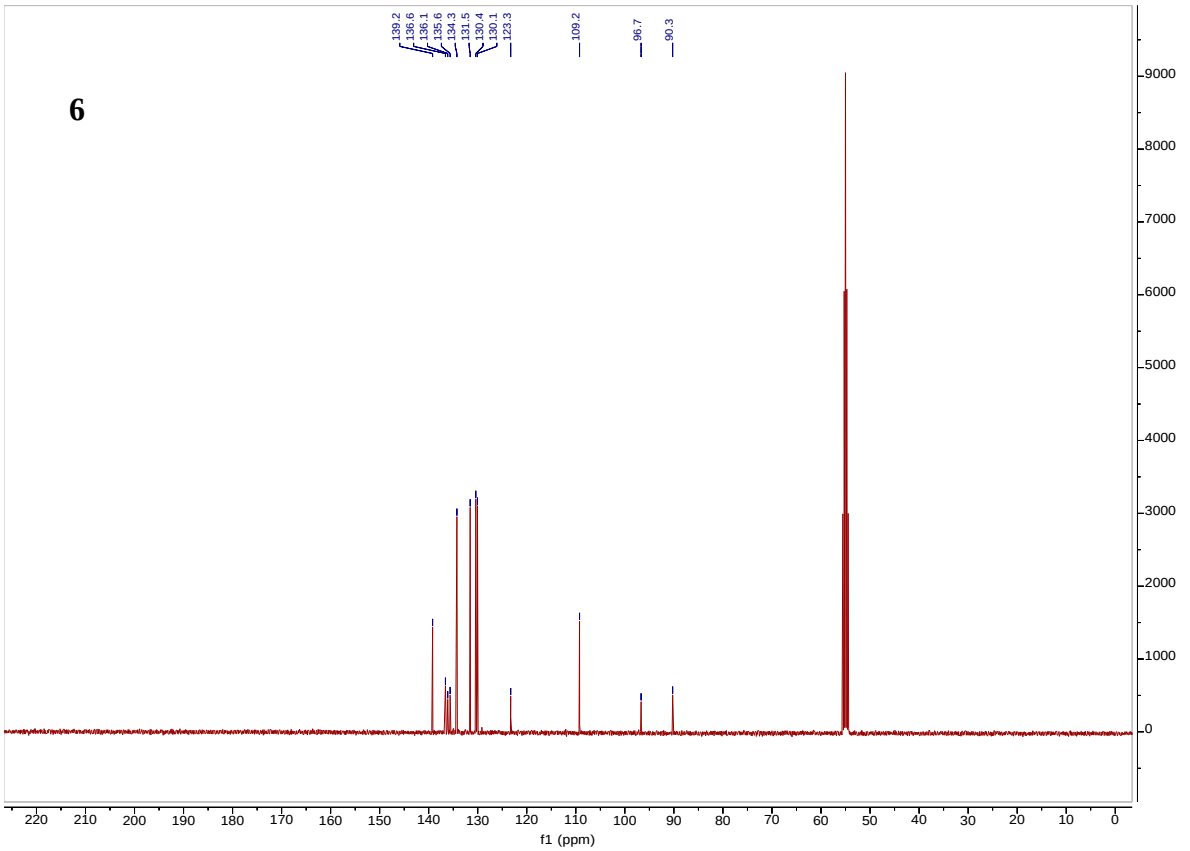
6
139.2
136.6
136.1
135.6
134.3
131.5
130.4
130.1
123.3
109.2
96.7
90.3
9000
8000
7000
6000
5000
4000
3000
2000
1000
0
220
210
200
190
180
170
160
150
140
130
120
110
100
90
80
70
60
50
40
30
20
10
0
f1 (ppm)

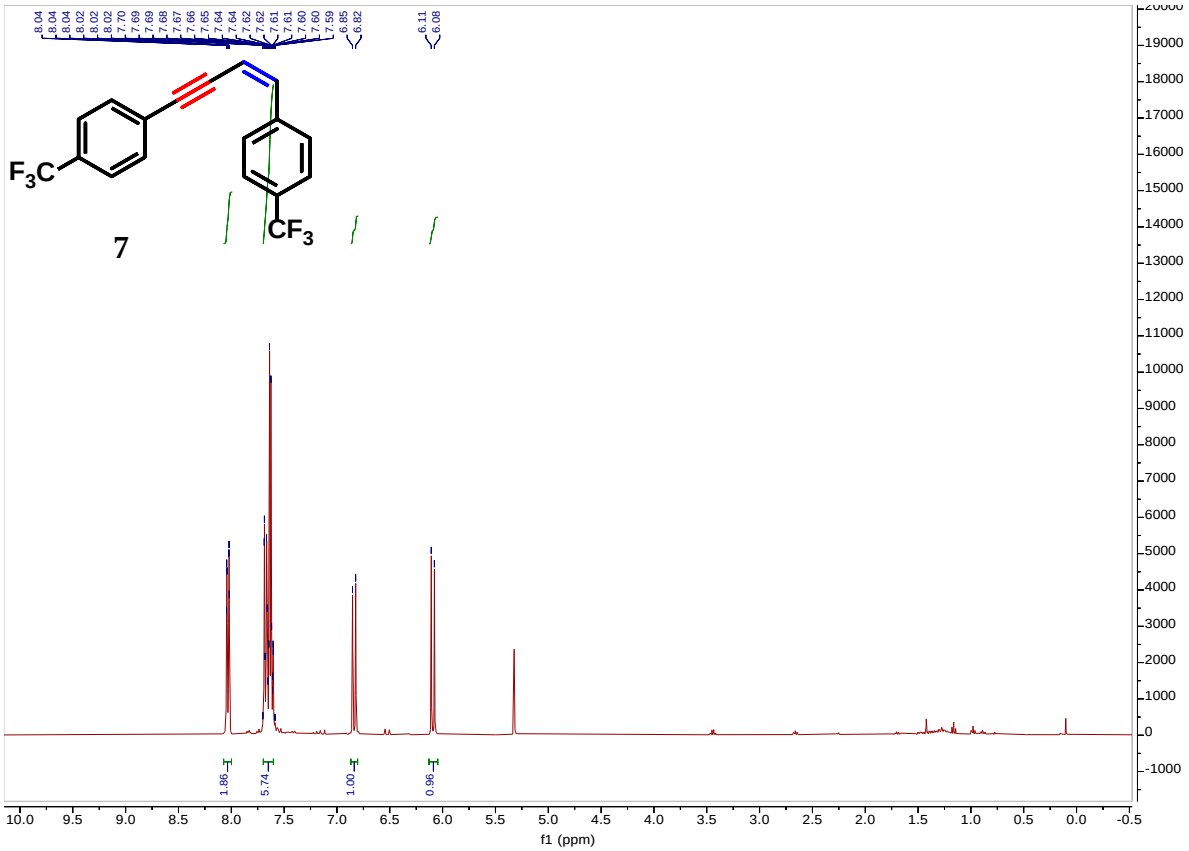
8.04
8.04
8.04
8.02
8.02
8.02
7.70
7.69
7.69
7.68
7.67
7.66
7.65
7.64
7.64
7.62
7.62
7.61
7.61
7.60
7.60
7.59
6.85
6.82
6.11
6.08
F3C
CF3
7
1.86
5.74
1.00
0.96
f1 (ppm)

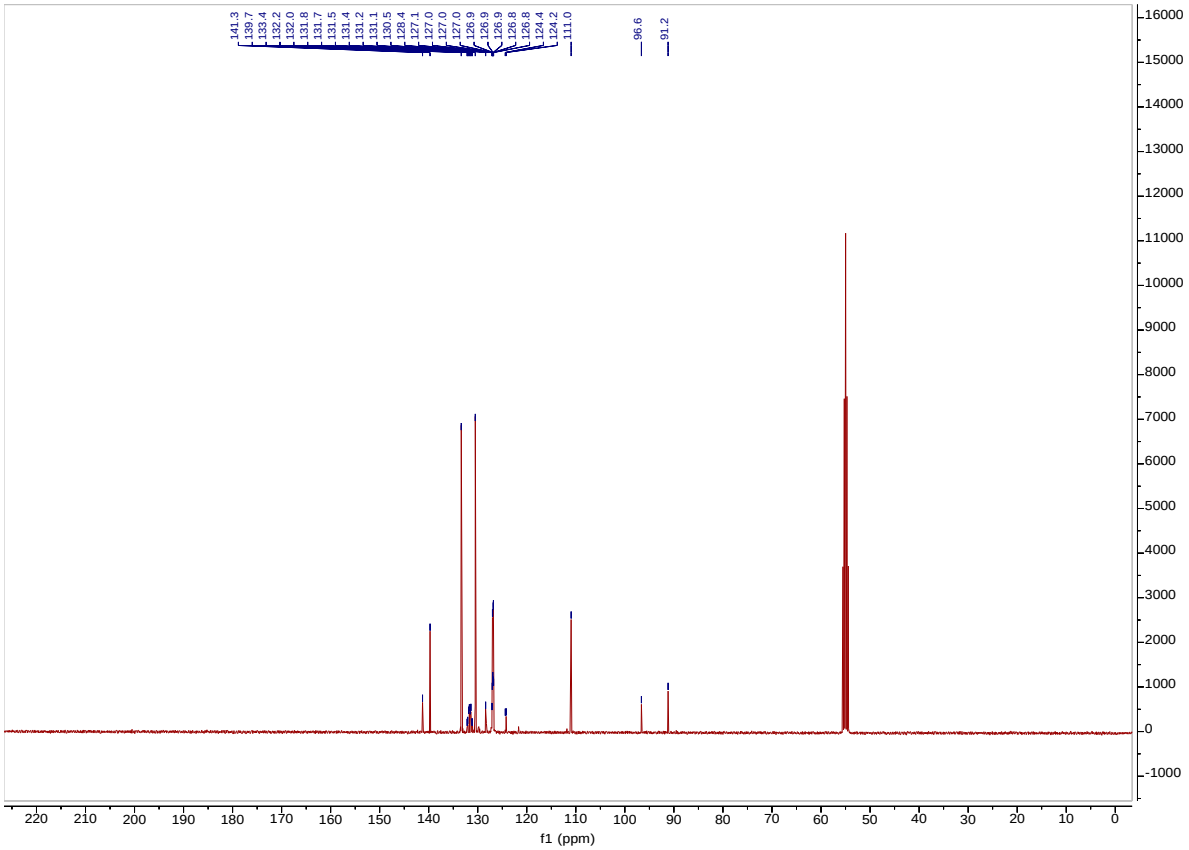
141.3
139.7
139.4
132.2
132.0
131.8
131.7
131.5
131.4
131.2
131.1
130.5
128.4
127.1
127.0
127.0
127.0
126.9
126.9
126.9
126.8
126.8
124.4
124.2
111.0
96.6
91.2
f1 (ppm)

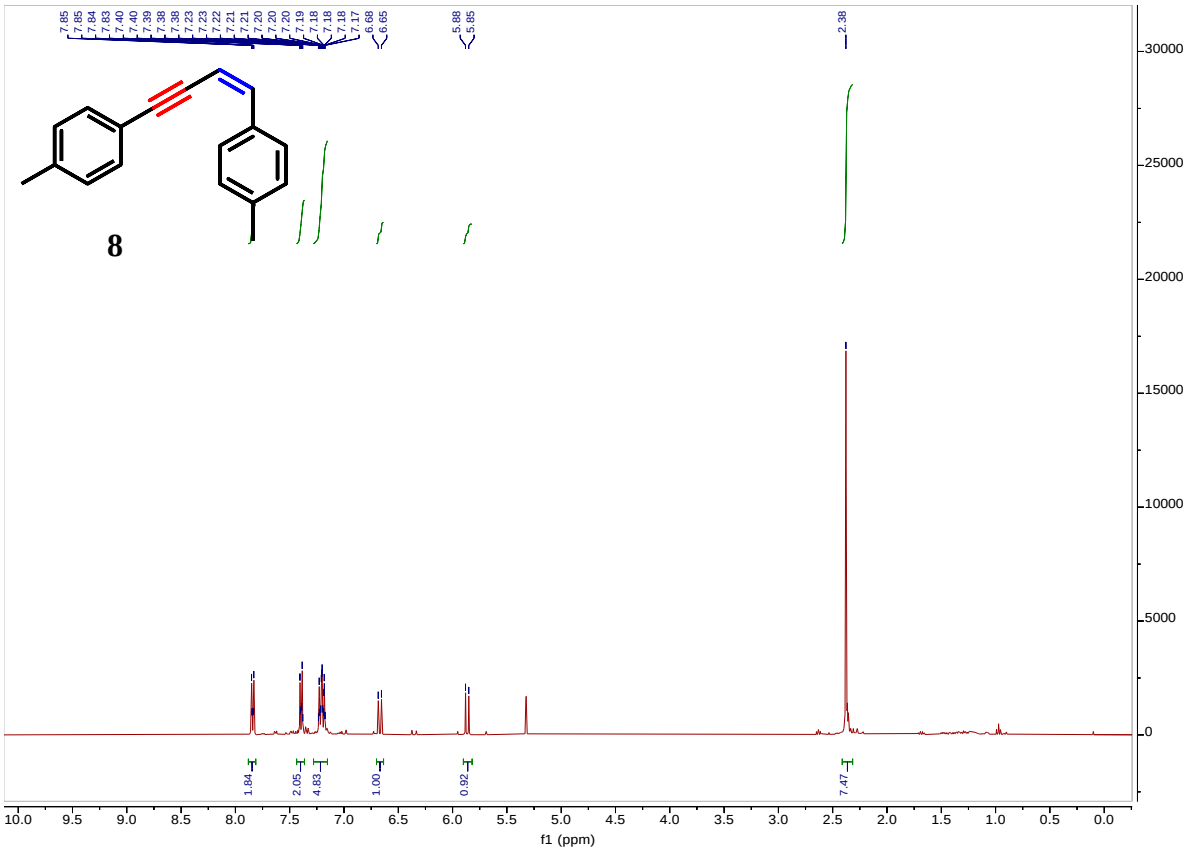
8
7.85
7.85
7.84
7.83
7.40
7.40
7.39
7.38
7.38
7.23
7.22
7.21
7.21
7.20
7.20
7.20
7.19
7.18
7.18
7.18
7.17
6.68
6.65
5.88
5.85
2.38
1.84
2.05
4.83
1.00
0.92
7.47
f1 (ppm)

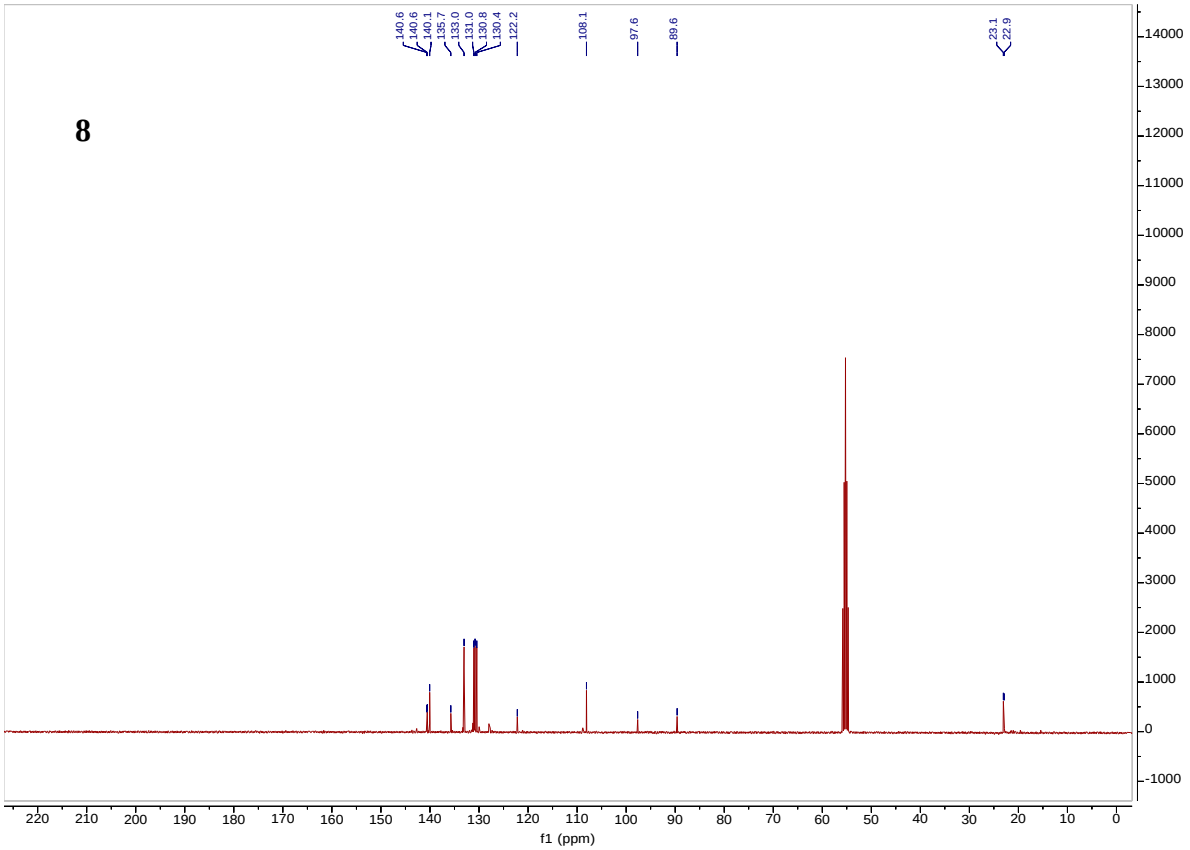
8
140.6
140.6
140.1
135.7
133.0
131.0
130.8
130.4
122.2
108.1
97.6
89.6
23.1
22.9
f1 (ppm)

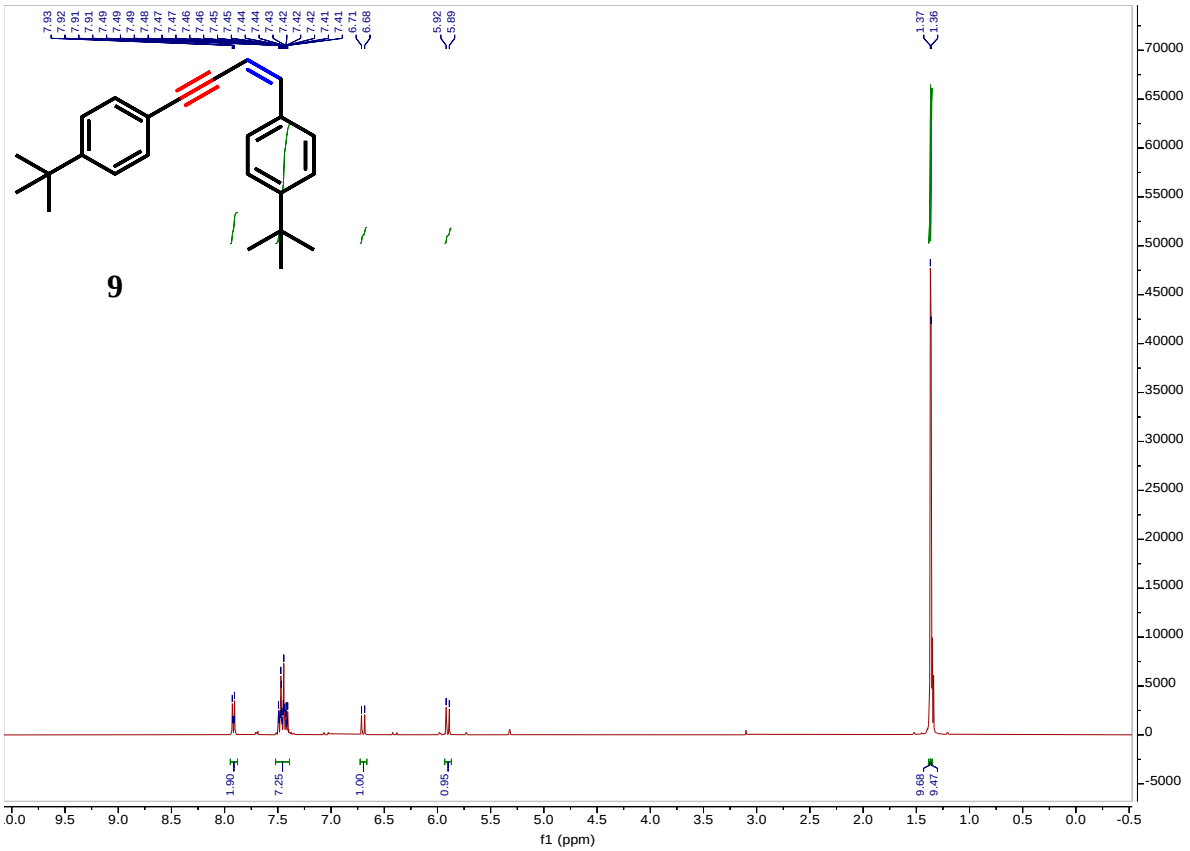
9
f1 (ppm)

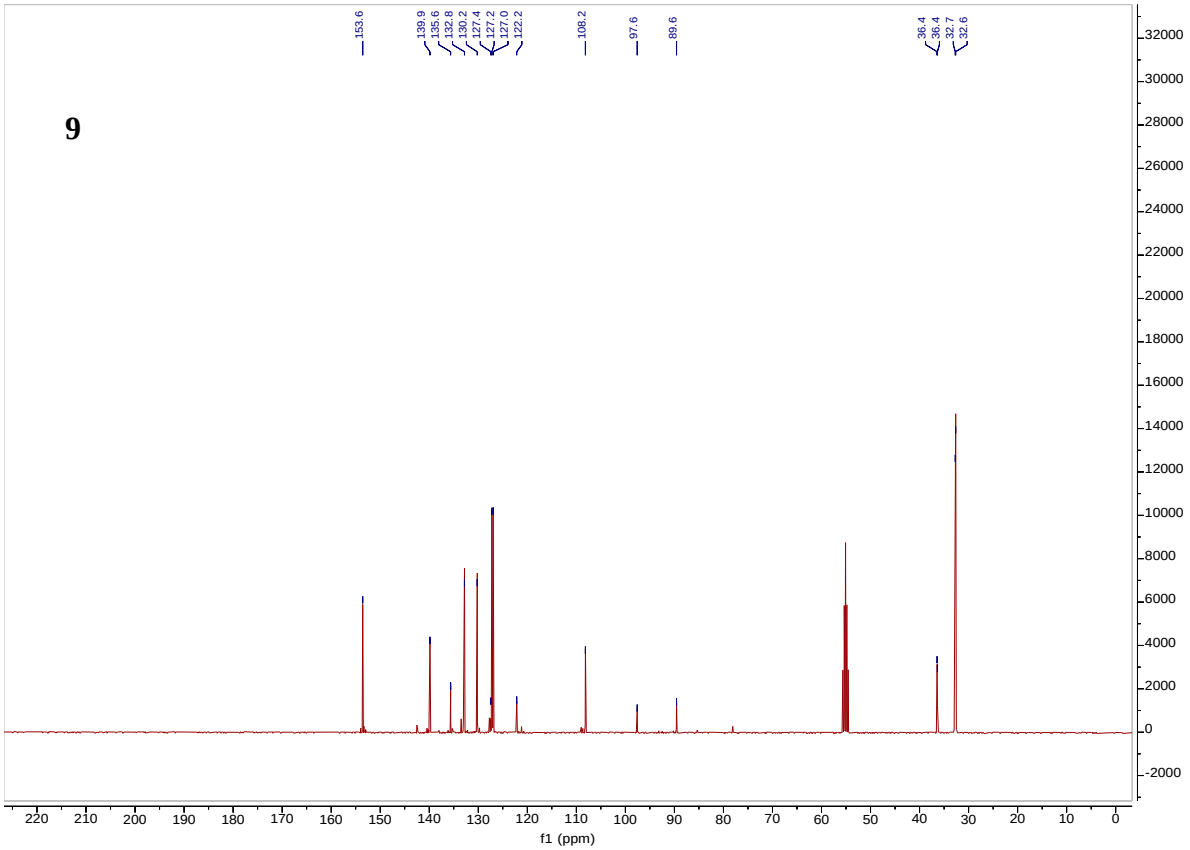
9
f1 (ppm)

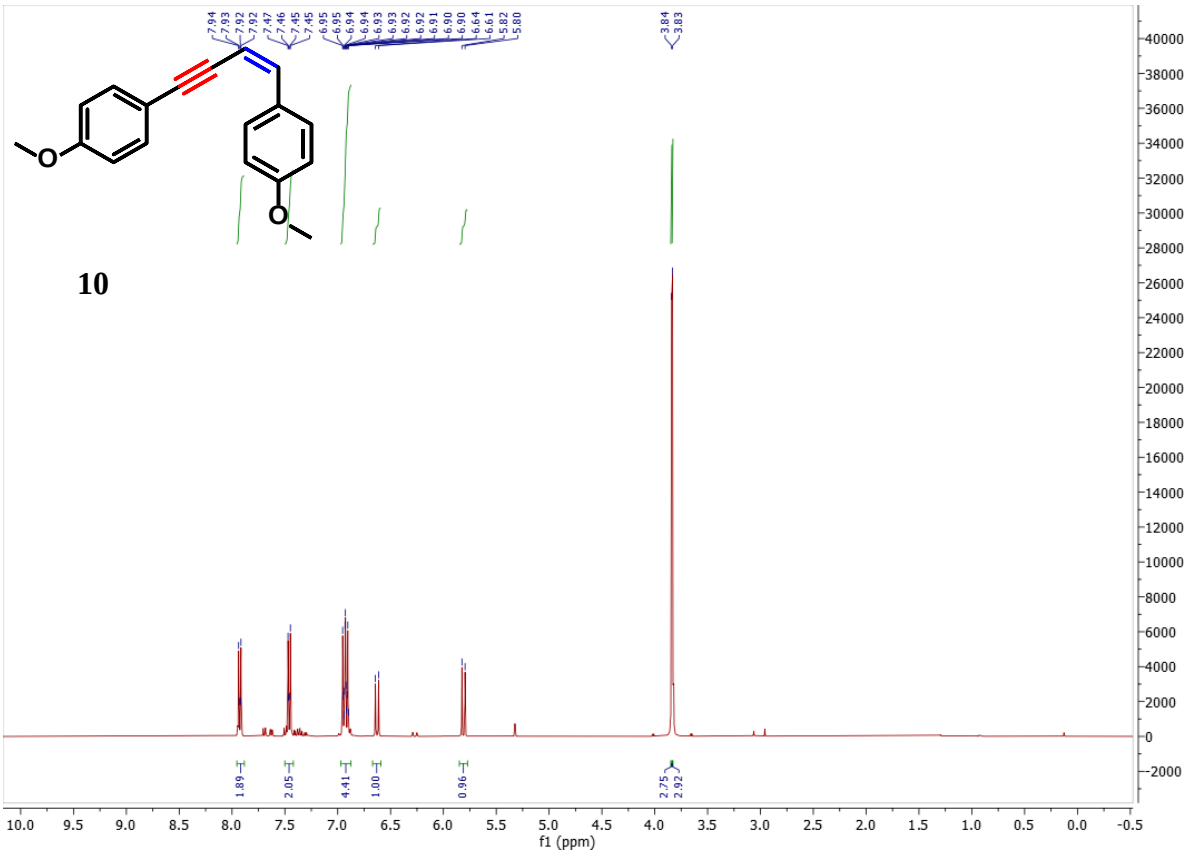
10
7.94
7.93
7.92
7.92
7.47
7.46
7.45
7.45
6.95
6.95
6.94
6.94
6.93
6.93
6.92
6.92
6.91
6.90
6.90
6.64
6.61
5.82
5.80
3.84
3.83
1.89
2.05
4.41
1.00
0.96
2.75
2.92
f1 (ppm)

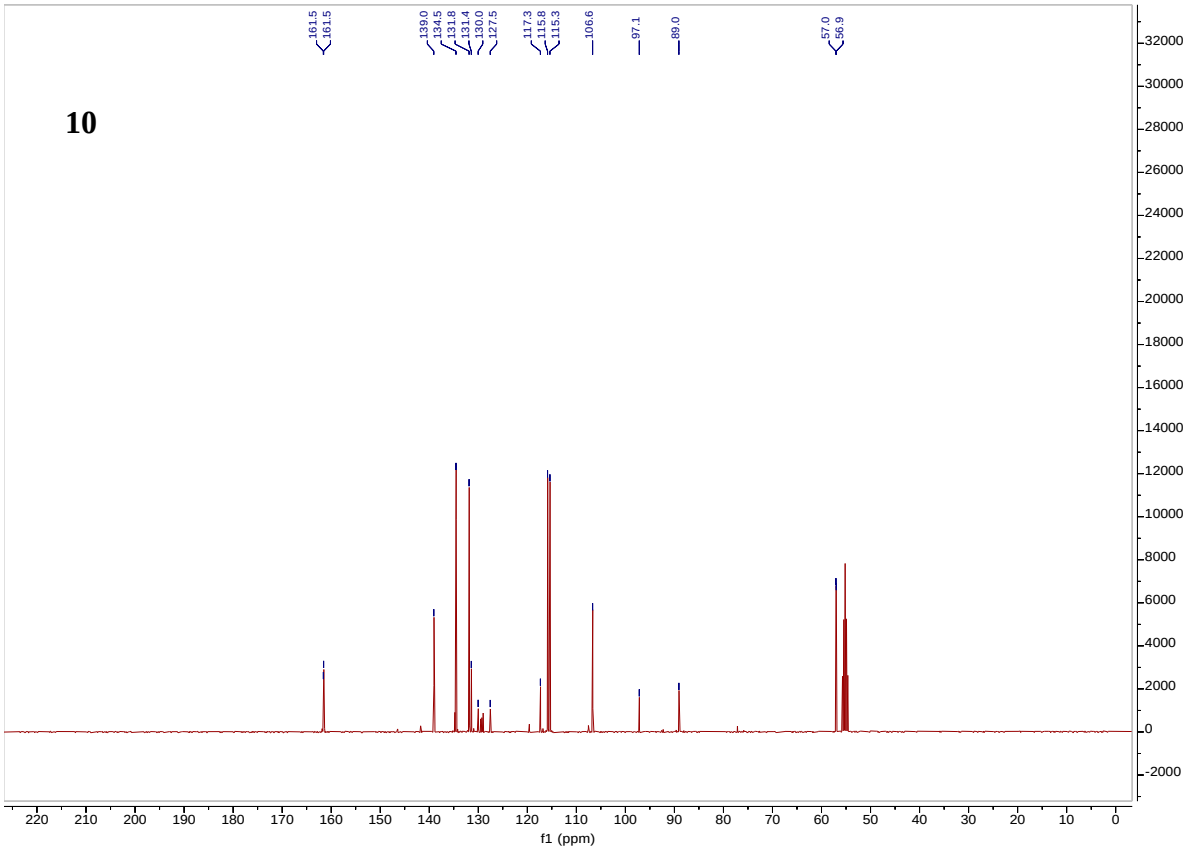
10
161.5
161.5
139.0
134.5
131.8
131.4
130.0
127.5
117.3
115.8
115.3
106.6
97.1
89.0
57.0
56.9
f1 (ppm)

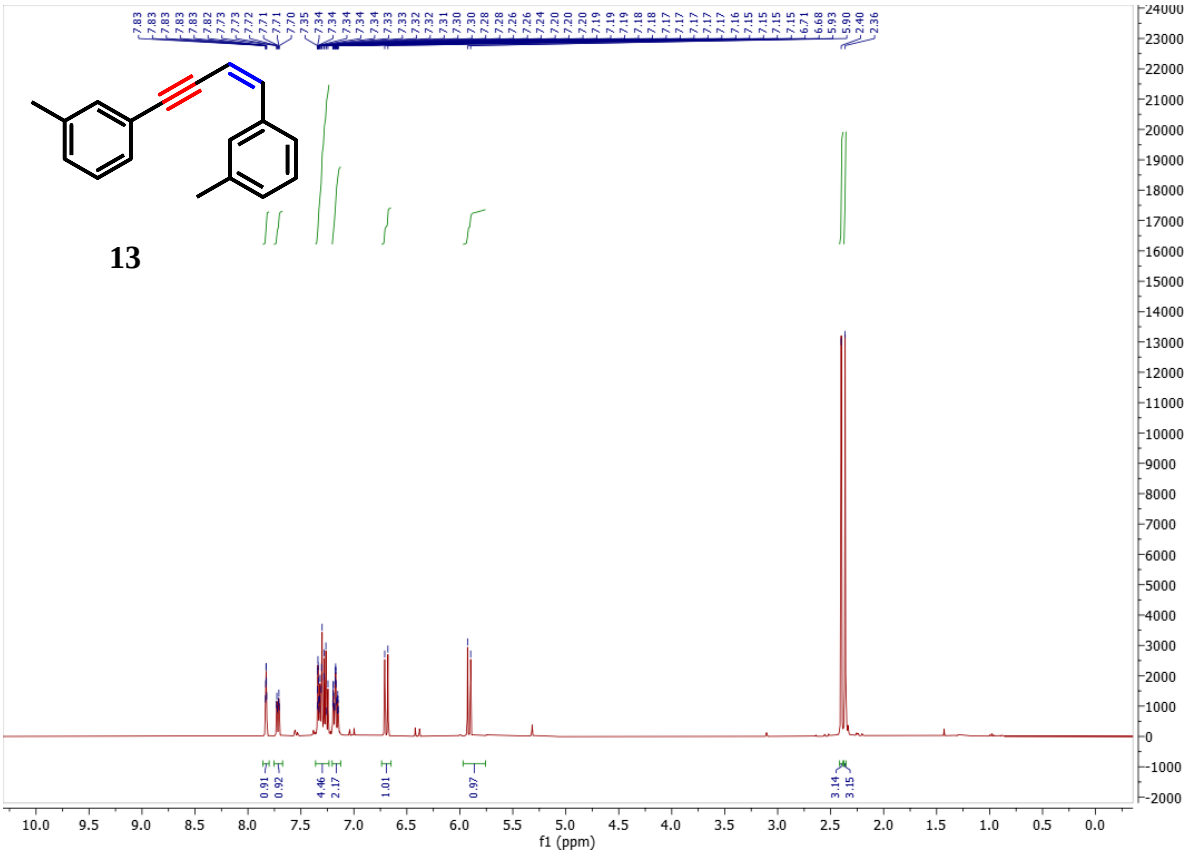
13
f1 (ppm)

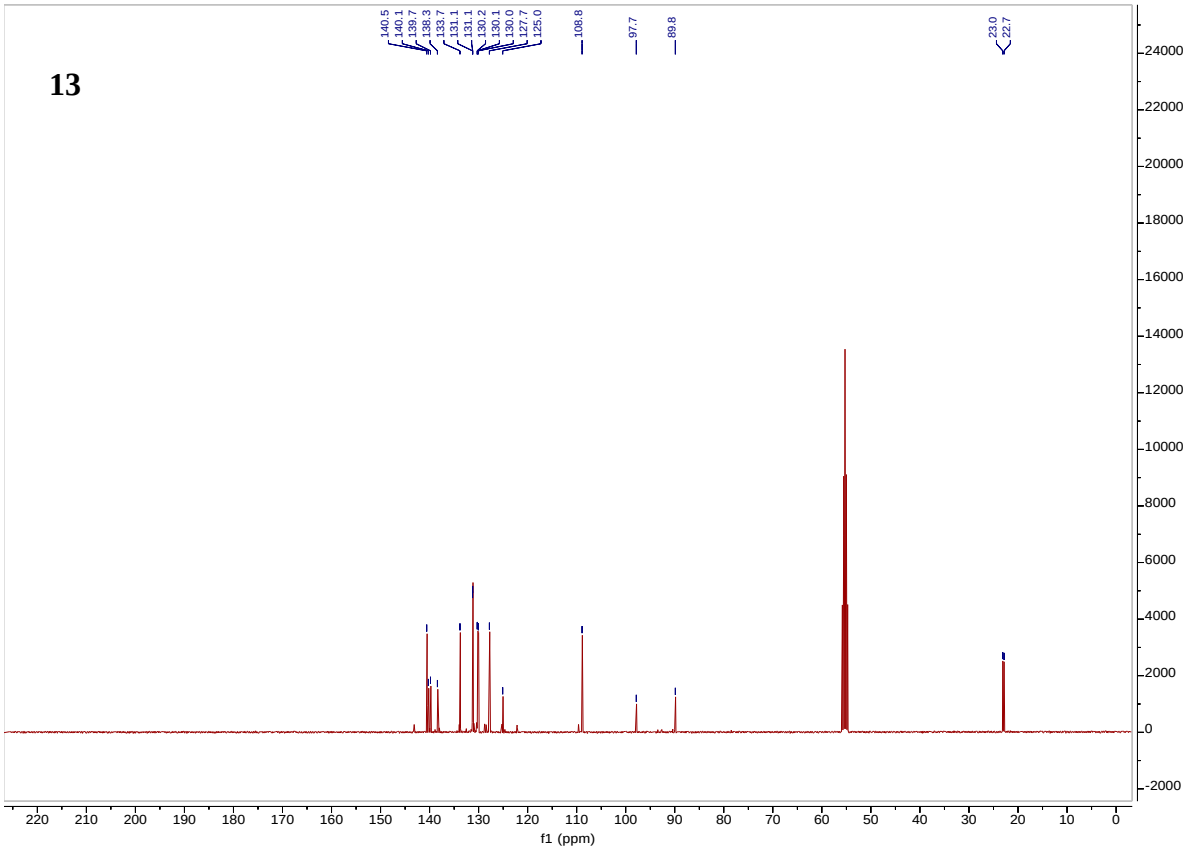
13
f1 (ppm)

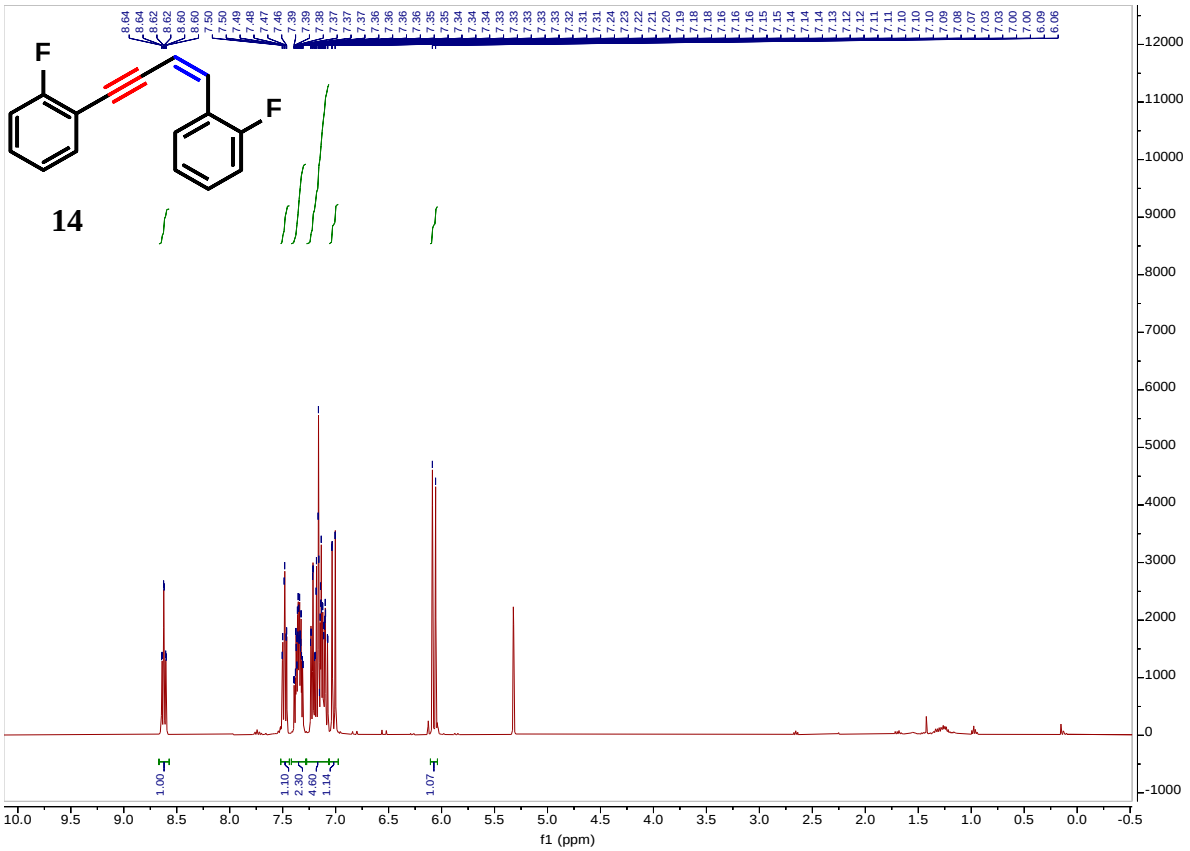
F
F
14
f1 (ppm)

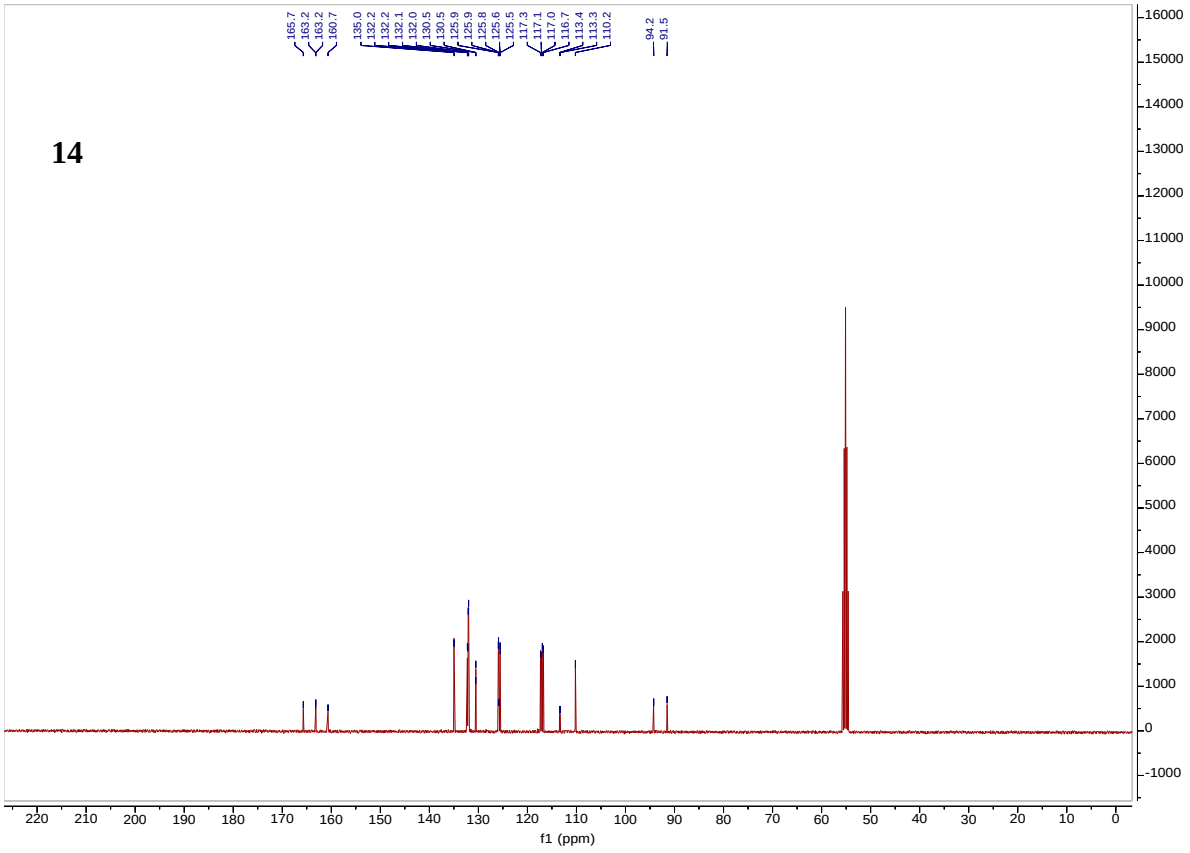
14
f1 (ppm)

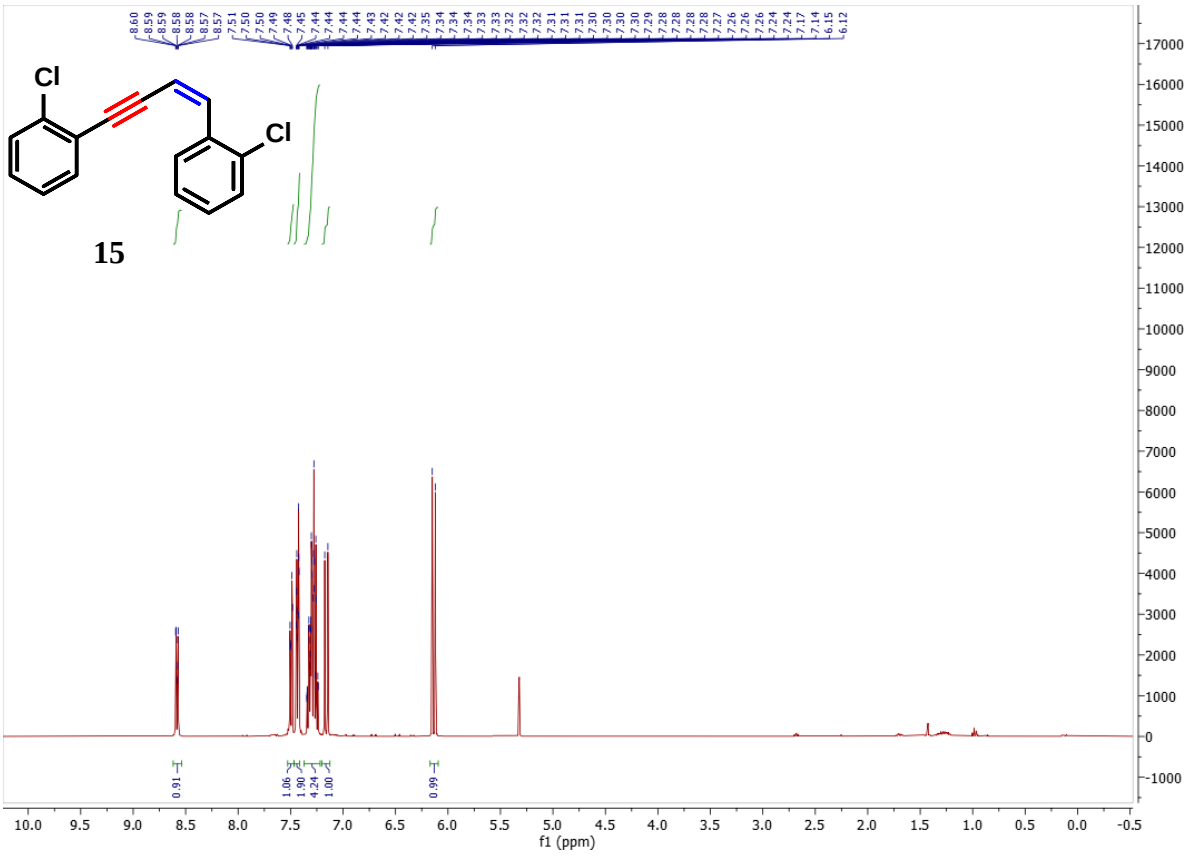
Cl
Cl
15
f1 (ppm)

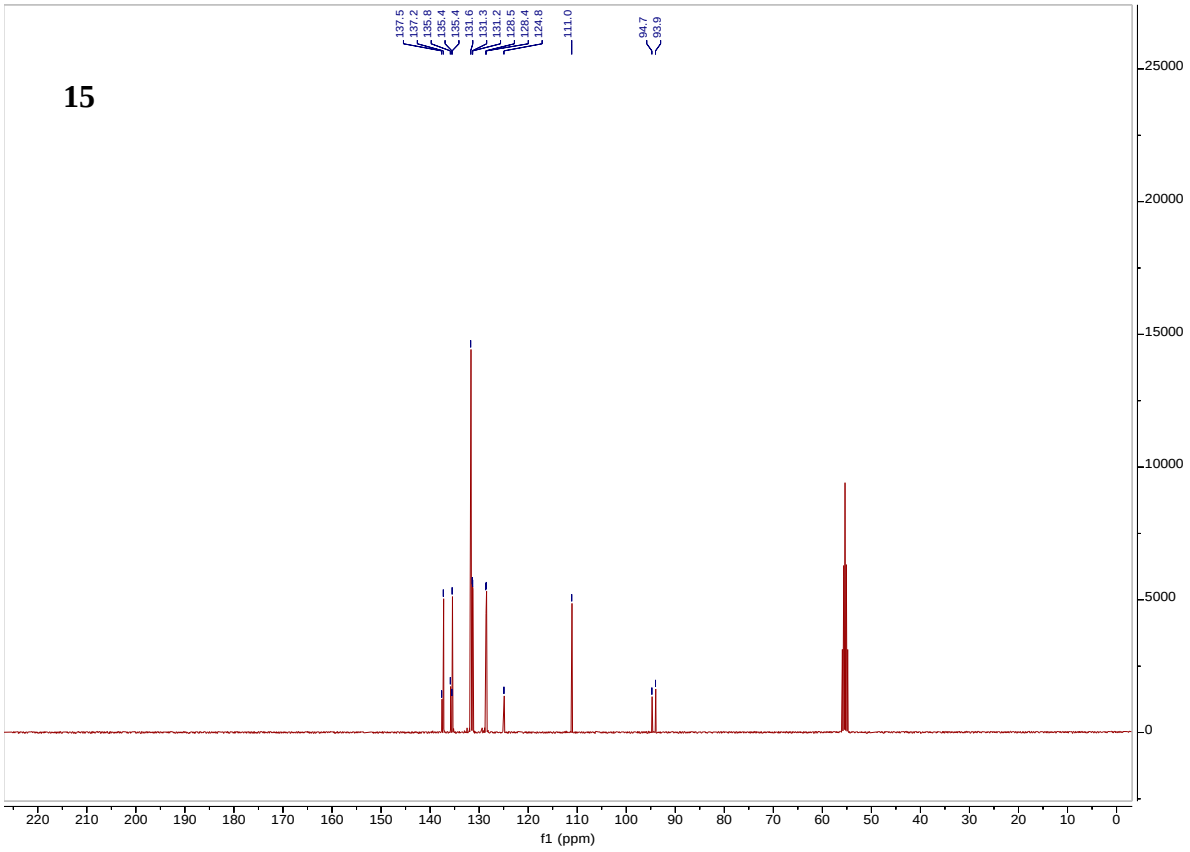
15
f1 (ppm)

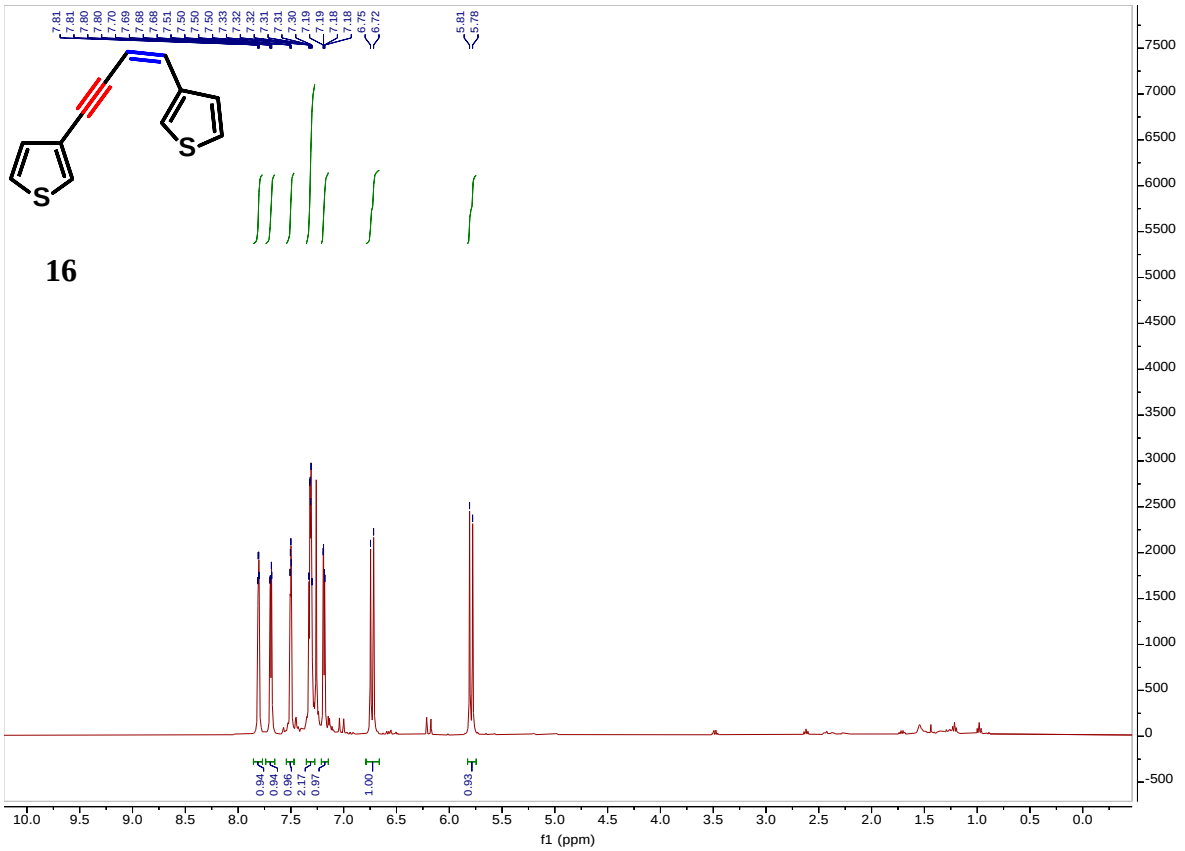
16
f1 (ppm)

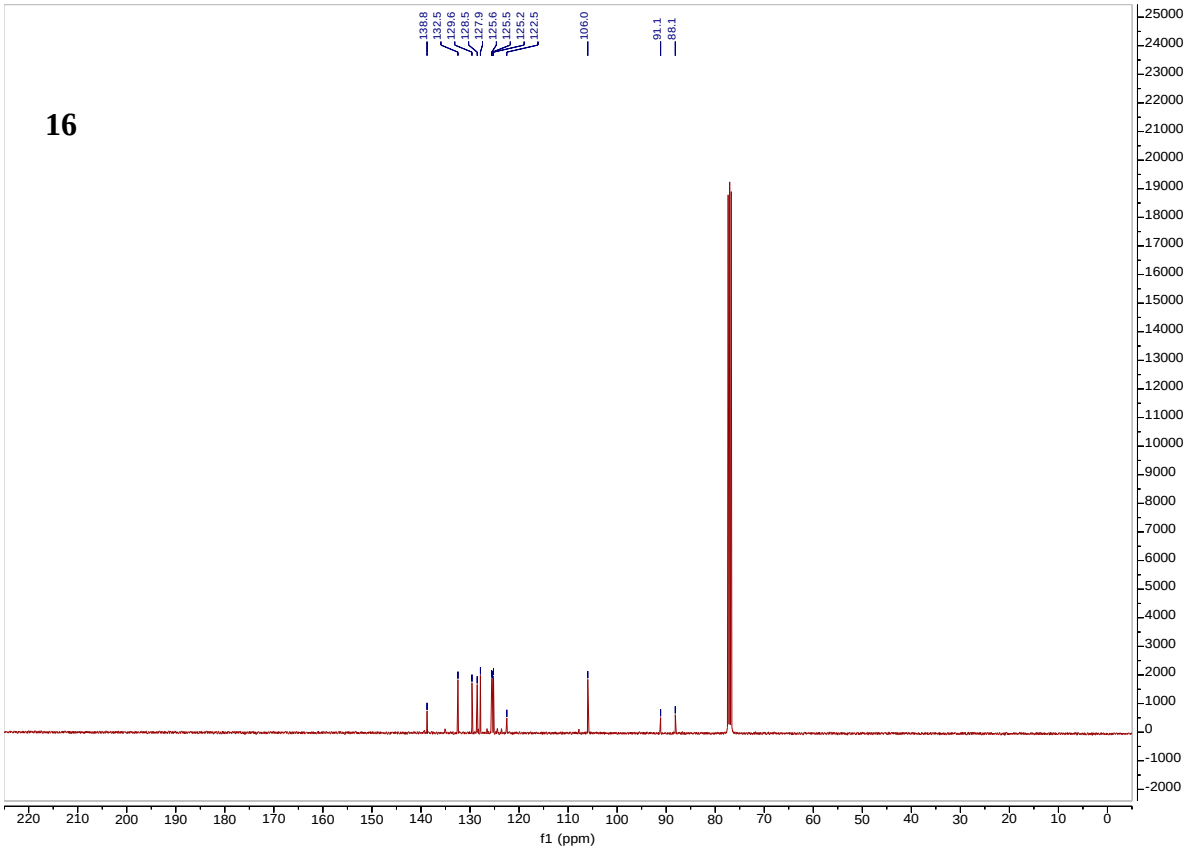
16
f1 (ppm)

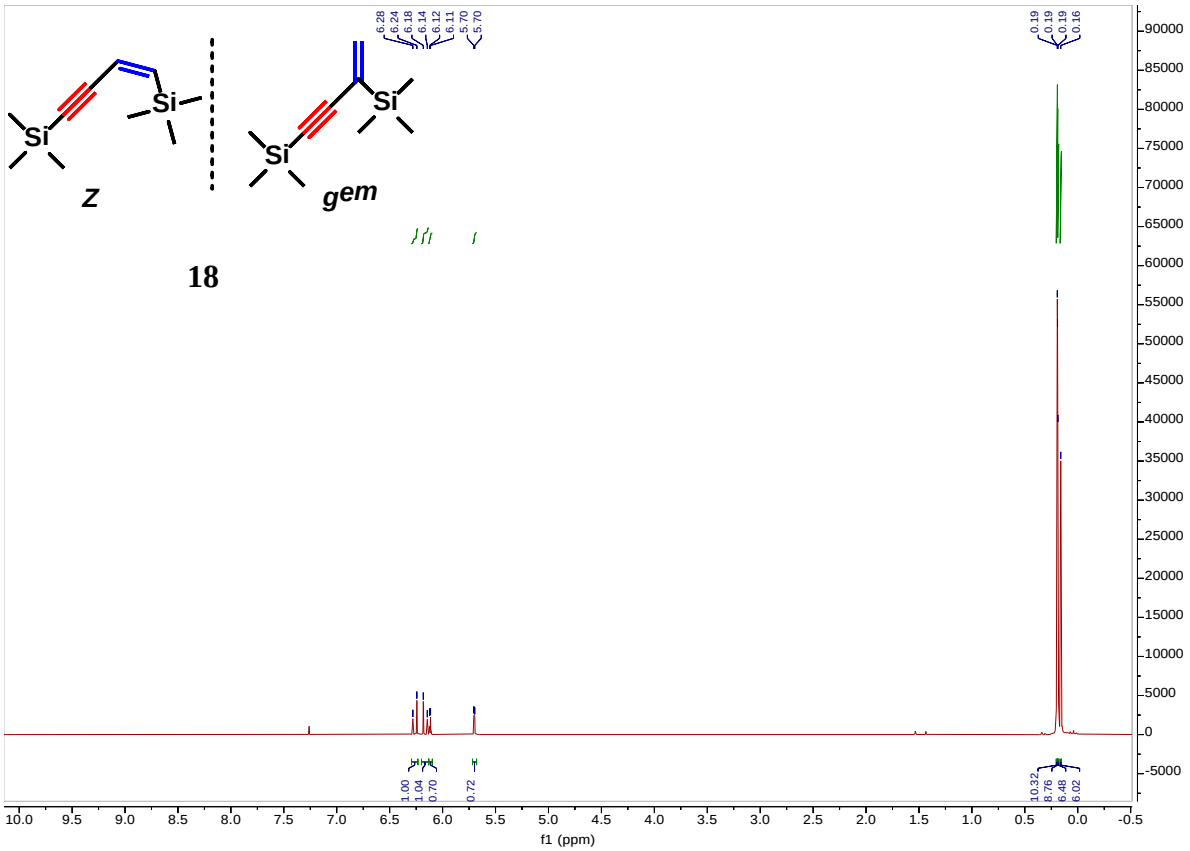
Si
Si
Z
Si
Si
gem
18
6.28
6.24
6.18
6.14
6.12
6.11
5.70
5.70
0.19
0.19
0.19
0.16
1.00
1.04
0.70
0.72
10.32
8.76
6.48
6.02
f1 (ppm)

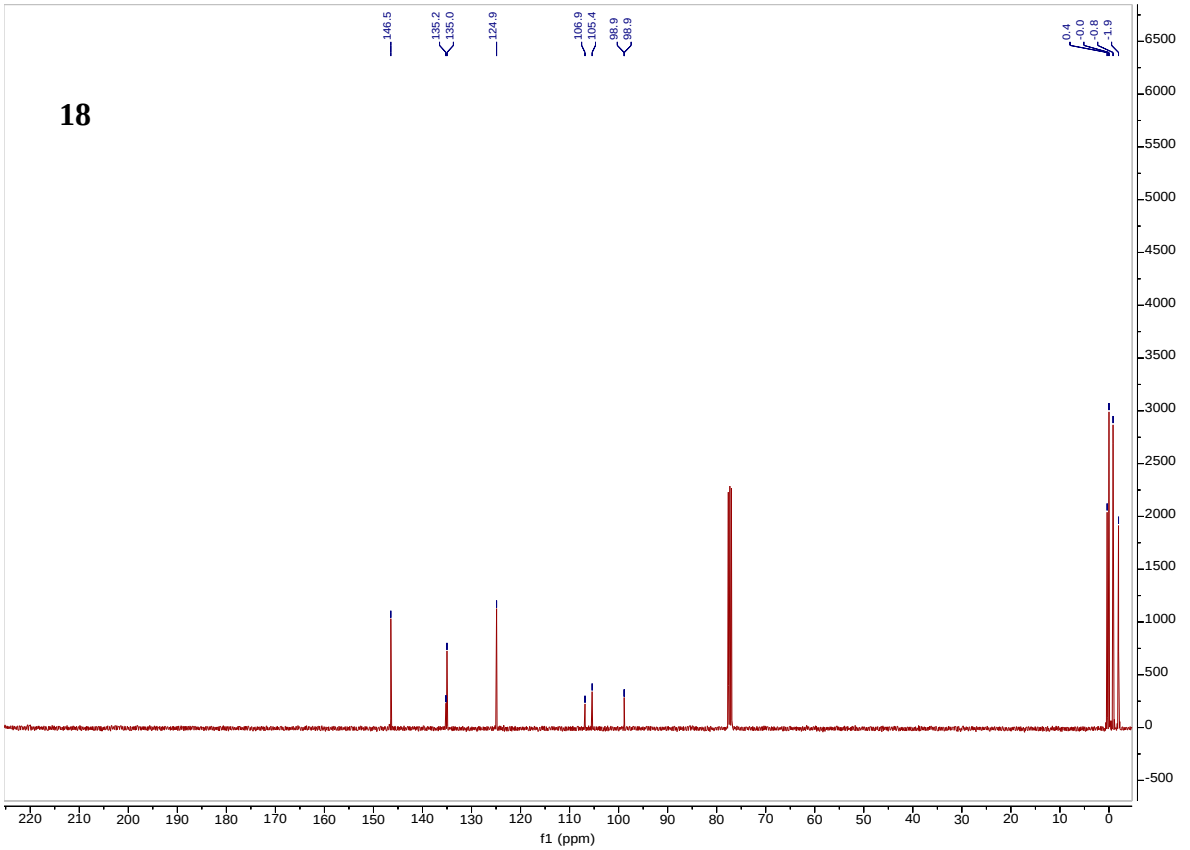
18
146.5
135.2
135.0
124.9
106.9
105.4
98.9
98.9
0.4
-0.0
-0.8
-1.9
f1 (ppm)

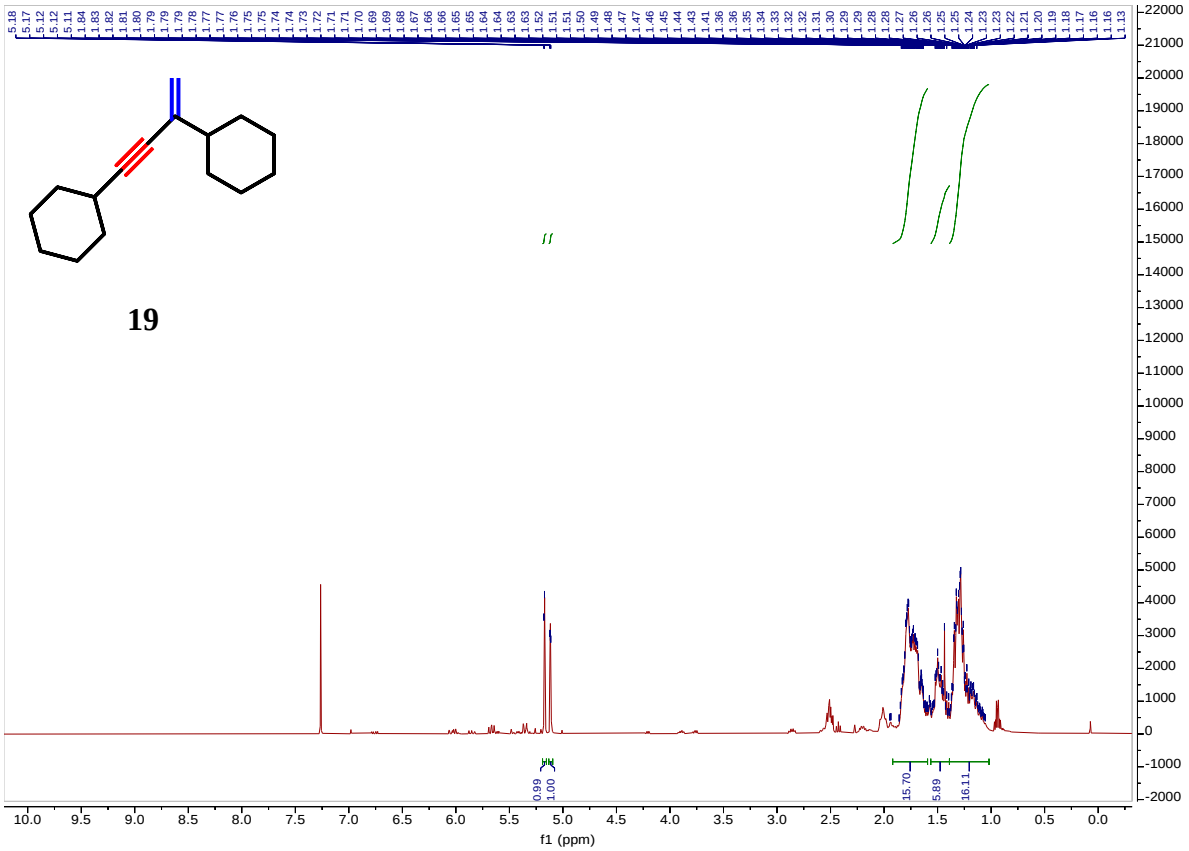
19
0.99
1.00
15.70
5.89
16.11
f1 (ppm)

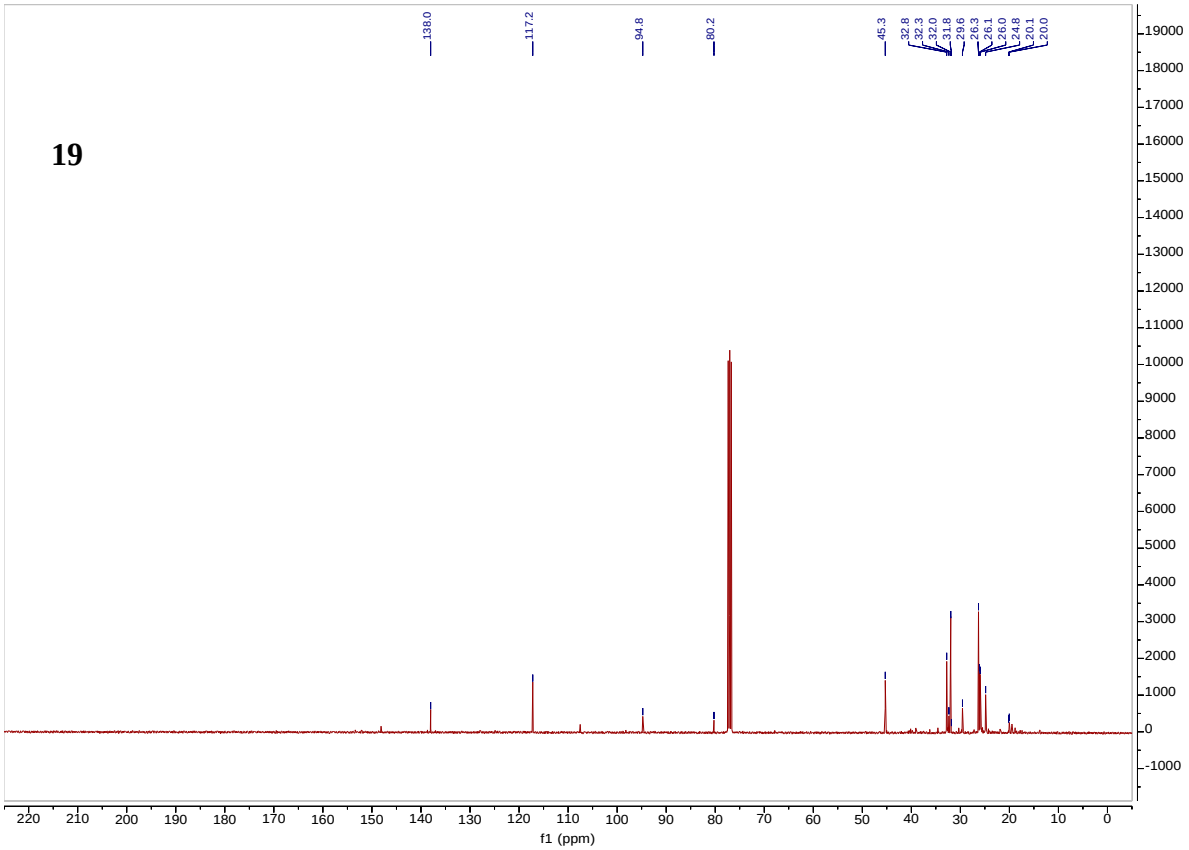
19
138.0
117.2
94.8
80.2
45.3
32.8
32.3
32.0
31.8
29.6
26.3
26.1
26.0
24.8
20.1
20.0
f1 (ppm)

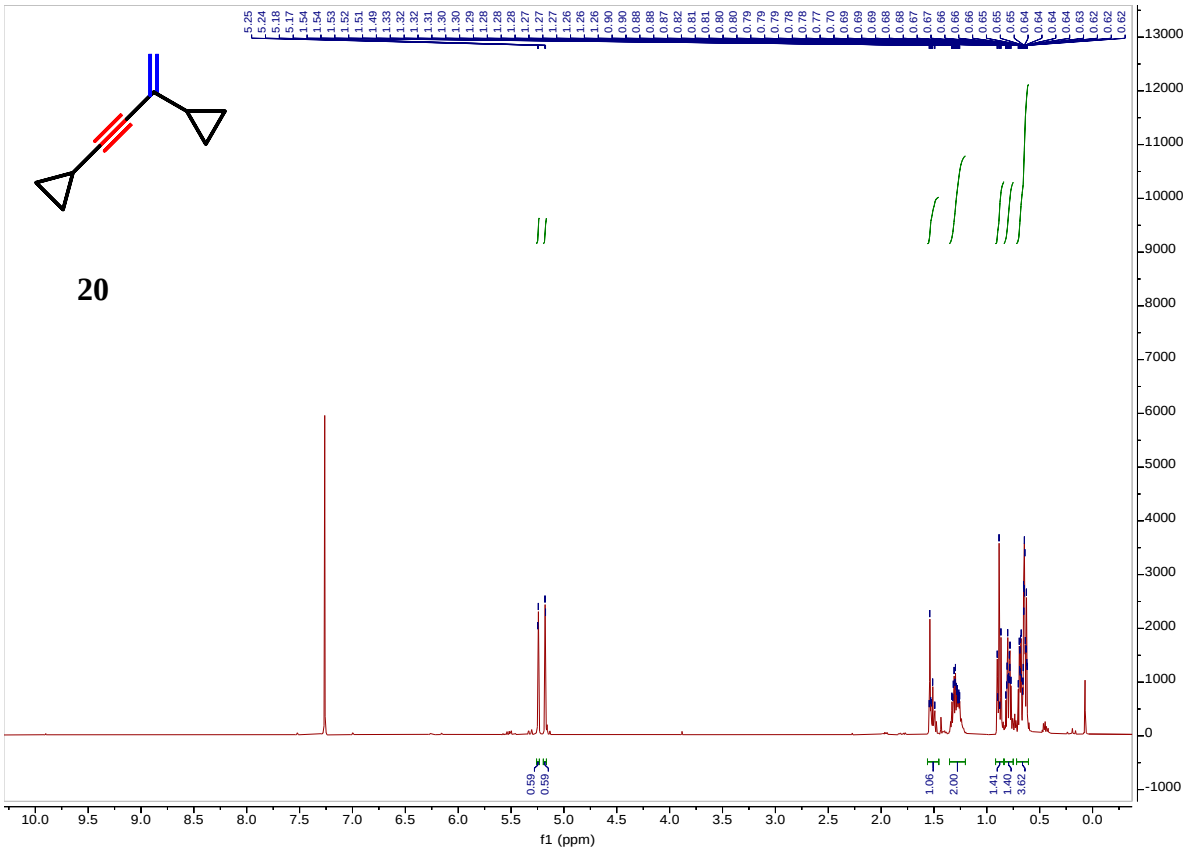
20
f1 (ppm)

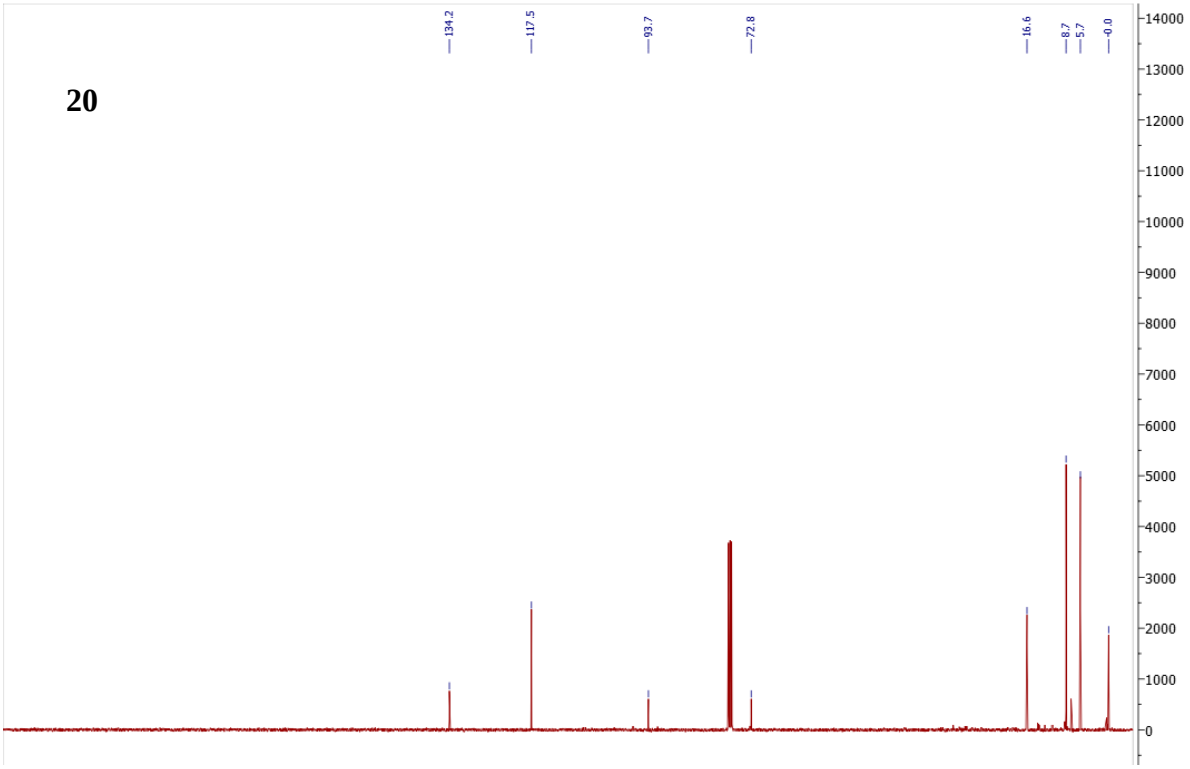
20

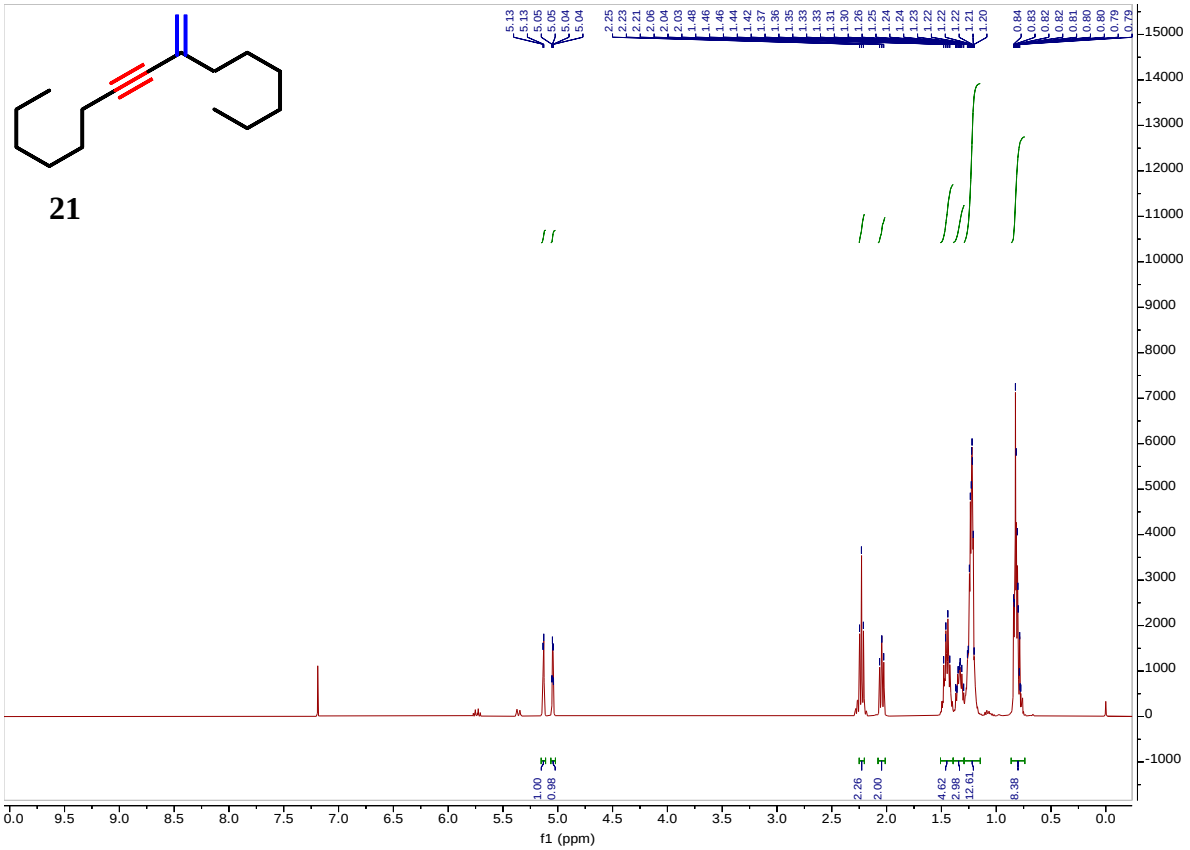
21
f1 (ppm)

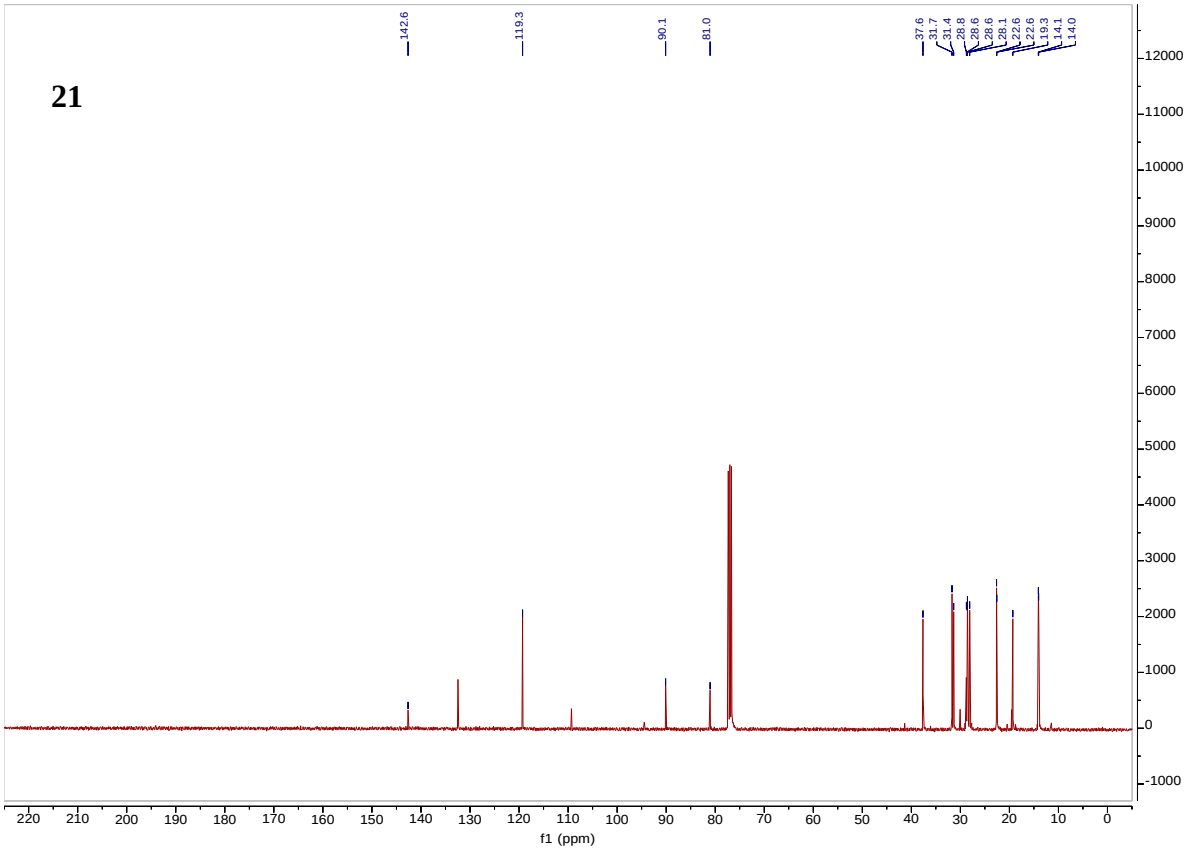
21
f1 (ppm)

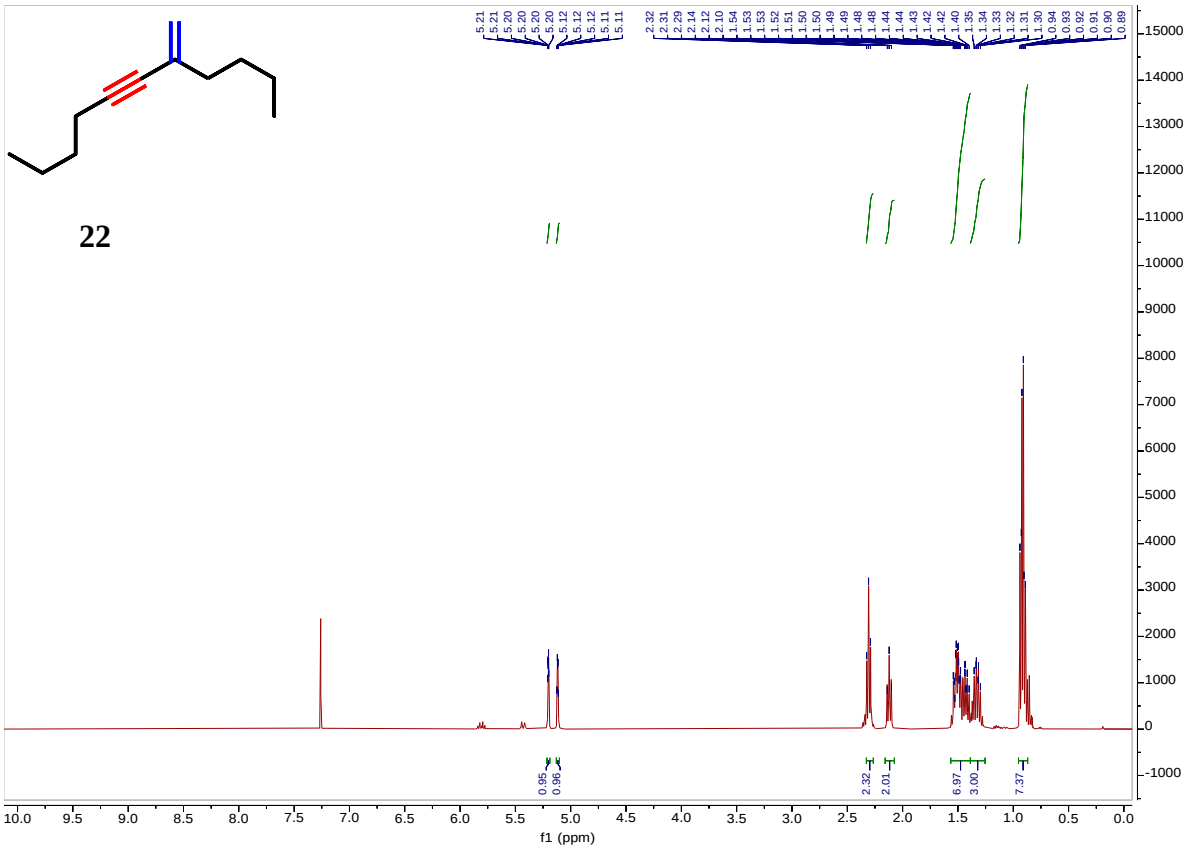
22
f1 (ppm)

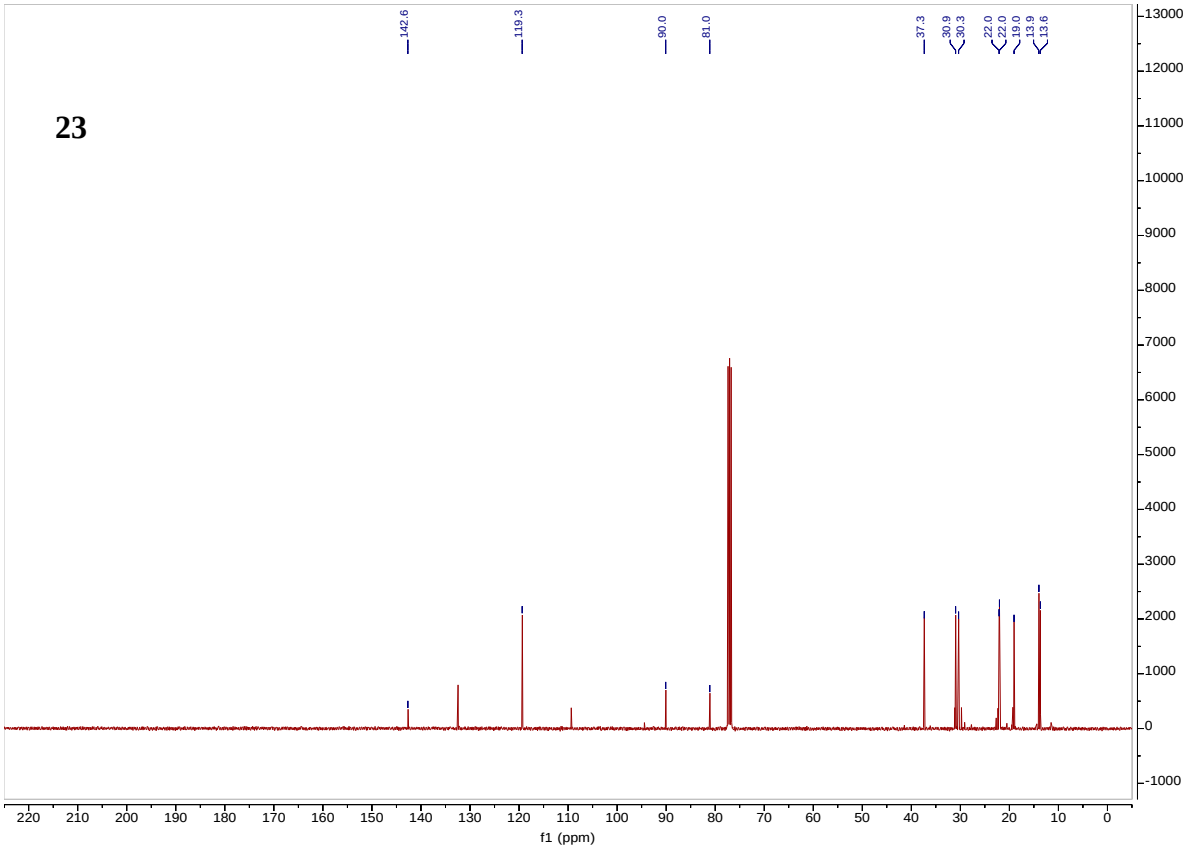
23
142.6
119.3
90.0
81.0
37.3
30.9
30.3
22.0
22.0
19.0
13.9
13.6
f1 (ppm)

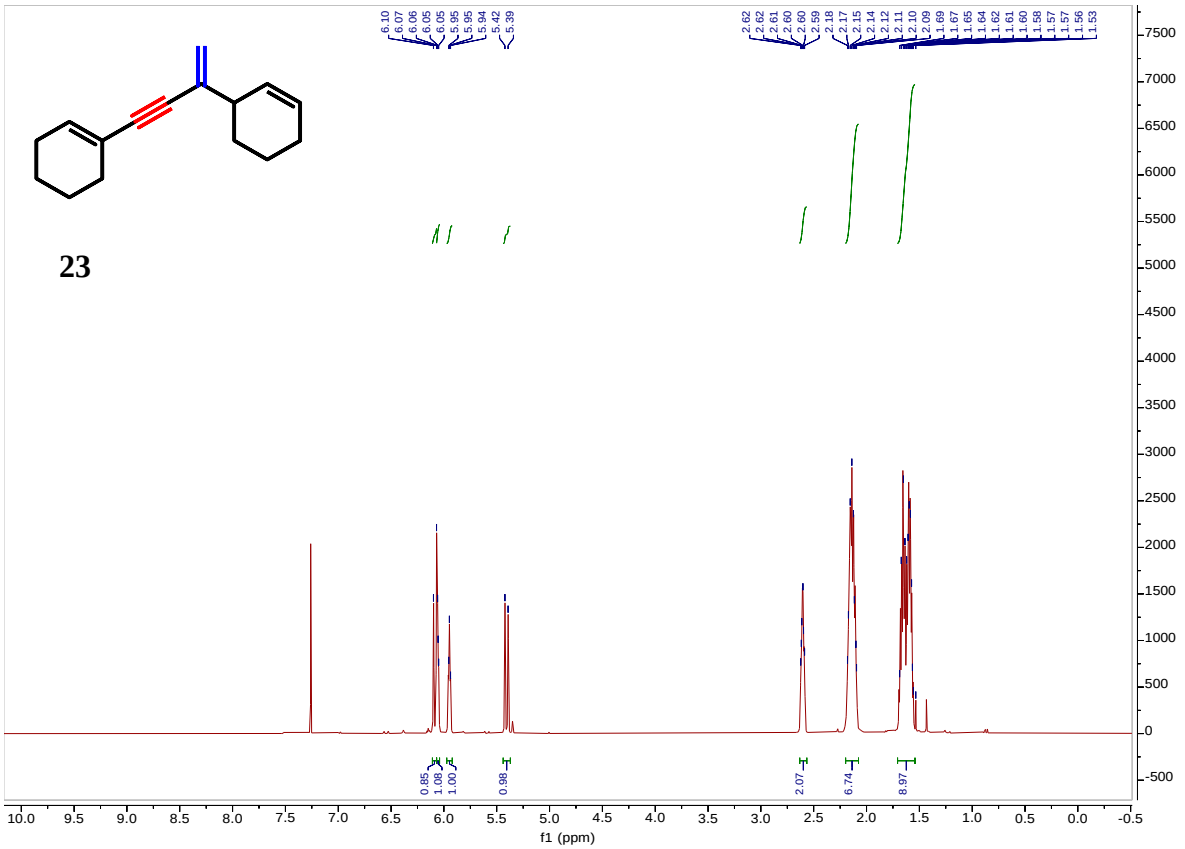
23
f1 (ppm)

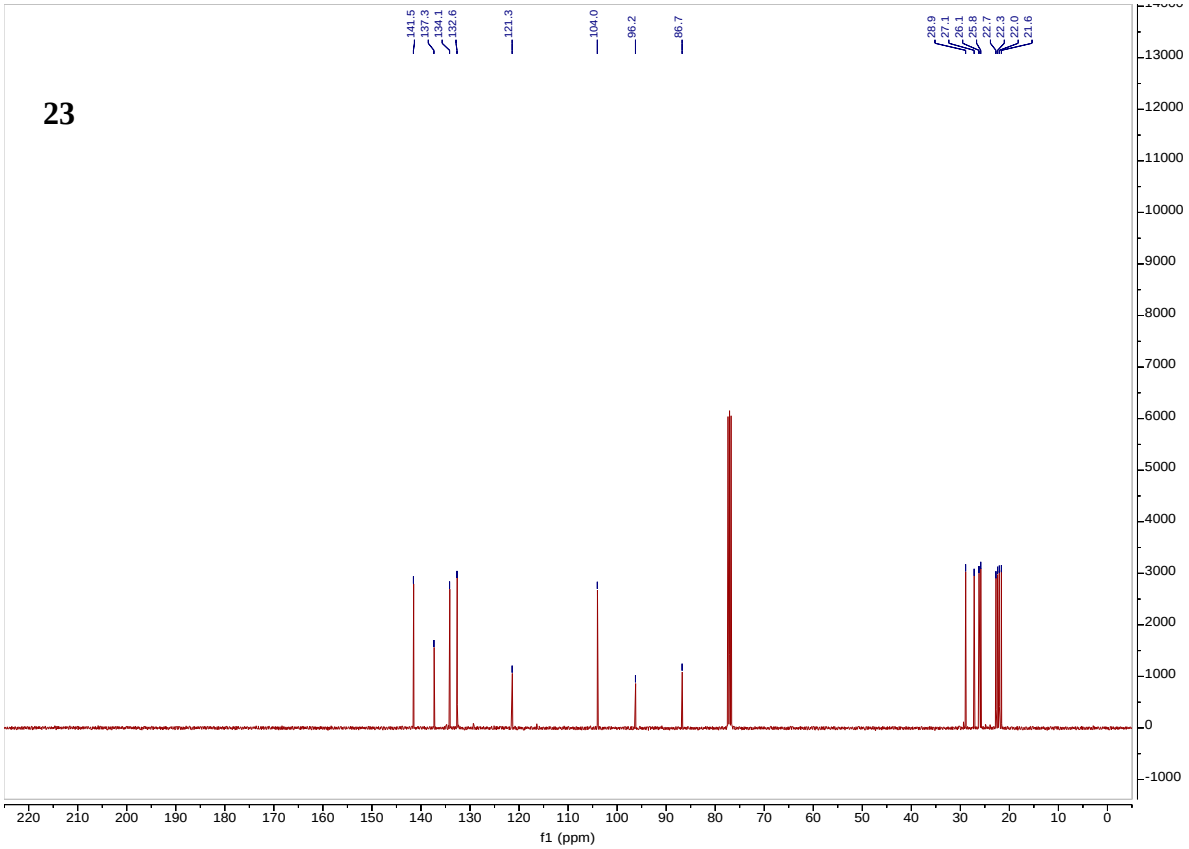
23
f1 (ppm)

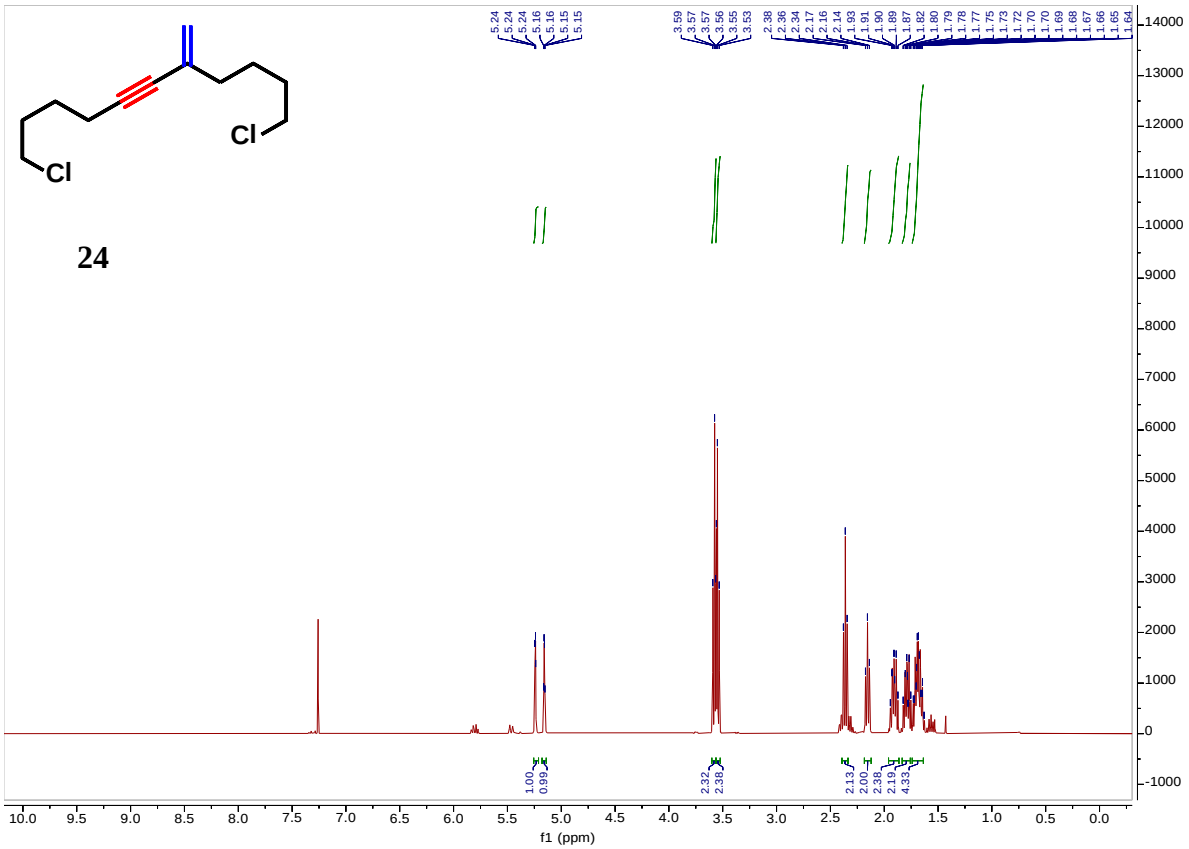
Cl
Cl
24
f1 (ppm)

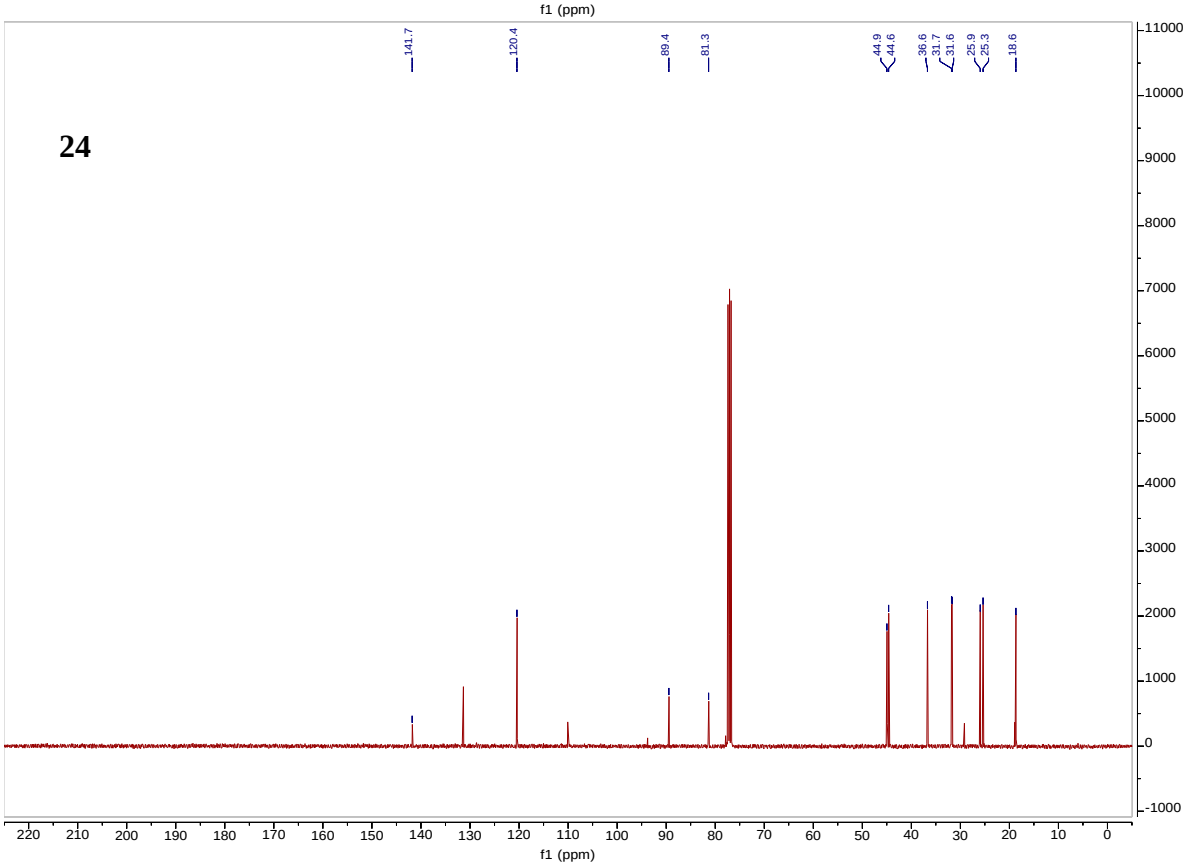
24
f1 (ppm)

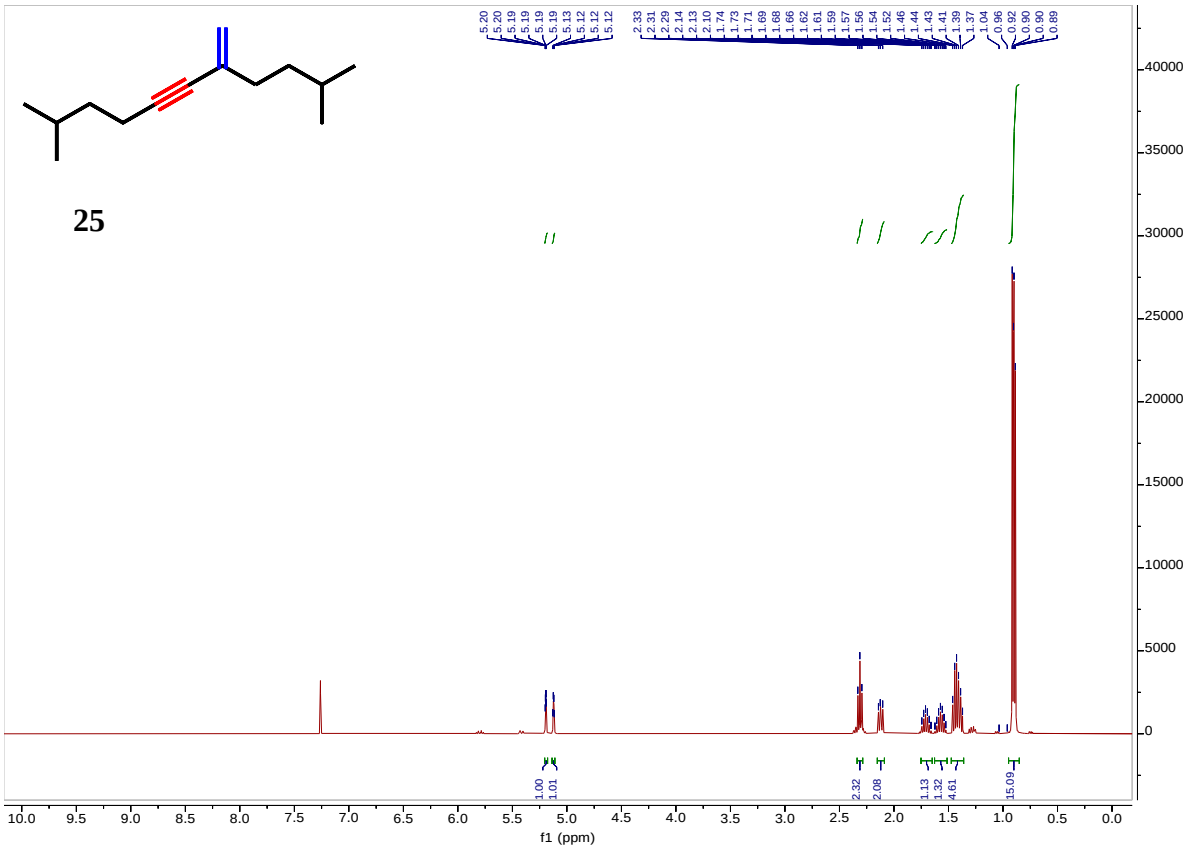
25
f1 (ppm)

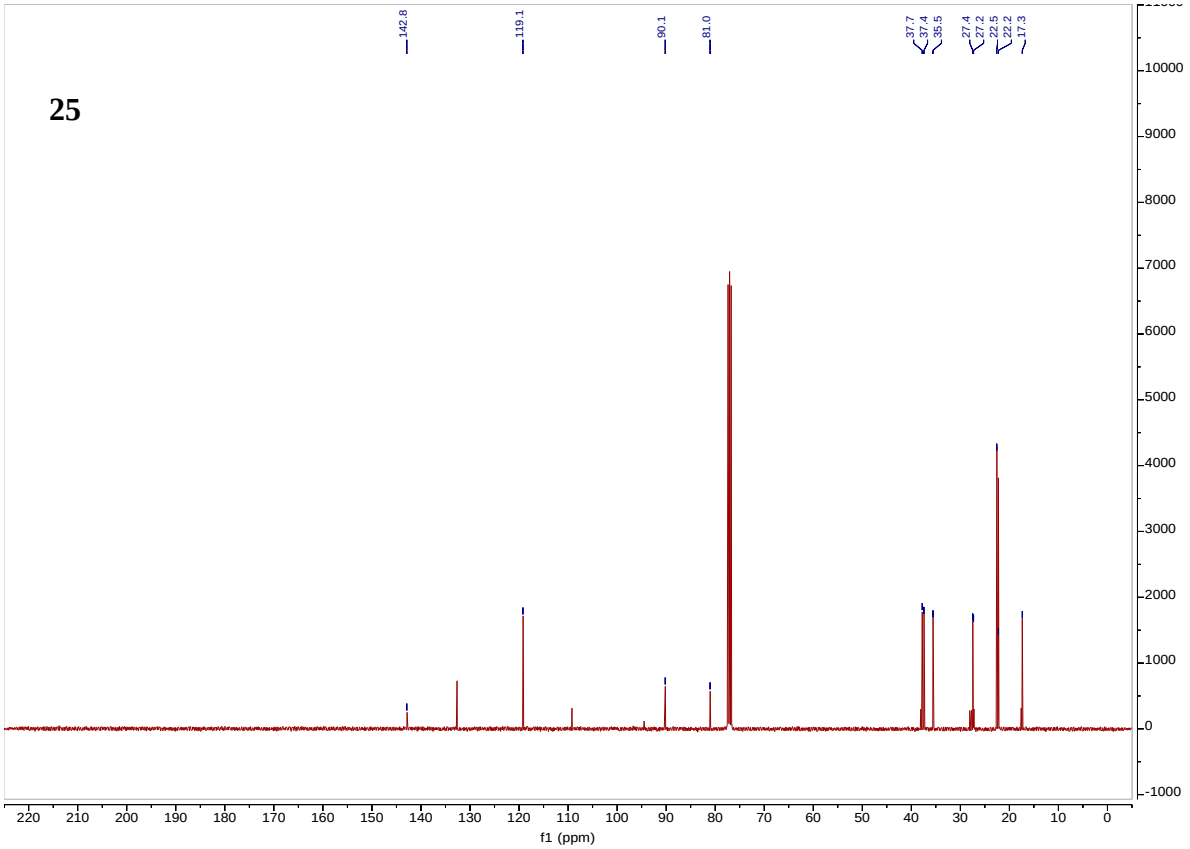
25
142.8
119.1
90.1
81.0
37.7
37.4
35.5
27.4
27.2
22.5
22.2
17.3
f1 (ppm)

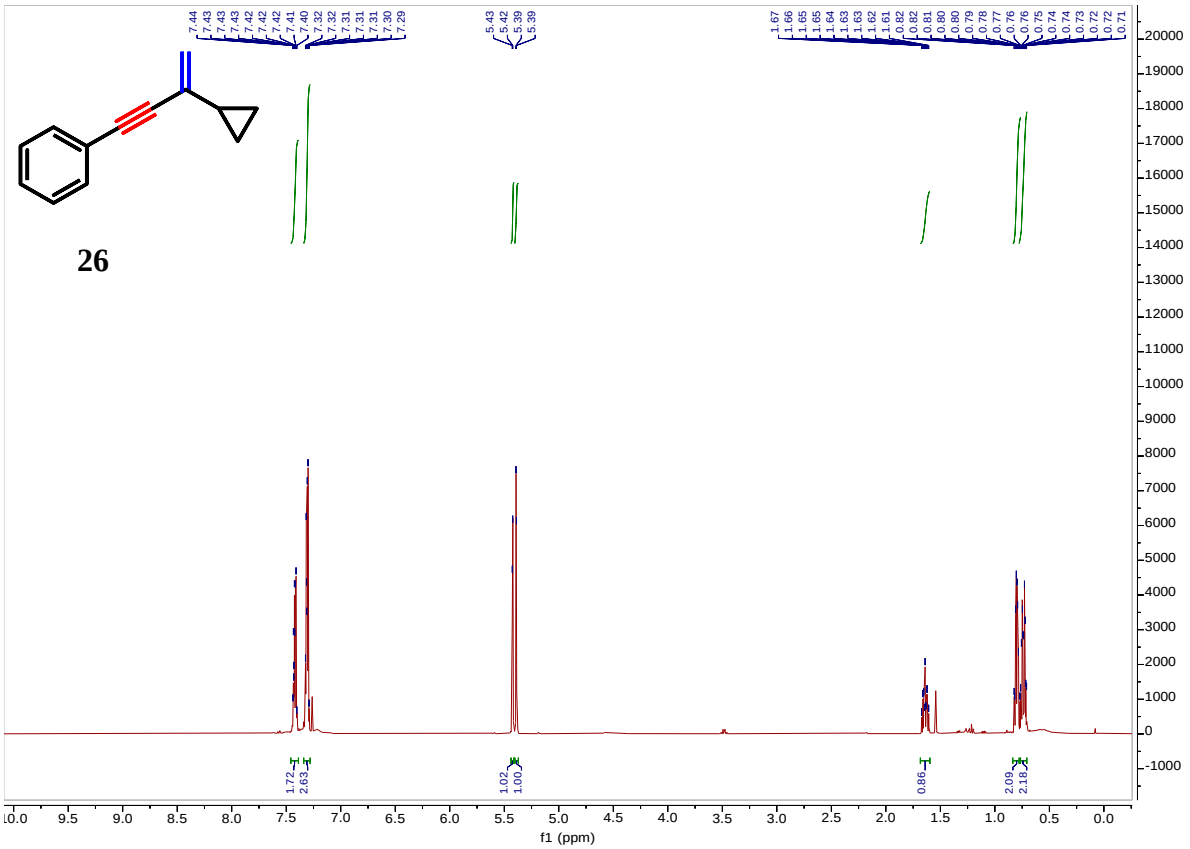
26
f1 (ppm)

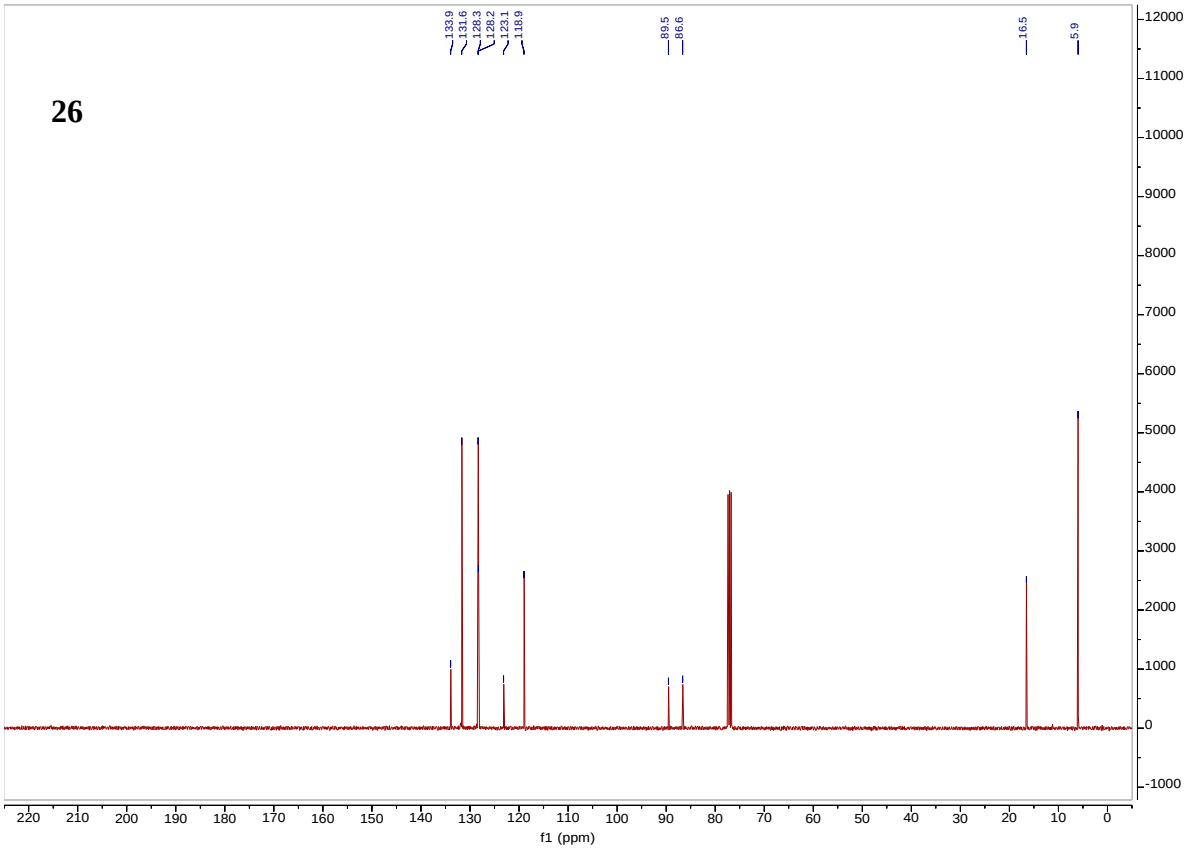
26
f1 (ppm)

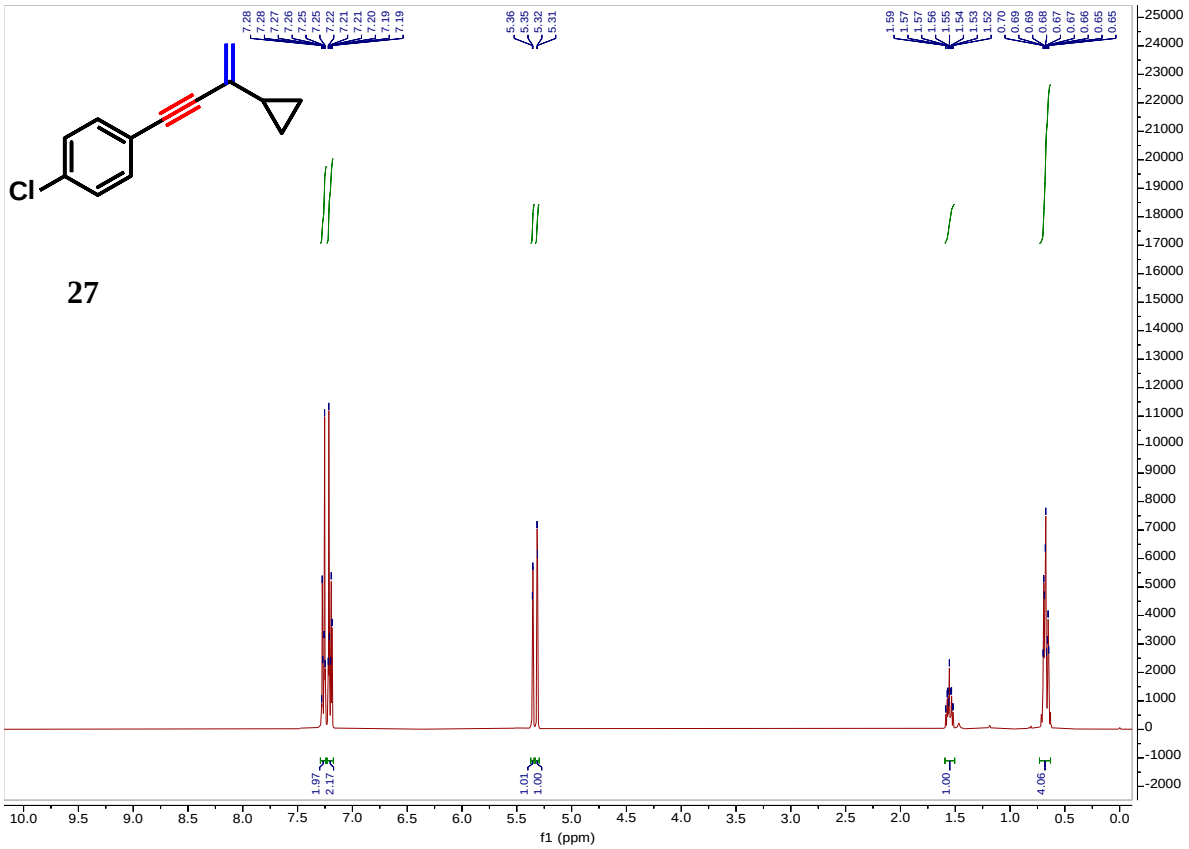
Cl
27
f1 (ppm)

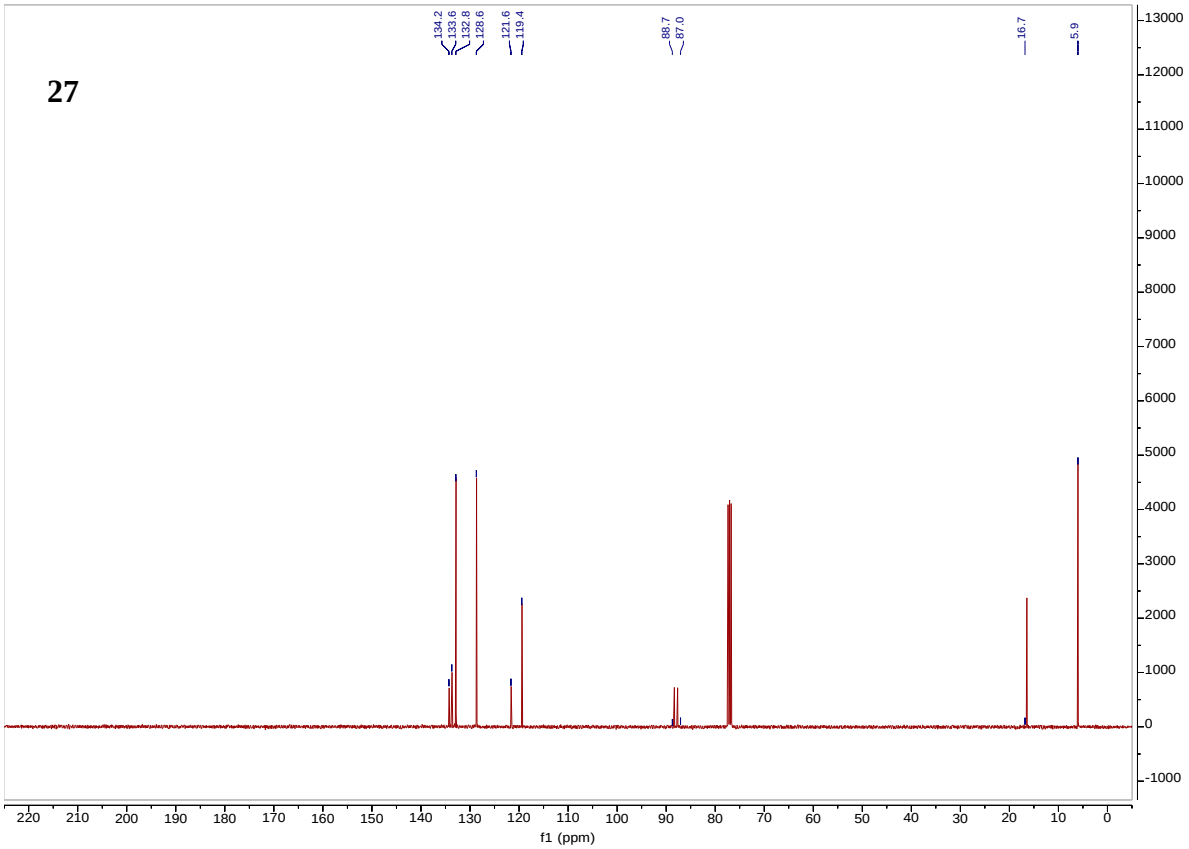
27
f1 (ppm)

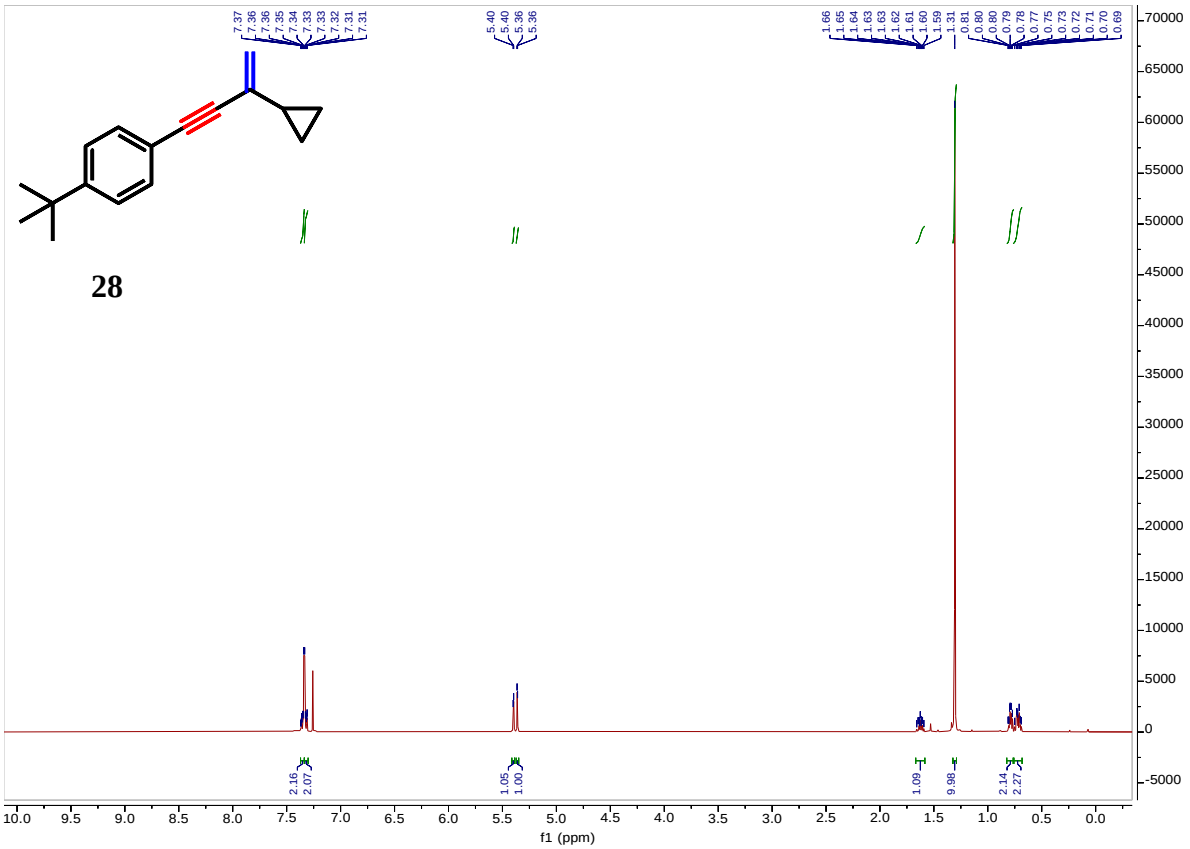
28
7.37
7.36
7.36
7.35
7.34
7.33
7.33
7.32
7.31
7.31
5.40
5.40
5.36
5.36
1.66
1.65
1.64
1.63
1.63
1.62
1.61
1.60
1.59
1.31
0.81
0.80
0.80
0.79
0.78
0.77
0.75
0.73
0.72
0.71
0.70
0.69
2.16
2.07
1.05
1.00
1.09
9.98
2.14
2.27
f1 (ppm)

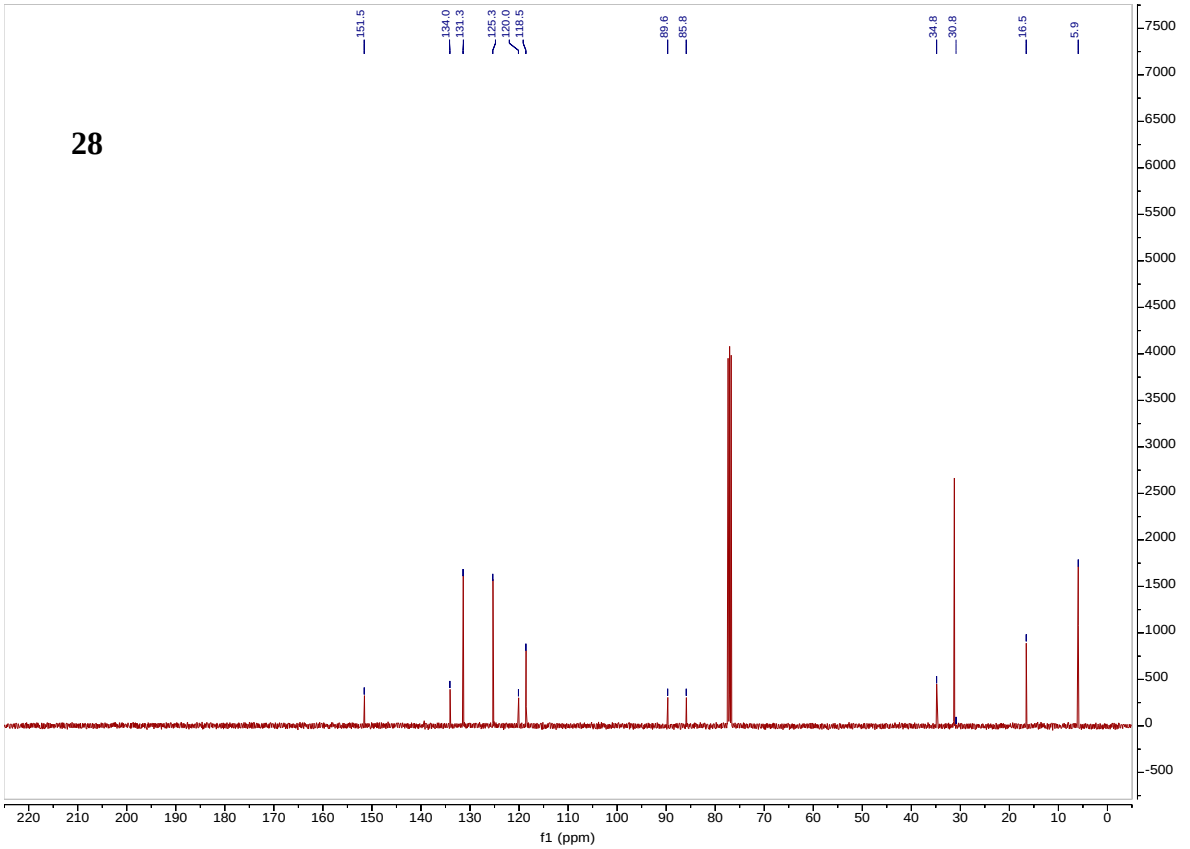
28
151.5
134.0
131.3
125.3
120.0
118.5
89.6
85.8
34.8
30.8
16.5
5.9
f1 (ppm)

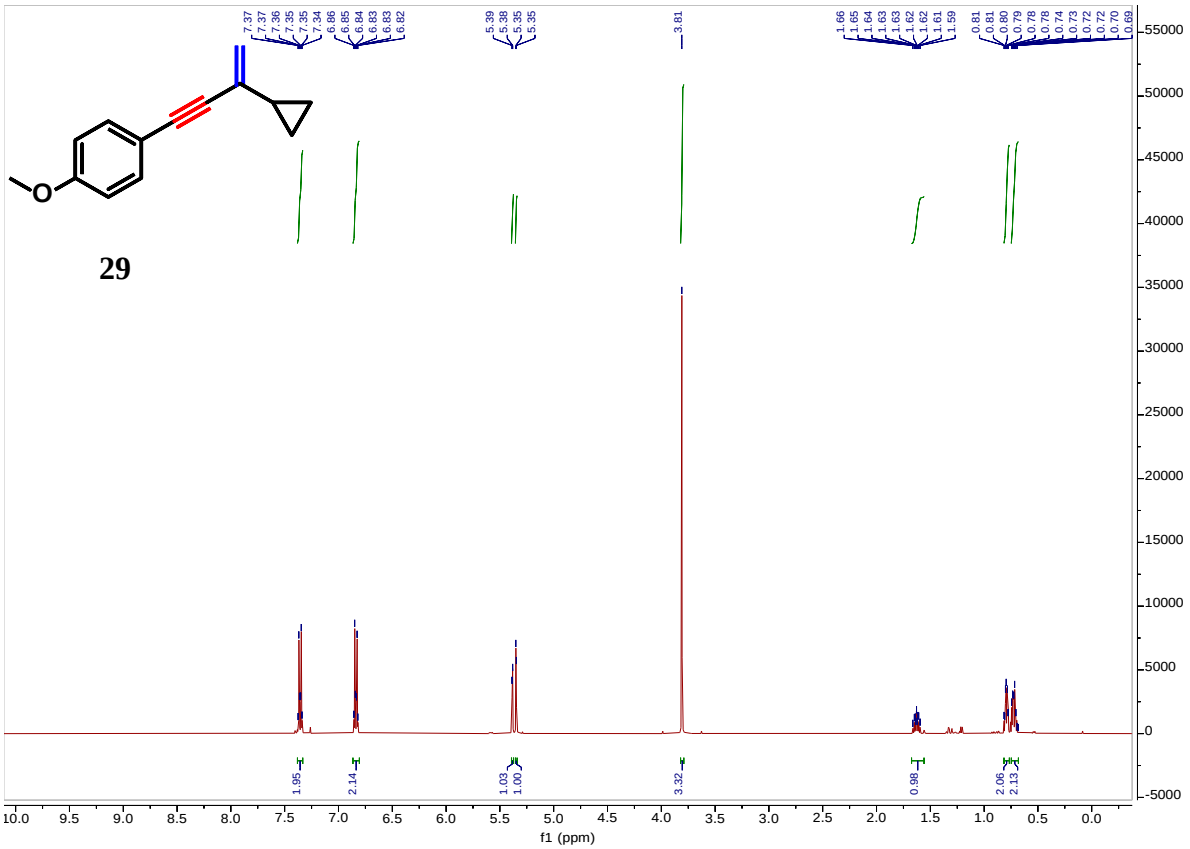
29
7.37
7.37
7.36
7.35
7.35
7.34
6.86
6.85
6.84
6.83
6.83
6.82
5.39
5.38
5.35
5.35
3.81
1.66
1.65
1.64
1.63
1.63
1.62
1.62
1.61
1.59
0.81
0.81
0.80
0.79
0.78
0.78
0.74
0.73
0.72
0.72
0.70
0.69
1.95
2.14
1.03
1.00
3.32
0.98
2.06
2.13
f1 (ppm)

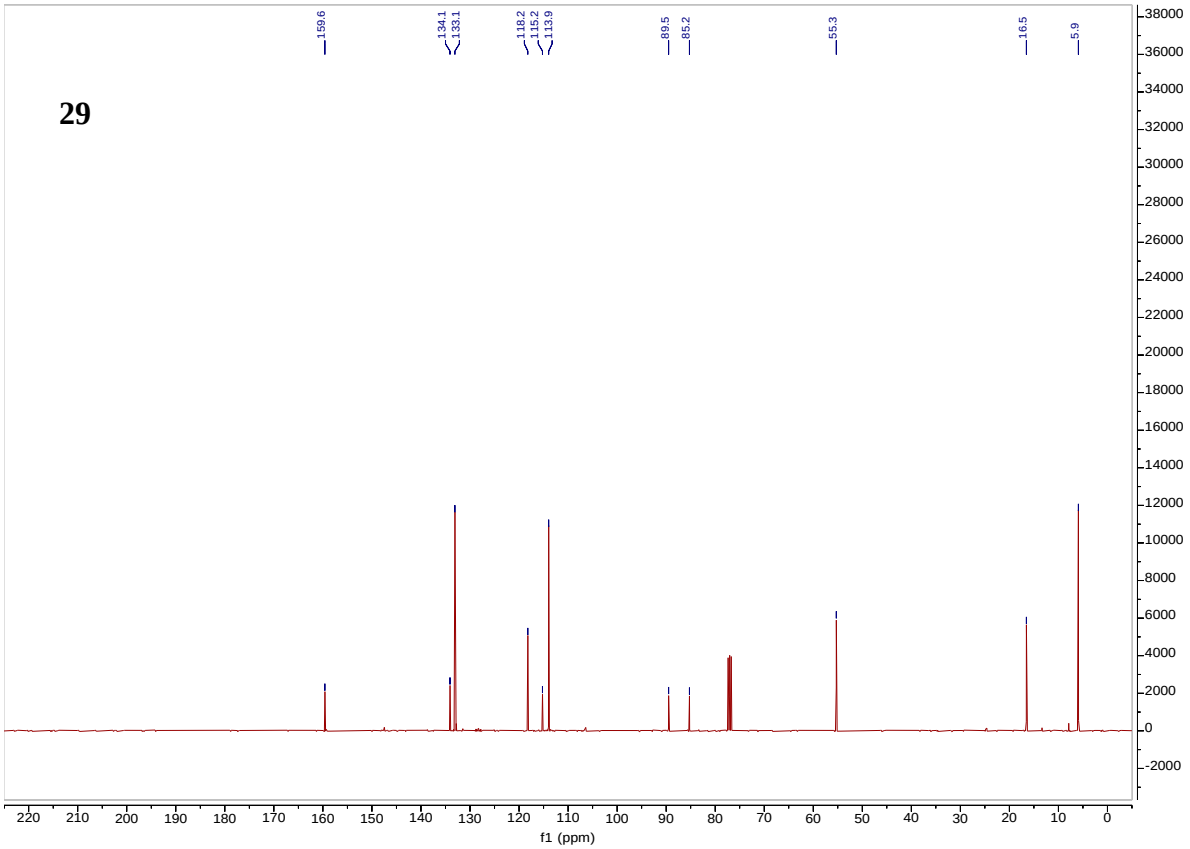
29
159.6
134.1
133.1
118.2
115.2
113.9
89.5
85.2
55.3
16.5
5.9
f1 (ppm)

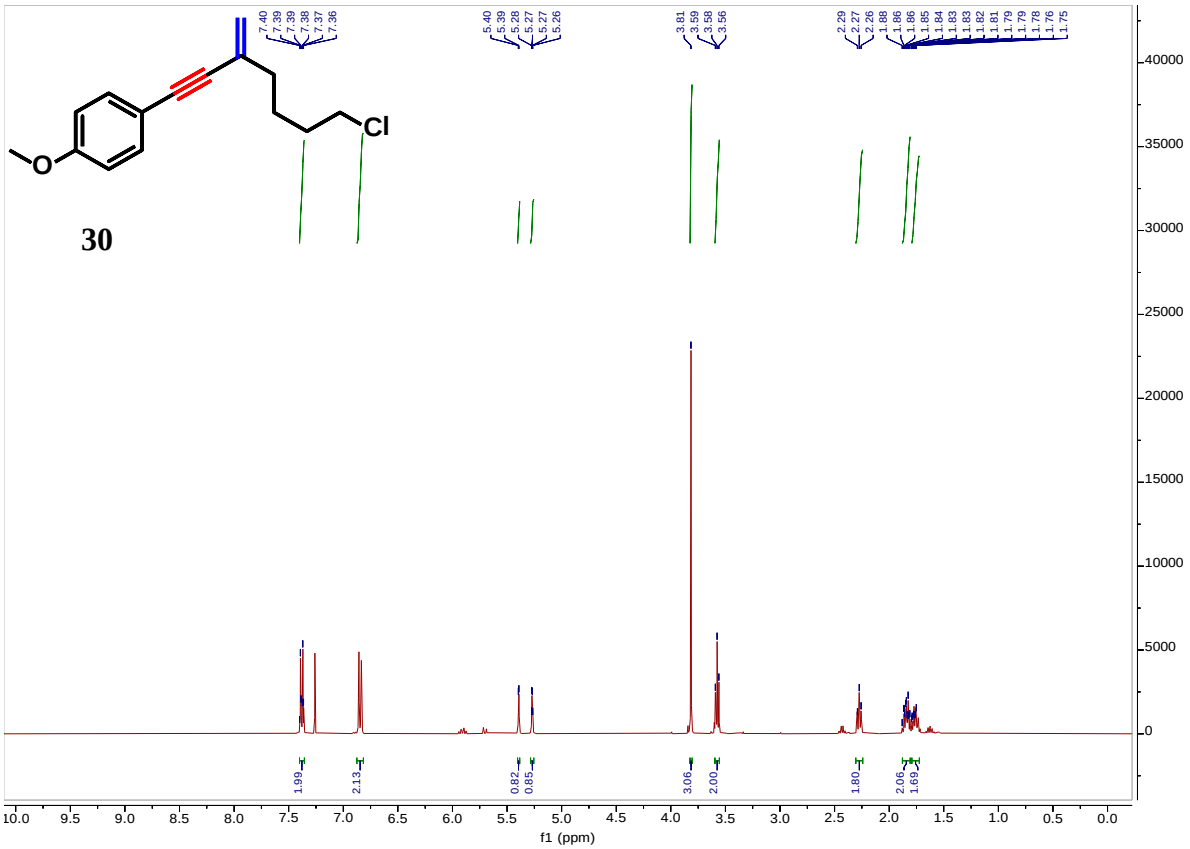
30
Cl
O
7.40
7.39
7.39
7.38
7.37
7.36
5.40
5.39
5.28
5.27
5.27
5.26
3.81
3.59
3.58
3.56
2.29
2.27
2.26
1.88
1.86
1.86
1.85
1.84
1.83
1.83
1.82
1.81
1.79
1.79
1.78
1.76
1.75
1.99
2.13
0.82
0.85
3.06
2.00
1.80
2.06
1.69
f1 (ppm)

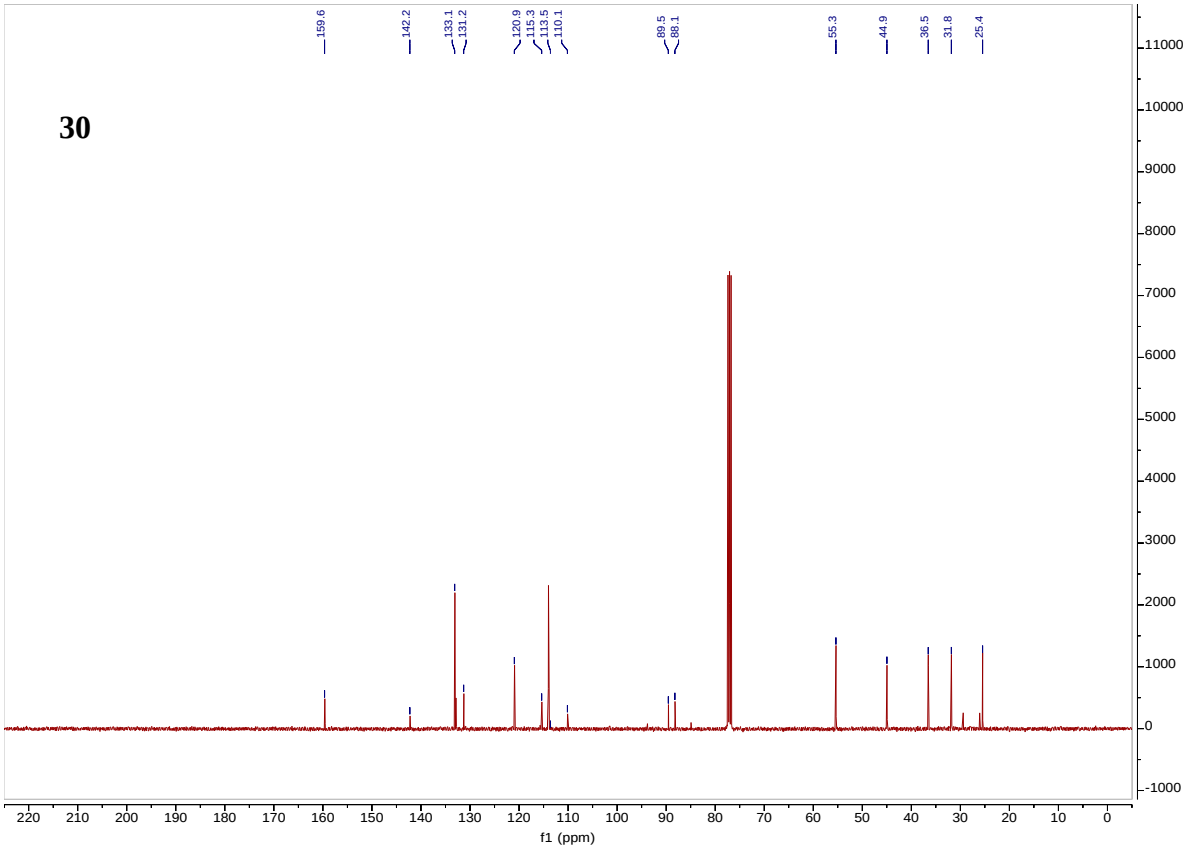
30
159.6
142.2
133.1
131.2
120.9
115.3
113.5
110.1
89.5
88.1
55.3
44.9
36.5
31.8
25.4
f1 (ppm)

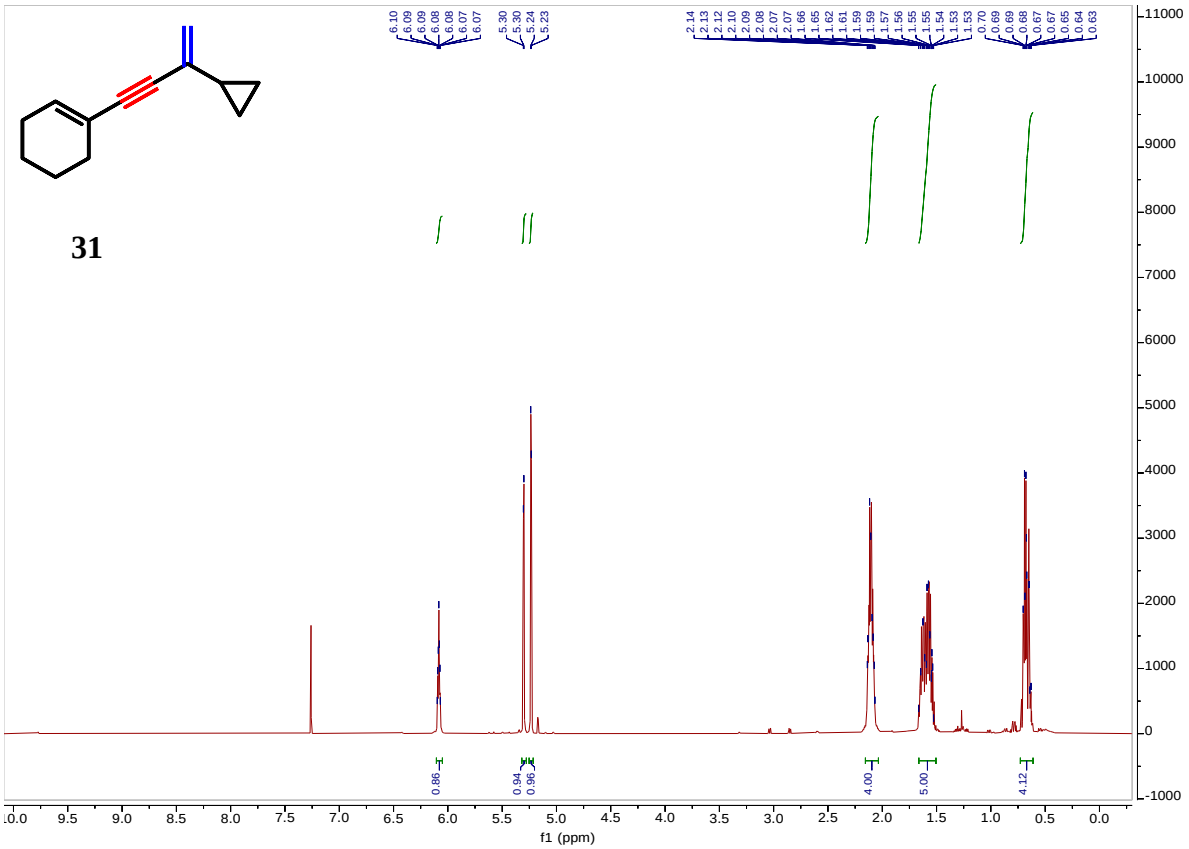
31
f1 (ppm)

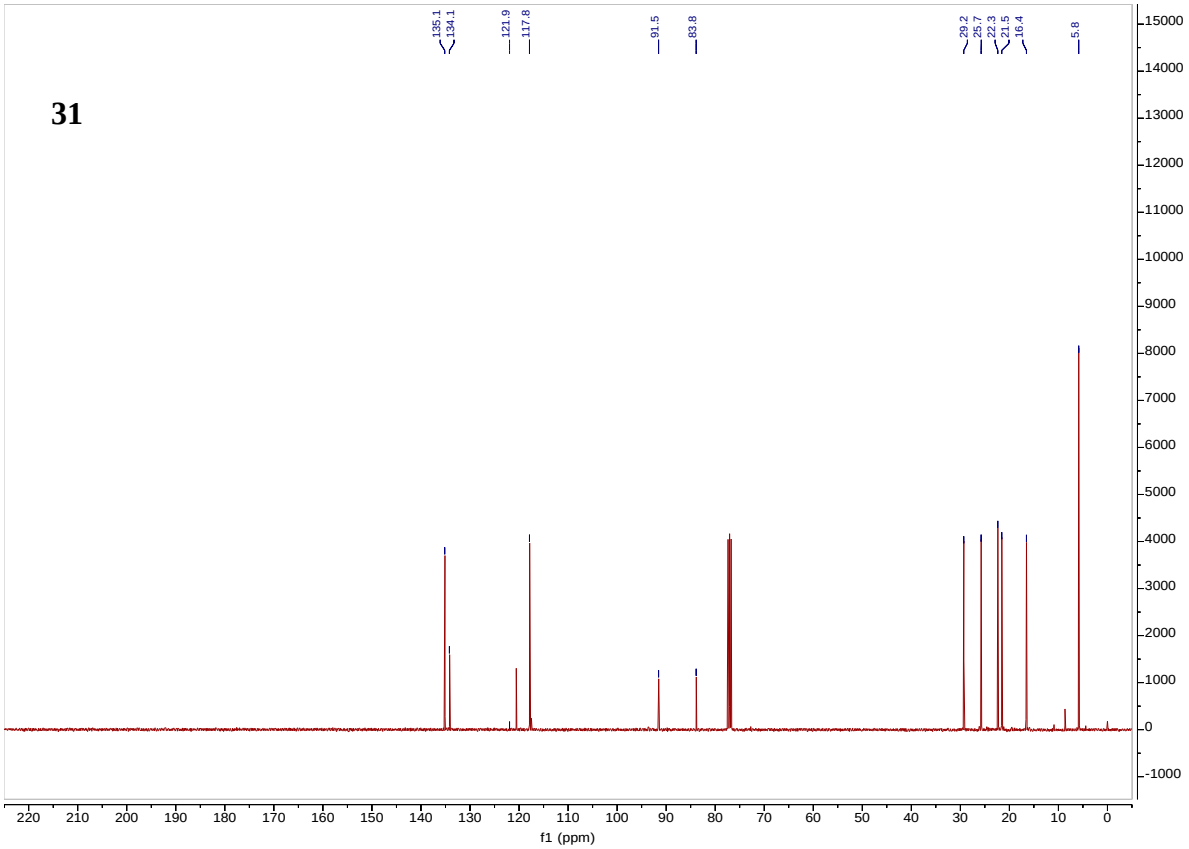
31
f1 (ppm)

6. References

(1) Weber, S.; Stöger, B.; Veiros, L. F.; Kirchner, K. Rethinking Basic Concepts - Hydrogenation of Alkenes Catalyzed by Bench-Stable Alkyl Mn(I) Complexes. *ACS Catal.* **2019**, *9*, 9715-9720.

(2) Garduño, J.A.; Arévalo, A.; Flores-Alamo, M.; García, J.J. Mn(I) organometallics containing the $^{i}Pr_2P(CH_2)_2P^{i}Pr_2$ ligand for the catalytic hydration of aromatic nitriles. *Catal. Sci. Technol.* **2018**, *8*, 2606-2016.

(3) Garduño, J. A.; García, J. J. Non-Pincer Mn(I) Organometallics for the Selective Catalytic Hydrogenation of Nitriles to Primary Amines. *ACS Catal.* **2018**, *9*, 392-401.

(4) Gorgas, N.; Alves, L.G.; Stöger, B.; Martins, A.M.; Veiros, L.F., Kirchner, K. Stable, Yet Highly Reactive Nonclassical Iron(II) Polyhydride Pincer Complexes: *Z*-Selective Dimerization and Hydroboration of Terminal Alkynes. *J. Am. Chem Soc.* **2017**, *139*, 8130 – 8133.

(5) Xu, D.; Sun, Q.; Quan, Z.; Wang, X.; Sun, W. Cobalt-Catalyzed Dimerization and Homocoupling of Terminal Alkynes. *Asian J. Org. Chem.* **2018**, *7*, 155 – 159.

(6) Brar, A.; Mummadi, S.; Unruh, D.K.; Krempner C. Verkade Base in FLP Chemistry– From Stoichiometric C–H Bond Cleavage to the Catalytic Dimerization of Alkynes. *Organometallics* **2020**, *39*, 4307 – 4311.

(7) Rubio-Pérez, L.; Azpíroz, R.; Di Guiseppe, A., Polo, V.; Castarlenas, R.; Pérez-Torrente, Oro, L.A. Pyridine-Enhanced Head-to-Tail Dimerization of Terminal Alkynes by a Rhodium–N-Heterocyclic-Carbene Catalyst. *Chem. Eur. J.* **2013**, *19*, 15304 – 15314.

(8) Chen, T.; Guo, C.; Goto, M.; Han, L.-B. A Brønsted acid-catalyzed generation of palladium complexes: efficient head-to-tail dimerization of alkynes. *Chem. Commun.* **2013**, *68*, 7498-7500.

(9) Chen, J.-F.; Li, C. Cobalt-Catalyzed gem-Cross-Dimerization of Terminal Alkynes. *ACS Catal.* **2020**, *10*, 3881 – 3889.

(10) Liu, C.-H.; Zhuang, Z.; Bose, S.; Yu, Z.-X. $Fe_2(CO)_9$-mediated [5+1] cycloaddition of vinylcyclopropanes and CO for the synthesis of α,β-cyclohexenones. *Tetrahydron* **2016**, *72*, 2752 – 2755.

(11) Gaussian 09, Revision A.01, Frisch, M. J.; Trucks, G. W.; Schlegel, H. B.; Scuseria, G. E.; Robb, M. A.; Cheeseman, J. R.; Scalmani, G.; Barone, V.; Mennucci, B.; Petersson,

G. A.; Nakatsuji, H.; Caricato, M.; Li, X.; Hratchian, H. P.; Izmaylov, A. F.; Bloino, J.; Zheng, G.; Sonnenberg, J. L.; Hada, M.; Ehara, M.; Toyota, K.; Fukuda, R.; Hasegawa, J.; Ishida, M.; Nakajima, T.; Honda, Y.; Kitao, O.; Nakai, H.; Vreven, T.; Montgomery, Jr., J. A.; Peralta, J. E.; Ogliaro, F.; Bearpark, M.; Heyd, J. J.; Brothers, E.; Kudin, K. N.; Staroverov, V. N.; Kobayashi, R.; Normand, J.; Raghavachari, K.; Rendell, A.; Burant, J. C.; Iyengar, S. S.; Tomasi, J.; Cossi, M.; Rega, N.; Millam, J. M.; Klene, M.; Knox, J. E.; Cross, J. B.; Bakken, V.; Adamo, C.; Jaramillo, J.; Gomperts, R.; Stratmann, R. E.; Yazyev, O.; Austin, A. J.; Cammi, R.; Pomelli, C.; Ochterski, J. W.; Martin, R. L.; Morokuma, K.; Zakrzewski, V. G.; Voth, G. A.; Salvador, P.; Dannenberg, J. J.; Dapprich, S.; Daniels, A. D.; Farkas, Ö.; Foresman, J. B.; Ortiz, J. V.; Cioslowski, J.; Fox, D. J. Gaussian, Inc., Wallingford CT, 2009.

(12) (a) Haeusermann, U.; Dolg, M.; Stoll, H.; Preuss, H.; Schwerdtfeger, P.; Pitzer, R. M. Accuracy of energy-adjusted quasirelativistic ab initio pseudopotentials *Mol. Phys.* **1993**, *78*, 1211-1224. (b) Kuechle, W.; Dolg, M.; Stoll, H.; Preuss, H. Energy-adjusted pseudopotentials for the actinides. Parameter sets and test calculations for thorium and thorium monoxide *J. Chem. Phys.* **1994**, *100*, 7535-7542. (c) Leininger, T.; Nicklass, A.; Stoll, H.; Dolg, M.; Schwerdtfeger, P. The accuracy of the pseudopotential approximation. II. A comparison of various core sizes for indium pseudopotentials in calculations for spectroscopic constants of InH, InF, and InCl *J. Chem. Phys.* **1996**, *105*, 1052-1059.

(13) (a) Ditchfield, R.; Hehre, W. J.; Pople, J. A. Self-Consistent Molecular-Orbital Methods. IX. An Extended Gaussian-Type Basis for Molecular-Orbital Studies of Organic Molecules *J. Chem. Phys.* **1971**, *54*, 724-728. (b) Hehre, W. J.; Ditchfield, R.; Pople, J. A. Self-Consistent Molecular Orbital Methods. 12. Further extensions of Gaussian-type basis sets for use in molecular-orbital studies of organic-molecules *J. Chem. Phys.* **1972**, *56*, 2257-2261. (c) Hariharan, P. C.; Pople, J. A. Accuracy of AH equilibrium geometries by single determinant molecular-orbital theory *Mol. Phys.* **1974**, *27*, 209-214. (d) Gordon, M. S. The isomers of silacyclopropane *Chem. Phys. Lett.* **1980**, *76*, 163-168. (e) Hariharan, P. C.; Pople, J. A. Influence of polarization functions on molecular-orbital hydrogenation energies *Theor. Chim. Acta* **1973**, *28*, 213-222.

(14) Hehre, W. J., Radom, L., Schleyer, P. v.R. & Pople, J. A. *Ab Initio Molecular Orbital Theory*, John Wiley & Sons, NY, 1986.

(15) Parr, R. G.; Yang, W. Density Functional Theory of Atoms and Molecules; Oxford University Press: New York, 1989.

(16) (a) Perdew, J. P.; Burke, K.; Ernzerhof, M. Generalized Gradient Approximation Made Simple *Phys. Rev. Lett.* **1996**, *77*, 3865-3868. (b) Perdew, J. P.; Burke, K.; Ernzerhof, M. Generalized Gradient Approximation Made Simple *Phys. Rev. Lett.* **1997**, *78*, 1396-1396. (c) Perdew, J. P. Density-functional approximation for the correlation energy of the inhomogeneous electron gas *Phys. Rev. B* **1986**, *33*, 8822-8824.

(17) (a) Peng, C.; Ayala, P. Y.; Schlegel, H. B.; Frisch, M. J. Using redundant internal coordinates to optimize equilibrium geometries and transition states *J. Comp. Chem.* **1996**, *17*, 49-56. (b) Peng, C.; Schlegel, H. B. Combining Synchronous Transit and Quasi-Newton Methods for Finding Transition States *Israel J. Chem.* **1993**, *33*, 449-454.

(18) (a) McClean, A. D.; Chandler, G. S. Contracted Gaussian basis sets for molecular calculations. I. Second row atoms,*Z*=11-18 *J. Chem. Phys.* **1980**, *72*, 5639-5648. (b) Krishnan, R.; Binkley, J. S.; Seeger, R.; Pople, J. A. Self-consistent molecular orbital methods. XX. A basis set for correlated wave functions *J. Chem. Phys.* **1980**, *72*, 650-654. (c) Wachters, A. J. H. Gaussian Basis Set for Molecular Wavefunctions Containing Third-Row Atoms *J. Chem. Phys.* **1970**, *52*, 1033-1036. (d) Hay, P. J. Gaussian basis sets for molecular calculations - representation of 3D orbitals in transition-metal atoms *J. Chem. Phys.* **1977**, *66*, 4377-4384. (e) Raghavachari, K.; Trucks, G. W. Highly correlated systems: Excitation energies of first row transition metals Sc-Cu *J. Chem. Phys.* **1989**, *91*, 1062-1065. (f) Binning Jr., R. C.; Curtiss, L. A. Compact contracted basis-sets for 3rd-row atoms - Ga-Kr *J. Comp. Chem.* **1990**, *11*, 1206-1216. (g) McGrath, M. P.; Radom, L. Extension of Gaussian-1 (G1) theory to bromine-containing molecules *J. Chem. Phys.* **1991**, *94*, 511-516. (h) Curtiss, L. A.; McGrath, M. P.; Blaudeau, J.-P.; Davis, N. E.; Binning Jr., R. C.; Radom, L. Extension of Gaussian-2 theory to molecules containing third-row atoms Ga-Kr *J. Chem. Phys.*, **1995**, *103*, 6104-6113. (i) Clark, T.; Chandrasekhar, J.; Spitznagel, G. W.; Schleyer, P. v. R. Efficient diffuse function-augmented basis-sets for anion calculations. 3. The 3-21+G basis set for 1st-row elements, Li-F *J. Comp. Chem.* **1983**, *4*, 294-301. (j) Frisch, M. J.; Pople, J. A.; Binkley, J. S. Self-Consistent Molecular Orbital Methods. 25. Supplementary Functions for Gaussian Basis Sets *J. Chem. Phys.* **1984**, *80*, 3265-3269.

(19) Zhao, Y.; Truhlar, D. G. The M06 suite of density functionals for main group thermochemistry, thermochemical kinetics, noncovalent interactions, excited states, and transition elements: two new functionals and systematic testing of four M06-class functionals and 12 other functionals *Theor. Chem. Acc.*, **2008**, *120*, 215-241.

(20) (a) Zhao, Y.; Truhlar, D. G. Density Functionals with Broad Applicability in Chemistry *Acc. Chem. Res.* **2008**, *41*, 157-167. (b) Zhao, Y.; Truhlar, D. G. Applications and validations of the Minnesota density functionals *Chem. Phys. Lett.* **2011**, *502*, 1-13.

(21) (a) Cancès, M. T.; Mennucci, B.; Tomasi, J. A new integral equation formalism for the polarizable continuum model: Theoretical background and applications to isotropic and anistropic dielectrics *J. Chem. Phys.* **1997**, *107*, 3032-3041. (b) Cossi, M.; Barone, V.; Mennucci, B.; Tomasi, J. Ab initio study of ionic solutions by a polarizable continuum dielectric model *Chem. Phys. Lett.* **1998**, *286*, 253-260. (c) Mennucci, B.; Tomasi, J. Continuum solvation models: A new approach to the problem of solute's charge distribution and cavity boundaries *J. Chem. Phys.* **1997**, *106*, 5151-5158. (d) Tomasi, J.; Mennucci, B.; Cammi, R. Quantum mechanical continuum solvation models *Chem. Rev.* **2005**, *105*, 2999-3094.

(22) Marenich, A. V.; Cramer, C. J.; Truhlar, D. G. Universal solvation model based on solute electron density and a continuum model of the solvent defined by the bulk dielectric constant and atomic surface tensions *J. Phys. Chem. B*, **2009**, *113*, 6378-6396.

Other files

coordinates alkynes DFT.xyz (106.62 KiB) view on ChemRxiv • download file